Instrumented Ergonomic Risk Assessment Using Wearable Technology and Marker-less Optical Sensor

By

Ahmed Humadi

A thesis submitted in partial fulfillment of the requirements for the degree of
Master of Science

Department of Mechanical Engineering

University of Alberta

Abstract

Work-related musculoskeletal disorders (WMDs) are reported as the primary category of non-fatal work-related diseases in the industrial environment that affect joints, ligaments, tendons, and muscles. The contributing factors to the WMDs could be awkward postures adopted by workers, forceful exertions, repetitive motions, vibration, and psychological and environmental factors. Various assessment methods based on the kinematics and kinetics of the body were proposed for preventing WMDs. Self-report methods, including questionnaires, checklist, and interviews, are used for this purpose, based on a subjective report of the individuals about their behavior, symptoms, and attitude. Although the self-report methods have low cost and cover a wide range of samples, personal reporting has drawbacks originating from the individuals' inaccurate perception of the WMDs factors exposure. Additionally, self-report methods could have low validity and reliability compared to other methods. At the same time, the observational methods were proposed for evaluating and reducing the WMDs factors. The previous studies showed that inter-observer reliability is the major shortcoming of these methods. Besides, accurate and reliable advanced observational methods such as marker-based systems are challenging to use in real workplaces. Therefore, a reliable system based on marker-less motion trackers or wearable technologies combined with an observational method is required for evaluating postures and movements, causing WMDs and overcome the shortcomings mentioned above.

The objective of this thesis is to investigate the accuracy and reliability of using a marker-less motion tracker and a wearable technology against a gold-standard marker-based

system combined with an observational ergonomic method for different manual material handling tasks.

To this end, eleven able-bodied individuals participated in two manual material handling tasks while their motion was recorded by a marker-based system (reference), marker-less motion tracker (Microsoft Kinect), and a system of inertial measurement units (IMUs). Then, joint angles were calculated and inserted into an observational risk assessment tool: Rapid Upper Limb Assessment (RULA). The calculated joint angles and the associated RULA scores obtained by the marker-less motion and IMU-based systems were compared against a marker-based system (reference) using the proportion agreement index (Po), Cohen's Kappa coefficient (κ) for RULA scores, and root mean square error (RMSE) for joint angles. Also, the intra-class correlation coefficient (ICC) was used to assess inter-participant reliability for each system. The IMU-based system showed "moderate" to a "substantial" agreement with the marker-based system in most of the tested manual handling tasks with the median of $\kappa > 0.6$, according to Landis and Koch scale. Also, it showed an "excellent" agreement in the RULA scores median between participants for most of the manual handling tested tasks (ICC > 0.75). While the reference marker-based system showed an "excellent" agreement for all manual handling tested tasks (ICC > 0.75) in the RULA scores median between participants, according to Cicchetti guidelines for interpretation of ICC.

On the other hand, the marker-less system showed "fair" to a "moderate" agreement with the median of $\kappa < 0.4$ and $\kappa > 0.41$ with the maker-based system over the same scale, affected by both self-occlusion and object occlusion. In addition, the ICC showed "fair" to an excellent agreement in the RULA scores median, between participants for the tested

manual handling tasks (ICC < 0.59) and (ICC > 0.75), according to the same guidelines for interpretation of ICC.

Preface

This thesis is an original work of Ahmed Humadi. The research project, of which this thesis is a part, received research ethics approval from the Health Research Ethics Board of the University of Alberta, Project Name "Ergonomic risk assessment using in-field motion sensors," study ID_Pro00083309.

Parts of this thesis were presented as a poster at the 20th Annual Alberta Biomedical Engineering Conference 2019 (Banff, Canada) and selected for a five-minute presentation competition at the same conference.

Dedicated to

My mother,

my sister,

And

Eng. Abdullah Ahmed Bugshan.

Acknowledgments

I would first like to thank my supervisor Dr. Hossein Rouhani and co-supervisor Dr. Rafiq Ahmad.

I would also like to thank the godfather of education in Yemen, Eng. Abdullah Bugshan, who is always willing to lend a hand to students.

I would also like to thank Milad Nazarahari, Aminreza Khandan, and Alireza Noamani, who were involved in the experiments and data analysis of this research project. Without their passionate participation and input, the experiments and data analysis could not have been successfully conducted.

Finally, I must express my very profound gratitude to my mother and to my friends Ahmed Aldhaleai and Hamed Namoura for providing me with unfailing support and continuous encouragement throughout my years of study and through the process of researching and writing this thesis. This accomplishment would not have been possible without them. Thank you.

Table of Contents

List of Tables

List of Figures

Chapter 1

This chapter provides an introduction to the risk factors of work-related musculoskeletal disorders (WMDs) and their evaluation. First, the rise of ergonomics as an upstanding discipline is introduced. Then, the working areas of ergonomics science and the contributing risk factors in each area are described. After that, a light spot was shed on the physical ergonomics and its factors that cause WMDs, and ergonomic methods that proposed to prevent these factors. Lastly, the thesis objective and outline are provided.

1. Introduction

1.1 Work-related risk assessment

The field of ergonomics, or human factors as it is known in North America, is a new discipline compared to other disciplines such as human motion biomechanics. The first appearance of ergonomics goes back to the early 1900s. However, it became an identifiable and noticeable profession only in its sixth decade of existence [1]. Since then, the number of ergonomists increased from a few individuals in industrialized countries to thousands of professional ergonomists in both industrialized and developing countries. In addition, the field of ergonomics has experienced an evolution, and currently, the ergonomists are working in a broad range of systems (e.g., simple hand tools, and software).

The field of ergonomics has been defined both as a science and as a practice [1]. Firstly, as a science, ergonomists are interested in identifying human performance capabilities, limitations, and other characteristics in human-machine interaction. Secondly, as a practice, ergonomics investigates the applications of the human-system interface to foster safety, health, comfort, and quality of life. In addition, the National Research Council of Canada defines ergonomics as “the application of scientific knowledge to the workplace in order to improve the well-being and efficiency of both the individual and the organization.”

The most important specialization areas of ergonomics, as reported in the IEA triennial report [2], are (1) physical ergonomics, (2) cognitive ergonomics, and (3) organizational ergonomics. The physical ergonomics concerns preventing work-related musculoskeletal disorders (WMDs) that are primarily associated with physical activities such as workers’ postures, manual material handling, and repetitive movements by maintaining a healthy

and safe human-environment interaction. The cognitive ergonomics concerns the mental processes such as perception and reasoning and their effects on human-environment interference. In contrast, the organizational ergonomics is concerned with the optimization process of the human-technology interaction.

The musculoskeletal system is made of the bones, muscles, cartilages, tendons, ligaments, and joints. Any kind of sprain, strain, tear, soreness, or pain of one or more of the musculoskeletal system's component(s) is considered a disorder. Three main factors are causing musculoskeletal disorders: physical, psychological, and environmental [3]. The physical factors, such as forces exerted on the musculoskeletal system, postures adopted, or work cycles, are considered as the main factors contributing to WMDs by causing muscles and joint fatigue. The psychological factors can be categorized into mental, psychosocial, and organizational factors. Psychological factors are not considered as a direct cause of WMDs. However, their hazard to the musculoskeletal system exists whenever the workers are mentally stressed as they try to maintain a certain posture. Finally, environmental factors such as noise, light, and temperature can develop WMDs or decrease the worker's productivity [3].

The WMDs are reported as the major cause of nonfatal occupational injuries in industrial countries [1]. According to the Canadian Community Health Survey (CCHS), in 2013, 16.0% of Canadians aged 15 or older have suffered injuries that limited their activities, while for 14.5% of this population, the injury took place during work. The majority of those with workplace-related injuries were male (71.2%), while most of them worked in trades, transport, equipment operation, and related occupations (34.0%), followed by sales and service (24.0%). In addition to severe consequences for the Canadian workforce, WMDs are a significant financial burden for the Canadian health care system; they cost $19.8 billion annually, according to CCHS [4].

To reduce the negative effects of WMDs on workforce and healthcare systems, various methods were proposed during the past decades to assess the risk exposure of the WMDs factors, such as the Rapid Upper Lim Assessment (RULA) tool. Such assessments would benefit both workforces and the healthcare system by decreasing the injury-related costs.

These assessment methods can be categorized based on their method of data collection into three groups: self-report, observational, and instrumental [5].

Numerous self-report methods have been developed to measure different WMDs factors, such as the physical load, muscle use, and body discomfort. Self-report methods depend on the subjective report of the individuals about their behavior, symptoms, and attitude. They take different forms, such as questionnaires [6]-[7]-[8]-[9], checklist [10], and interview [11]-[12]. The advantages of self-reporting methods are as follows: (1) the person expresses precisely the experience of overloading and discomfort, regardless of what the behavioral measures show by reporting his/ her situation, (2) a wide range of samples could be assessed, and (3) they have a low cost. However, subjective reporting has many drawbacks coming from the inaccurate perception of the WMDs factors exposure among workers [13]. In addition to the low reliability, researchers believe that the use of the other methods increases the assessment accuracy and reliability compared to self-reporting methods [14].

In addition to the self-report proactive attempts to prevent WMDs, the observational methods are also common in the industry in order to evaluate and manage the WMDs factors. Observational methods could be classified into two groups [15]: (1) simple, and (2) advanced. Simple observational methods or pen-paper based observational methods, record the worker postures in pre-designed pro-forma sheets by an independent observer. For example, the Ovako Working Posture Analysis System (OWAS) [16] is a practical observational method for recording and analyzing the whole-body posture. The OWAS defines the postures of the back, arms, and legs by different codes to indicate their positions plus three codes for the load definition. Based on the OWAS, a new method called Rapid Upper Limb Assessment (RULA) [17] was developed to provide a quick upper limb disorder factors assessment for the working population. Also, it identifies muscle fatigue originated from the adopted postures, exerting forces, and the frequency of muscle use.

The RULA method utilizes silhouettes of the body segments' postures and three coding tables to indicate the exposure risk level. Body segments in the RULA method are grouped to Group 1 containing Arm and Wrist and Group 2 containing Neck, Trunk, and Leg in order to provide a quick assessment. Each body segment is given a number, which

represents its range of motion, i.e., number 1 indicates a minimal range of motion, while number 4 is a high range of motion. The scoring system in the RULA method requires a single number from each group to indicate the amount of load exerted on the musculoskeletal system.

As the RULA method was developed for sedentary task evaluation [15], the Rapid Entire Body Assessment method (REBA) was designed to assess dynamic tasks [16]. The REBA method is similar to the RULA in terms of using diagrams to represent the body segments and the scoring system. However, in addition to RULA purposes, the REBA method aims to have a comprehensive evaluation that is sensitive to a variety of tasks. For example, the power of grip, rapid or unstable postures, and the knee position are the additional parts in the REBA method. In addition to the posture and force factors, other factors such as biomechanical, physiological, and psychophysical could cause serious WMDs. Thus, a new method called the Revised NIOSH equation for the design and evaluation of manual lifting tasks has been developed to consider these factors [16]. While simple observational methods have advantages such as having a low cost, not requiring highly trained staff and being able to assess a variety of physical activities, the low inter-observer repeatability is the major shortcoming of these methods [5].

On the other hand, advanced observational methods, based on video recording and computer analyzing, could be used to assess a variety of postures in fast-paced environments in real-time [15]. Examples of these advanced observational methods are HARBO [18], PEO [19], The TRAC-system [20], ARBAN [21], and SIMI [22]. Using these methods, physical activities could be observed and analyzed on-site or recorded for later analysis. For example, using marker-based systems, a 3D view of the workplaces could be recorded and analyzed to measure biomechanical parameters such as the distance of movement, range of motion of segments, and segments' velocity and acceleration. Yet, the practical functionality of these systems in real workplaces is questionable because of problems such as occlusion and limited field of view. Also, these methods have a high operating cost [13].

Direct methods for WMDs assessment are defined as the methods that have the measuring or sensing device attached directly to the person [13]. According to risk factors, the direct

measurement methods could be divided into a direct assessment of the posture and muscle fatigue measurements [15]. The posture direct measurement methods are based on simple, e.g., inclinometer, or sophisticated, e.g., electric goniometer, hand-held equipment [23]-[24] that continuously monitor a joint angle during the task. In addition to the electric goniometer, other direct technologies such as optical scanning system, sonic system, electromagnetic system, and accelerometer-based systems have been developed for joint angle measurement [15]. However, these systems were developed mainly for clinical applications rather than in workplaces. The muscle fatigue measurement methods are based on muscle tension measurement, and the most common device is the Electromyography (EMG) sensor. However, distinguishing between different postures using EMG signals is highly challenging due to different muscle lengths [15].

Recently, the fusion of direct methods and observational methods for assessing WMDs factors have been investigated to overcome the low inter-observer repeatability and increase the accuracy of data collection [25]. For example, the fusion of the EMG sensor and video image system has been used to collect information about postures and muscle activity [15]. However, there are a few research studies regarding the use of wearable inertial measurement units (IMUs) [26] and marker-less systems.

IMUs could be used to measure various quantities such as body segment acceleration and angular velocity, by means of miniature sensors, i.e., accelerometer, magnetometer, and gyroscope integrated into one chip [26]. Considering the advantages of IMUs such as low cost, small size, and long battery life, they can be an ideal choice for ergonomic assessment studies. IMUs can stream the data to a computer wirelessly and allow a pre-designed software to monitor the worker's motion in real-time and provide proper feedback when needed. Among the studies that addressed the use of IMUs for WMDs factors evaluation, [27]-[28]-[29] combined IMUs as a direct measurement tool with simple observational methods for ergonomic assessment.

A marker-less optical sensor is capable of capturing depth and color RGB images. The depth image contains the 3D information of the scene in the camera's field of view, which can be beneficial for ergonomic assessment in many ways, such as creating a 3D map for the workplace. To capture the depth image, the sensor emits infrared rays and receives the

rebounds from objects in its field of view. Moreover, it uses the time of flight principle to determine the distance between the sensor and an object in its field of view by calculating the total time that the emitted rays take to strike that object and bounce back. Also, the depth and RGB image resolution are 512x424 and 1920x1080 pixels, respectively, for Microsoft Kinect V2 [30]. Besides, marker-less optical sensors allow the user to create a 3D skeletal for the human body in its field of view using different programming languages such as C++/CLI, C#, or Visual Basic .NET [31]. The mentioned features of these marker-less sensors provide an opportunity for researchers, especially in ergonomics, to develop algorithms that harness these features for the sake of WMDs risk assessment.

1.2 Thesis objective

The main objective of this study is to investigate the validity of an instrumented RULA assessment tool based on kinematic models obtained by (i) wearable IMUs and (ii) a marker-less optical sensor (Microsoft Kinect V2) against the kinematic model obtained by marker-based optical cameras, as the gold-standard reference. The validation has been performed through an experimental study including five different manual material handling tasks by investigating the convergent validity and accuracy of both joint angles and RULA score calculation using (i) IMUs and (ii) Kinect against marker-based optical cameras.

1.3 Thesis outline

Chapter 2 reviews the literature: a review of human movement tracking systems, an overview of WMDs in manual material handling tasks, and a review of psychophysiological and physical factors assessment methods of WMDs. Chapter 3 presents the methodology that we used to build kinematic models based on (i) marker-based cameras, (ii) IMUs, and (iii) Kinect to calculate the joint angles and, subsequently, RULA scores. Figure 1 depicts the measurement methodology proposed in this thesis. Chapter 4 presents the results of joint angles obtained by the IMUs and Kinect in terms of root mean square error (RMSE) with respect to those obtained by marker-based cameras. In addition, the proportion agreement index and Cohen's Kappa coefficient are presented to measure the RULA scores median. Finally, Chapter 5 presents the discussion, conclusion, and future perspectives.

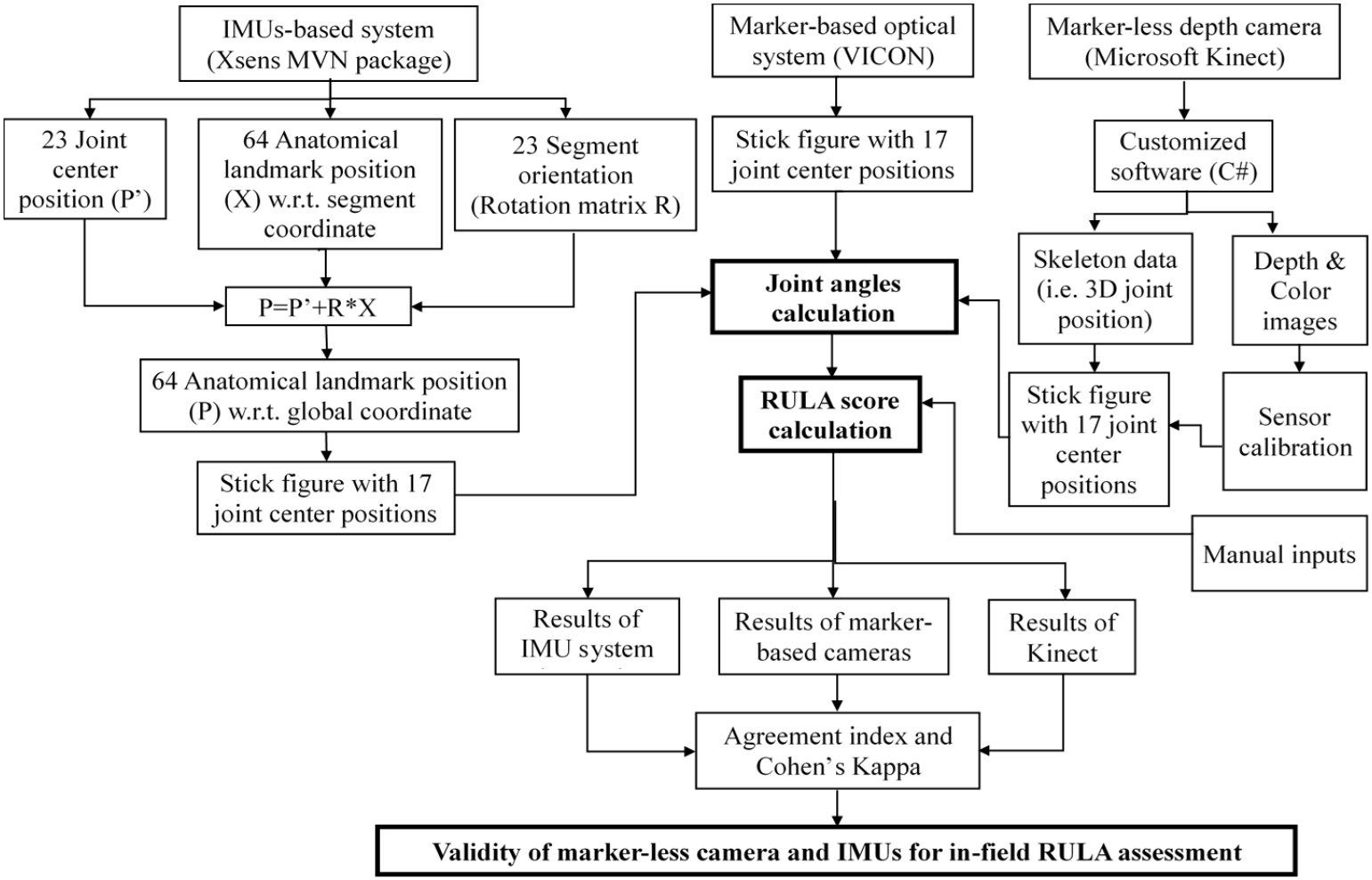

Figure 1. Thesis outline and summary of the methodology used to validate the IMU-based system and marker-less system with Marker-based system.

Chapter 2

Chapter 2 provides a literature review on the strength and weaknesses of various movement tracking systems, the relation between WMDs and Manual material handling tasks (MMH), and the recent psychophysiological and physical factors assessment methods.

2. Literature review

2.1 Human movement tracking

Human motion assessment has been of enormous interest for ergonomists since it can provide a robust means to solve severe ergonomic problems such as task modification and injury prevention. The quantitative analysis of human motion contains measurement (both kinematics and kinetic), storage, retrieval, processing, and presentation. The kinematic measurement of human movement is essential to picture underlying risks due to the task performance, and it excels the statistical analysis, which the latter just suggests the potential risk [1].

The kinematic analysis requires information on the three-dimensional (3D) position of the anatomical landmarks of the body to quantify the relative orientation between two linked segments (Figure 2) [32]. Kinematic quantities such as the linear and angular position, velocity, and acceleration can be obtained from the position of anatomical landmarks [33]. In addition to technologies such as stereophotogrammetric optoelectronic camera systems, marker-less motion tracking systems (i.e., depth cameras), and wearable inertial measurement units (IMUs) are exploited to provide a practical measurement of human movement kinematics.

2.1.1 Stereophotogrammetric optoelectronic camera systems

Stereophotogrammetric optoelectronic camera systems provide a comprehensive tool to obtain kinematic quantities for a large number of ergonomic and biomechanical applications because of their ability to rebuild the 3D position of a point in a global coordinate system. For 3D ergonomic or biomechanical analysis, a body segment position and orientation can be determined using at least three non-collinear markers positioned on the desired segment [33]. The 3D coordinates of bony landmarks are reconstructed from photographs, radiographs, and video images [34]. The video imaging method allows human participants to move more naturally [1]. In addition,

Chiari et al. [34] reported potential advantages of the video imaging method over the other stereophotogrammetric methods: lower cost, requiring less processing time, less images distortion. Therefore, video-based measurements have become the most common approach in biomechanical motion tracking. The video-based systems reconstruct the three spatial coordinates of a point in space by using either retroreflective (passive) or light-emitting (active) marker. The passive markers reflect the infrared and incandescent light emitted for external sources usually positioned around the lens in the camera periphery, while the active markers act as light sources. The active markers are robust in providing continuous marker identification with a higher sampling rate; however, they are more cumbersome than passive markers since they need wires to power them [1]-[34]. The markers are mounted either on the anatomical landmarks or a rigid plate fixed on the body segments [2]. The identification of the passive markers in the video frames is made either by pattern recognition software [35] or by dedicated hardware [36]. On the contrary, the active markers are detected by the pulse timing [34].

As mentioned above, each body segment's kinematics can be determined by three non-collinear markers; however, some studies recommended the use of four non-collinear markers to reconstruct a body segment, to reduce the possibility of missing a marker. To track markers, at least two cameras should simultaneously capture each marker [34].

Figure 2. Illustration of body markers placement

2.1.1.1 Limitations of Stereophotogrammetric optoelectronic systems

The limitations of stereophotogrammetric optoelectronic systems are due to three types of errors: 1) instrumental errors [34], 2) anatomical landmark misplacement [37], and 3) soft tissue artifacts [38]. These errors can lead to inaccuracy in the marker identification coordinates. The instrumental errors can be systematic due to the calibration inaccuracies or due to nonlinearities, or random instrumental error owed to electronic noise, marker jittering [34]. As forementioned, markers are placed either as a cluster on a plate or as a single marker placed on a palpable bony landmark. The latter placement procedure may affect the kinematic measurements, mainly inter- participant reliability [37]. Several factors contribute to the accuracy of anatomical landmarks determination, which is a milestone in the kinematic measurements using video-based systems. Examples are the soft tissue thickness over the bony landmarks, the shape of these bony prominences, and the experience of the examiner that plays a significant role in the anatomical landmarks determination [37]. The third type of error in the trajectory measurement of anatomical landmarks using stereophotogrammetric systems is the soft tissue artifacts (STA). Leardini et al. defined the STA as the relative movement of the marker and the bone under study [38]. This relative movement can be due to muscle contractions and skin deformation, and it is difficult to separate this movement from the actual bone motion by any kind of filer because of the similarity in their frequency content. It is worth mentioning that the STA depends on the experimental protocol and differs among participants [38].

The stereophotogrammetric systems have high precision and also are the most common motion capture instruments in biomechanics research; however, the system set-up is time-consuming and requires technical personnel to calibrate it and to determine the anatomical landmarks for markers placement [39]. Moreover, using the stereophotogrammetric systems for kinematic measurements requires a dedicated laboratory volume. Thus, these systems can hardly be used out of the laboratory and in real-world workplaces.

2.1.1.2 Definition of global and local coordinate systems

Each marker's 3D position is captured using at least two two-dimensional (2D) cameras with respect to a global coordinate system (GCS), defined to be fixed in the testing

space by a set of orthogonal axes (X_g, Y_g, Z_g) [40]. The GCS is defined after the calibration process, by which the location and orientation of each camera are identified [1]. The local coordinate system (LCS) is used to quantify the segment orientation and is identified based on the positions of markers attached to the segment [40]. Typically, the LCS is denoted by (X_l, Y_l, Z_l).

After defining the segment's LCS using three markers, a point's position in the GCS can be obtained from its position in the LCS using a translational mapping (Eq. 2.1):

$$P_a^g = R_l^g \vec{P}_a^l + \vec{P}_o^g \qquad \text{(Eq. 2.1)}$$

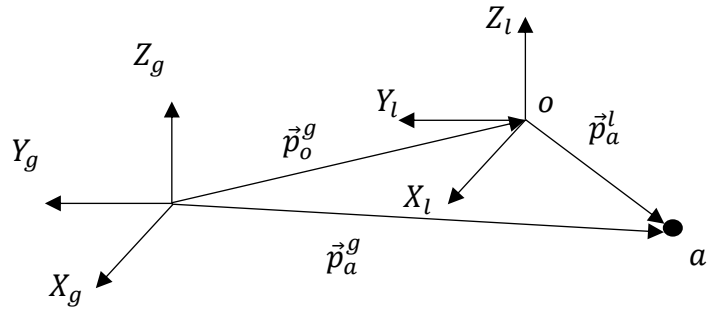

Figure 3. Depiction of Coordinate transformation of a point a from a local frame $[X_l,Y_l,Z_l]$ to the global frame $[X_g,Y_g,Z_g]$. Vectors $\vec{p}_o^g$, and $\vec{p}_a^g$ represent the position of points o, and a in space.

The rotation matrix R_l^g consists of the dot products of the unit vectors of the GCS and LCS as follow:

$$R_l^g = \begin{bmatrix} \vec{X}_g.\vec{X}_l & \vec{Y}_g.\vec{X}_l & \vec{Z}_g.\vec{X}_l \\ \vec{Y}_g.\vec{X}_l & \vec{Y}_g.\vec{Y}_l & \vec{Z}_g.\vec{Y}_l \\ \vec{Z}_g.\vec{X}_l & \vec{Z}_g.\vec{Y}_l & \vec{Z}_g.\vec{Z}_l \end{bmatrix} \qquad \text{(Eq. 2.2)}$$

The rotation matrix and the Eq. 2.1 are used when two or more motion capture systems are compared together. For example, when a segment orientation is obtained by both the IMU-based system and the marker-based stereophotogrammetric system, then both obtained orientations should be expressed with respect to the same GCS using Eq. 2.1.

2.1.1.3 Calculations of biomechanical parameters

The computation of the kinematic parameters depends on the applications. Some applications require only the markers trajectories mounted on the body surface, while others require capturing the skeletal movement by placing the markers on the joint centers, which is impossible [1]. Therefore, to estimate the skeleton locations, the term of virtual markers arose. Typically, the 3D position of the virtual markers is calculated from the 3D position of the surface (actual) markers mounted on the segment based on mathematical equations. Virtual markers are used to determine the anatomical landmarks on the segment [40]. Kadaba et al. [41] used an empirical correlation to identify the hip joint center based on the anterior superior iliac spine (ASIS) marker location and pelvis orientations.

2.1.2 Marker-less motion tracking systems

Marker-less motion tracking is a system the can recognize precisely the human movement with clothing on, under varying illumination conditions, and without the use of reflective markers on the body [42]. In order to overcome the drawbacks of the marker-based motion tracking systems (i.e., soft tissue artifacts, and markers misplacement), marker-less motion tracking systems have been presented for 20 years [43]. In addition, they are promising for the human body kinematic assessment and can have an integrated usage with the marker-based motion tracking systems. However, the lack of using marker-less motion tracking systems for quantitative analysis of human motion can be attributed to the complexity of acquiring an accurate 3D kinematic model using marker-less techniques [39]. Moreover, the applications of marker-less motion capture systems are not limited to the motion analysis for clinical studies. Still, they are extended over the past decades to cover the surveillance systems, virtual reality, and user interfaces [44]. All vision-based motion capture systems follow a general structure that has four stages: initialization, tracking, pose estimation, and recognition [44]. The initialization includes choosing a model representing the participant. The models are a hierarchy of rigid segments linked at designated joints and are used to facilitate the tracking process by showing the human movement [42]. The stick figure (Figure 4) is a common representation of human models in the literature as in [45]. The main problem associated with model reconstruction is the self-occlusion that makes the segmentation of the human body difficult during tracking [46]. This problem can be solved by making simplified assumptions such as no occlusions, the camera faces the

participant, and constant illumination [44]. The initialization process also contains the camera calibration and adaption to the scene characteristics [44]. After choosing the model and making the simplifying assumptions, the tracking is performed by distinguishing the participant's limbs from the background in consecutive frames [42]. Tracking consists of three stages. The first one is the segmentation and separating the participant limbs from the background. The second stage decreases the complexity of data by transferring it to another more controllable representation. The third one uses the participant model to distinguish the motion between frames [44]. In pose estimation, the identification of the participant's segments in a scene is brought about. In other words, the position, orientation, and shape of each segment are identified. If there is no defined model at the initialization process, the pose estimation relies on the model-free class. In this class, the pose is represented by points [47], simple boxes [48], or a stick figure, which is an advanced level of pose representations (Figure 4). If the model was defined, the pose estimation depends on two classes: an indirect model or a direct model [44]. The indirect model is a reference model utilized to extract information that can interpret the pose. The extracted information is ranging from simple information (i.e., body height), to more dynamic details about the participant [46]. The direct model class uses a model that represents the human body continuously and contains very detailed information about the pose [49].

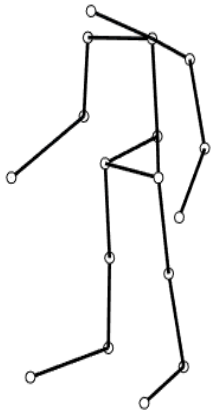

Figure 4. Stick figure for body pose representation

2.1.2.1 Limitations of marker-less motion tracking systems

All marker-less motion tracking systems up-to-date have been developed based on assumptions that made them more workable (i.e., no occlusion, known initial state, constant lighting, and tight clothes). However, in reality, the conditions are more

dynamic and non-expected. In addition to the occlusion issue that could happen due to obstacles in the scene under observation, the self-occlusion frequently arises due to body parts movement. Therefore, to solve this problem, more cameras can be used as many as the situation requires [50]. The use of multi-camera systems does not solve the problem entirely, and it just alleviates the problem [42]. The occlusion problem is a joint problem in all computer vision-based motion tracking systems (marker-less and marker-based). In systems that rely on the fixed background, the moving objects in the background are captured as a human [42]. High accuracy is not demanded in surveillance systems [44]; however, the captured motion must coincide with the actual motion for biomechanical and clinical applications. The marker-less motion systems suffer from such accuracy required for these applications, because of the complexity of extracting such biomechanical information 2D cameras. To increase the accuracy of marker-less systems, a direct model tracking system can be applied [39]. So far, no vision-based system can capture the actual human movement without markers on the body [51]. Finally, the computer vision-based systems are more attractive than other motion capture technologies (i.e., magnetic trackers, and accelerometers), since they are less cumbersome and non-intrusive to participants. However, data processing of computer vision-based systems is more complicated.

2.1.2.2 Microsoft Kinect marker-less motion tracker

On November 4, 2010, the first version of the Kinect sensor called (Microsoft Kinect) was released after a joint project between Microsoft and PrimeSense companies. The project aimed to build up a device for the user interface for video gaming based on gestures and voice. The use of the Kinect sensor did not stop in video gaming because shortly after its release, the competition to hack Kinect started as long as Kinect utilized the USB hardware feature that eased the mission. However, Microsoft Company did not want the Kinect sensor to work with other consoles other than the Xbox console; therefore, no drivers have been released. The first attempt to hack Kinect was by Adafruit, a New York-based company, when the company hosted a competition for making open-source drivers that could access Kinect's data. After that, the endeavors continued to hack Kinect such as, Hector Martin, who made the first version to access Kinect's depth image. In response to all of these efforts and on December 10,

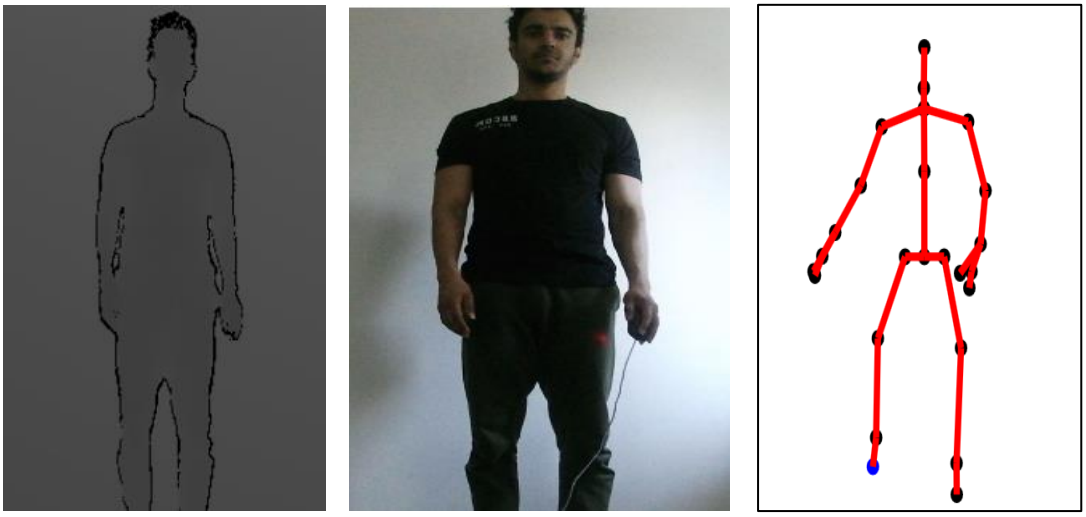

(a) (b) (c)

Figure 5. The output of Kinect sensors: (a) Depth image, (b) Color image, and (c) Kinect skeleton

2010, PrimeSense company launched its own software (OpenNI) for Kinect. The software was fascinating since it give not only access to the depth image (Figure 5.a) and RBG image (Figure 5.b) but also had the ability to detect the users' skeleton (Figure 5.c) and identify the joints positions in 3D by processing the depth image. However, a limitation of PrimeSense's software was that it requires the user to stand in T-pose to initialize the tracking algorithm. Later, on June 17, 2011, Microsoft announced the Kinect SDK beta for public use without any license. The Kinect SDK had the skeleton

tracking algorithm with no T-post initiation process and speech recognition system. Inspired by these huge steps on Kinect drivers' development, the interest among students and researchers excavated to develop their own computer application for many purposes, such as applications that use the skeleton data for ergonomic and biomechanics studies.

2.1.2.2.1 Kinect Hardware

Despite the lower cost of the Kinect sensor, its hardware pieces are revolutionary and contain advanced technologies. The hardware has four main components: color camera, infrared camera, IR emitter, and set of microphone (Figure 6). An infrared camera is used for depth data capturing. In addition, Kinect V1 utilized a USB 2.0 port, and Kinect V2 utilized USB 3.0 port, which is more advanced.

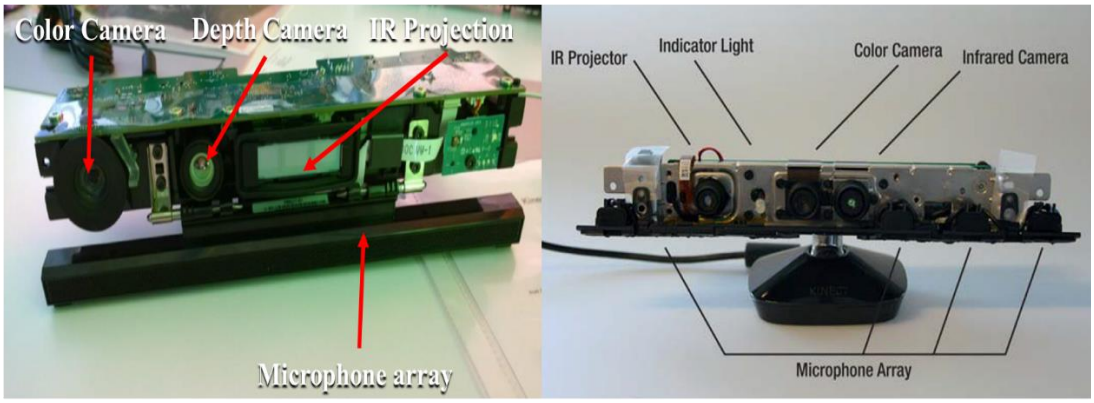

Figure 6. (a) Kinect V2 hardware (adopted from [31]). (b) Kinect V1 hardware (adopted from [95]).

The main differences between the two versions are summarized in Table 1. Moreover, the range of view is 0.5m to 8m for Kinect V2, and after 4.5m, the quality decreases. However, Kinect V1 has a default range of 0.8m to 4.5m [31].

2.1.2.2.2 Kinect applications

After the Kinect's drivers had been available for public use, there have been many research studies published investigating the usability, reliability, and validity of Kinect's data for different biomechanical, clinical, and ergonomic applications [45]-[50]-[43]-[32]-[30]-[25]-[5]. Bonnechère et al. [43] studied the validity and reproducibility of Kinect V1 for clinical analysis and rehabilitation. They designed the

study protocol to include shoulder abduction, elbow flexion, hip abduction, and knee flexion motion. To check the reproducibility, the same protocol was repeated after one week. The joint angles were recorded simultaneously using the Kinect sensor and a marker-based stereophotogrammetry system (reference). They used vector conventions to calculate the joint angles because the stick figure obtained by Kinect does not contain all anatomical landmarks that are required to use ISB recommendations. The comparison was made in terms of the range of motion between these systems. The study revealed that the range of motion is different between the systems, but the reproducibility is similar. This study was limited to simple tasks, and more complex tasks should be considered.

Table 1. Comparison between Kinect V1 and V2

	Kinect v1	Kinect v2
Color image	640 x 480 @ 30 Hz	1920 x 1080 @ 30 Hz
Depth image	320 x 240 @ 30 Hz	512 x 424 @ 30 Hz
Infrared image	640 x 480 @ 30 Hz	512 x 424 @ 30 Hz
Skeleton joints	20 joints	25 joints
Number of tracked bodies	6	6
Tilt motor	Yes	No
Angular Field of View	57.5 deg Horizontal & 43.4 deg Vertical	70 deg Horizontal & 60 deg Vertical

Clark et al. [52] validated Kinect V1 against a marker-based stereophotogrammetry system for quantifying the postural control tests such as forward reach, lateral reach, and single-leg eyes-closed standing balance. They studied different kinematic parameters for each test. The reach tests included the reached distance and trunk angles in sagittal and frontal planes. For standing balance, the range of motion and variation of movement in the position of the anatomical landmarks provided by Kinect were studied compared to a marker-based system for the sternum, pelvis, knee, and ankle. They found that Kinect was able to provide anatomical landmarks and trunk angles with excellent validity. In addition, they suggested that Kinect data were usable for clinical screening. However, the study lacks the day-to-day reliability test, which is not feasible

to perform due to the placement of the marker cannot be identical between days. Another study by the same author [53] aimed to validate Kinect V1 data with marker-based systems for gait retraining programs. During the study, real-time feedback of the lateral trunk angle was displayed to the participants. Both systems (marker-based and marker-less systems) recorded concurrently in order to assess the similarity and equivalence in the lateral trunk angle measurement. Their result showed good accuracy of Kinect data for gait retraining after the implementation of a simple calibration procedure. Yet, for more dexterous movements, the precision of Kinect is required more research. Fernández-Baena et al. [54] studied the precision of joint angles calculation of Kinect V1 marker-less sensor for a wide range of clinical rehabilitation treatments, including movements of the hip, knee, and shoulder in comparison with a marker-based system (as reference). They calculated the mean error and the range of motion and found that Kinect was very suitable for rehabilitation treatments, but its precision could be increased by putting length restriction on the bones provided by the Kinect algorithm. Inspired by the lower cost and the promising published results regarding Kinect accuracy Müller et al. [50] proposed a Kinect-based marker-less motion capture system for gait analysis. They validated the proposed system in terms of the accuracy of obtaining gait parameters, especially step width compared to a marker-based system. To decrease the self-occlusion while walking, the system consists of six Microsoft Kinect v2 sensors connecting to the main computer for control and monitoring. The sensors recorded synchronously by using Greyware's DomainTime II that allowed them to achieve a difference of two milliseconds between the internal clock of mini-computers hosting the sensors. The general finding of this study was that the multi-Kinect sensors system provided accurate results for gait analysis if the spatial-temporal calibration and sensors arrangement were bearing in mind. In the same context for solving the self-occlusion problem, other studies investigated the validity of using multiple Kinect sensors, especially for gait analysis [55]-[56]-[57]-[58]. Indeed, the multiple Kinect systems can cover different orientations, but the system accuracy would decrease if the sensors' placement is not carefully chosen, due to the interference of the infrared light of each sensor, which affects the posture recognition [25].

The research studies that have been accomplished so far regarding the validity and reliability of Microsoft Kinect sensor data were not confined to the gait analyses and rehabilitation. The validation studies extended to cover the usability of Kinect data in

ergonomic studies and workplace monitoring to prevent the associated injuries and to give early warnings. Diego-Mas and Alcaide-Marzal [25] proposed a computerized OWAS observational method based on Kinect measurement to evaluate the ergonomic risk factors in workplaces. The study protocol was chosen to cover many orientations of the sensor with respect to the participant during task performance. The input of the OWAS method was the joint angles calculated based on the vector dot product between segments projection into different planes. Three planes were defined sagittal, frontal, and trunk plane. The vector connected the R-hip, and L-hip position is normal to the sagittal plane. The frontal plane is parallel to the vertical axis and perpendicular to the sagittal plane. While the trunk passes through the spine-shoulder and hips position. The results were compared to the conventional OWAS observational method that depends on subjective visual observation. They found the best agreement when the participant faced the sensor. However, the study needed to be done over a larger population. Manghisi et al. [32] performed another fusion implementation of an observational method and Kinect data called (K2RULA). They automated the RULA method based on Kinect V2 for the purposes of wrong postures detection. The input of the RULA method was the joint angles calculated in the same way as in [25]; however, the definition of the planes was different. Two experiments were conducted to validate the system and the results compared to a marker-based system and to an expert observer. According to the proportion agreement index, they found a very strong agreement between K2RULA and the marker-based system and the expert observer. Yet, the evaluated tasks were simple according to static or dynamic tasks. In addition, the inter-participant repeatability was not checked. Haggag et al. [59] also used the Kinect V1 skeleton data to calculate RULA scores based on the joint angles and Voxel-based angle estimation. For prolonged sitting symptoms prevention, Paliyawan et al. [60] proposed a system to monitor the user and classify the position as stills or moves based on different classifiers (i.e., decision tree, neural network, and naive Bayes). The system provided feedback according to the risk score for prolonged sitting. The accuracy found to be 98% based on levels of health in ergonomics. However, the system was affected by the environment noise (i.e., participant's clothes and hair). Various studies have tried to improve the Kinect's performance, such as the jumpiness of the occluded joints. Martin et al. [61] proposed a system using Kinect skeleton data to evaluate the risk factors associated with lifting tasks in incorporation with OSHA ergonomic lifting model. The system embraced different iterations to process the streaming data from the

Kinect sensor. The first iteration was to use Kinect to calculate the user joint angles and insert it to the OSHA model. In the second iteration, they tried to improve the joint angles calculation accuracy by using multiple Kinects. However, synchronization was not achieved. The biggest problem was the occlusion; therefore, they used an additional Kinect sensor. The last iteration was to make the necessary changes to the system as a response to the problems in the second iteration and to the participants' feedback. The system was not able to recognize some objects that required assessing the lifting tasks; also, a real demonstration of the system is needed. Instead of using multiple Kinect sensors to solve the occlusion problem Plantard et al. [62] proposed a Kinect-RULA system that used a corrected Kinect skeleton data. According to Plantard et al. [45], the Kinect skeleton data can be optimized by creating an accurate database of the human poses that could be adopted by workers in a certain task. The database was created using a marker-based system with a couple of constraints such as (1) the database should consist of movements similar to those that would be conducted in real workplaces, and (2) it should contain many examples for a reasonable variability. Then, a pose reconstruction algorithm based on the Filtered Pose Graph method was implemented to find identical poses from the database. In contrast to the other Kinect-based observational methods systems such as [25], and [32], the joint angles were defined to be close to the ISB recommendation. For example, the trunk orientation was represented by the spine-shoulder, L-shoulder, and midpoint between spine-shoulder and spine-base. For the angles that could not be defined this way, they used the vectors dot product described in [43]. They validated the system in the lab using a marker-based system. Although the study in the lab was limited to simple movements, the overall performance of the system was improved using the corrected Kinect skeleton data.

Finally, the literature shows that most of the studies validated marker-less systems against marker-based systems using simple movements without any environmental occlusions as duplication of real manual material handling tasks. In addition, the sample size was small (n=1), as in [32].

2.1.3 Inertial measurement unit (IMU)

2.1.3.1 Frames

The motion capture systems have been divided into active and passive motion capture systems [51]. The active systems are directly attached to the human body to collect

spatial and temporal parameters (i.e., electromagnetic devices, mechanical devices, and accelerometers). Since they are intrusive and cumbersome, the motivation arose to come up with passive motion capture systems, such as marker-based and marker-less computer vision-based systems. However, with the rapid development in microchips and wireless technologies, the intrusiveness and cumbersomeness of the active systems regressed, and they have become more workable in non-controlled environments. The wearable IMUs, surface electromyography (EMG), and hand-held dynamometers are demonstrative examples of this huge development (Figure 7), due to their small size and wireless data transmission ability.

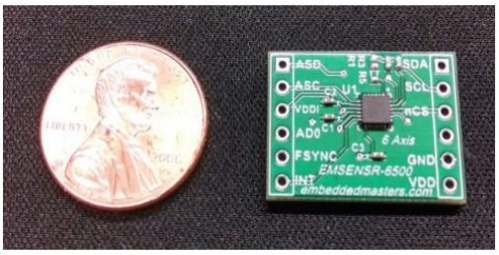

Figure 7. MPU-6500 6-axis Sensor Breakout Board (retrieved from https://variense.com/blog/difference-between-mems-and-imus/)

The IMU is a sensor module for measuring the kinematic parameters of a rigid body, such as the acceleration and angular velocity. IMU consists of an accelerometer, gyroscope, and magnetometer integrated inside a miniature chip. Since these sensors embrace the inertia principle, the term inertial explicitly appears [26]. Many companies manufacture IMUs, such as XSens (Netherlands) and Innalabs (Russia). An accelerometer is used to measure a rigid body's acceleration. Gyroscope is a sensor to measure a rigid body's angular velocity. A magnetometer measures the magnetic field [63]. However, the magnetometer is sensitive to the electromagnetic fields in workplaces [26]. As mentioned above, these sensors have been utilized in a few ergonomic studies that used automated risk factors evaluation methods instead of subjective visual observation methods [26]. Vignais et al. [29] proposed a real-time approach for assessing industrial tasks. They used seven wireless IMUs placed on the upper body segments to calculate the angles and goniometers for calculating wrist angles. The RULA method was used as an assessment method for the tasks based on the angles measured in a 20 degree-of-freedom (DOF) biomechanical model. The RULA scores displayed to the user through a head-mounted screen. They validated the

system using two groups of participants, the first group received auditory and visual feedback during task performance, and the other group did not receive such feedback. The results showed that the hazard associated with the tasks decreased among the group with the feedback. The system suffered from the magnetic field disturbances. In the same context, Peppoloni et al. [28] presented a novel wearable system for WMDs risk assessment consists of IMUs and surface EMG sensors for measuring the forearm's muscle efforts. A seven DOF model of the arm has been reconstructed. The model's angles and muscle strain were used as an input to two risk assessment indexes: RULA and the Strain Index (SI) [64] for a real-time ergonomic assessment. They validated their system in a simulated environment of the supermarket checkout position for assessing hazards associated with the handling material. For comparison, they compared the system's results to subjective observational inspection. The results of the proposed system proved to agree with the subjective observations. The system was limited to the arms motions only. Battini et al. [27] introduced a whole-body motion capturing system integrated with different WMDs risk assessment methods: the RULA, OWAS, OCRA [65], lift Index (LI), hands position, and hip movement tools. The authors developed the last two tools. They used 17 IMUs to rebuild 20 degrees of freedom biomechanical model. The assessment mentioned above tools processed the joint angles and data regarding the segment positions. The system was applied in two distributive places: fashion distribution center and supermarket warehouse. The system increased the productivity of the warehouses and alleviated the risk factors in the manual handling tasks. For comprehensive in-field ergonomic assessment, the system needs to integrate the EMG for muscle activities.

In addition to the systems that integrated IMUs technology with the observational methods, Yan et al. [66] proposed a standalone wearable IMUs system for preventing the WMDs risk factors related to the low back and neck positions. The system was composed of a smartphone that received the raw data from the wearable IMUs. The smartphone had an embedded application to alert the worker when an awkward posture was detected. The application sent a warning signal when the algorithm thresholds were surpassed. The proposed system was tested in the laboratory by mimicking the construction workers lifting and handling tasks. Also, for further validation, they applied the system on a real construction site. The system was proved feasible for WMDs factors prevention in the construction industry; however, the system worked for

a short period. Moreover, Ping Li et al. [67] introduced a smart safety helmet to detect head gestures and brain activities to prevent injuries. The smart safety helmet contained IMUs, EEG electrodes, and a haptic device. The IMUs were used to recognize the user's head gestures. The EEG electrodes recorded brain activities. While the haptic device was integrated to warn the user when the risk threshold is being surpassed. The study considered the probability of occurrence, the severity of the mishap, and exposure as risk factors. The interpretation of the collected data was made by the artificial intelligence algorithm, which received the raw data from the sensors and evaluated the risk factors of the workers. The results showed the ability of the system to find the relationship between the head movement and brain activities. However, the system was limited the head motion without any information about body movements and postures.

Finally, despite the great advantages of the IMUs (i.e., small size, occlusion-free), there have considerable shortcomings such as lack of reference and omitting the environment information, which important for hazard detection [68]. Therefore, the trade-off between the vision-based systems and wearable sensors for ergonomic studies relates to the tasks and the workplaces under study.

2.2 WMDs and Manual material handling tasks (MMH)

The MMH task is the task that workers manipulate objects using movements such as pulling, pushing, lifting, lowering, and carrying [69]. The U.S. Department of Labor defines the MMH as any working with the hand or hands, including seizing, holding, turning, and grasping. The fingers involving only conducting movements such as turn a switch. The MMH tasks are responsible for the majority of work time loss in workplaces, and 30% of accidents in the U.K. and U.S. were reported as MMH incidents [69]. Also, the major factors of WMDs come from MMH tasks (i.e., physical factors). Just in the U.S., about half a million WMD cases annually reported, including lower back, shoulders, and upper limb strain, are due to the MMH tasks [70]. Many endeavors to study the WMDs factors that related to MMH tasks. For example, Ciriello & Snook [69] conducted a comprehensive survey to summarize the features of MMH tasks that represent a wide base of the U.S. industry. The survey covered about 2,442 industries and reviewed MMH tasks, and analyses were performed over 13 years at the Liberty Mutual Research Center for Safety and Health. They concluded that most MMH tasks were not acceptable to a high percentage of the female group based on the psychophysical factors (i.e., heart rate, and muscle activity). Also, the load limit

recommended by the NIOSH in most of the MMH tasks was accessed, which means serious WMDs could occur. Dempsey [71] assessed 1,063 lifting and lowering tasks and summarized their parameters to provide a reference for the prevention of WMDs in workplaces. In 1983, Ciriello & Snook [72] studied the impact of the box size, lift distances, frequency, and push and pull heights among a group of male and female workers. The experiment was carried out using a psychophysiological methodology that gauged psychophysiological parameters such as heart rate and oxygen consumption. They found a significant contribution of those variables in defining the maximum limit for MMH tasks. Wahyudi et al. [73] have applied the Nordic Body Map (NBM) questionnaire [74] along with the OWSA method to determine physical WMDs factors (postural detection) in MMH tasks of a corn chip factory. The results showed the 51.6% of the MMH tasks had a high risk of WMDs, and immediate modification was required. Choobineh et al. [10] studied the existence of WMDs in industrial workshops by using the NBM questionnaire and Quick Exposure Checklist (QEC). Awkward postures, MMH, and standing for long hours were the most dominant factors contributed to WMDs among the workers. Based on the RULA method and a self-report questionnaire, Deros et al. [75] found that all MMH tasks in a production area had a high-risk level. In addition, Torres & Viña [76] reached the same conclusion using REBA and NIOSH methods. The hazard associated with MMH tasks is inevitable; however, well-advised workers selection, safety training in MMH, and re-designing the job to accommodate the worker can alleviate the occurrence of WMDs [77].

In conclusion, the MMH tasks are considered with great significance to the WMDs factors occurrence. Thus, more attention must be paid to the MMH tasks in workplaces by developing fast and easy-to-use ergonomic assessment methods to reduce the involving hazard.

2.3 Psychophysiological and physical risk assessment

There is a broad classification of the risk assessment methods according to the physical and psychophysiological risk factors. The physical and psychophysiological risk factors can be assessed based on any of the aforementioned WMDs risk factors assessment forms (i.e., self-report, observational methods, and direct measurement). The physical risk assessment deal with WMDs risk factors that include workers' posture, hazard in the workplace environment, muscle strain, and upper limb injuries. At the same time, the psychophysiological risk assessment deals with the evaluation of the exposure to

the risk of high heart rate, high blood pressure, high respiration rate, and high muscle activity.

Table 2. Psychophysiological and physical risk assessment methods

Psychophysiological risk assessment	Scope	Physical risk assessment	Scope
Electrodermal Measurement [78]	Mental strain and emotional strain in ergonomic studies	PLIBEL: A method to identify ergonomic hazards [79]	Musculoskeletal discomfort checklist
Electromyography (EMG) [80]	Muscles function	Musculoskeletal discomfort surveys used at NIOSH [81]	Lifting equation: weight limit
Estimating mental effort using heart rate and heart rate variability [82]	Mental effort	The Dutch Musculoskeletal Questionnaire (DMQ) [83]	Work-related musculoskeletal risk questionnaire
Ambulatory EEG methods and sleepiness [84]	Brain activity	Quick Exposure Checklist (QEC) [85]	Work-related musculoskeletal risk checklist
Assessing brain function and mental chronometry with event-related potentials (ERP) [86]	Brain function and mental chronometry	Rapid Upper Limb Assessment (RULA) [17]	Posture evaluation
Ambulatory assessment of blood pressure to evaluate workload [87]	Blood pressure	Rapid Entire Body Assessment [88]	Posture evaluation
Measurement of respiration in applied human factors and ergonomics research [89]	Respiration rate	The Strain Index [64]	Repetitive movement equation
		The Occupational Repetitive Action (OCRA) methods: OCRA Index and OCRA Checklist[65]	Repetitive movements evaluation checklist
		Posture checklist using Personal Digital Assistant (PDA) technology [90]	Posture evaluation checklist using a small computer

2.3.1 Rapid upper-limb assessment (RULA)

RULA is a physical risk assessment method based on the independent observation that can provide an evaluation of the WMDs risk factors focusing on the neck and upper limb. This method provides a single score that represents the posture, load, and movement risk. The score ranges from 1 (low risk) to 7 (high risk). The scores are classified into four risk indications (Table 3).

The RULA sheet (Figure 8) is used during the task observation. The sheet consists of three score tables and diagrams to illustrate the position of each body part position, accompanied by the required threshold.

2.3.1.1 RULA procedure

To use RULA for ergonomic analysis, three steps should be followed: (1) choose the postures to evaluate, (2) rate the selected posture, and (3) convert the scores to an action level.

Table 3. RULA action levels

1-2	Acceptable posture
3-4	Further investigation, change may be needed
5-6	Further investigation, change soon
7	Investigate and implement change

2.3.1.1.1 Choosing the postures to evaluate

RULA evaluation captures an instant in the work cycle. Therefore, it is essential to oversee the whole postures of the task or a period of task's cycle before selecting the posture to assess, in order to choose the most awkward posture or longest-held posture [17].

2.3.1.1.2 Rating the selected posture

According to the assessor, right, left, or both sides of the upper arms are required to be assessed. Using the RULA sheet diagrams (i.e., Group A and Group B), the posture of each body part is scored, along with the force and muscle use. The diagrams of Group A represent the position of the upper and lower arm and the wrist. The diagrams of Group B represent the positions of the neck, trunk, and legs.

2.3.1.1.3 Action level

Using tables A and B, each observation score can be obtained for the observation Groups A, and B, respectively. These tables assess the impact of the adopted posture so as to have a preliminary indication of the risk. In addition, the scores for the force and muscle use can be added to the initial posture score. The final action will be determined using table C (Figure 8).

2.3.1.2 Reliability and Validity

McAtamney and Corlett [17] have proposed and validated RULA in both industrial and office settings. They reported that RULA was found to be a useful evaluation tool in various packing operations, VDU-based tasks, garment-making operations, supermarket checkout operations, and operations in the car manufacturing industry. The validation test aimed to examine if the RULA assessment was able to provide a good indication of musculoskeletal onus during work. For checking the RULA reliability, 120 physiotherapists, industrial engineers, safety, and production engineers used it to evaluate packing, sewing, and brick sorting operations. The results showed a high agreement between the participants.

The advantages of RULA can be summarized as being quick and easy to use the assessment tool. RULA was reported to help demonstrate the musculoskeletal load during work. Also, it was useful in making fast decisions regarding the modifications that should be applied in the workplace. Furthermore, it was found to be practical in re-assessing the musculoskeletal load after the modifications.

Despite these advantages, the general disadvantage of all observational methods is bias due to subjective observations. A particular disadvantage of the RULA method is that the thresholds of most the movement are not defined, which means the door for the practitioners to speculate is open.

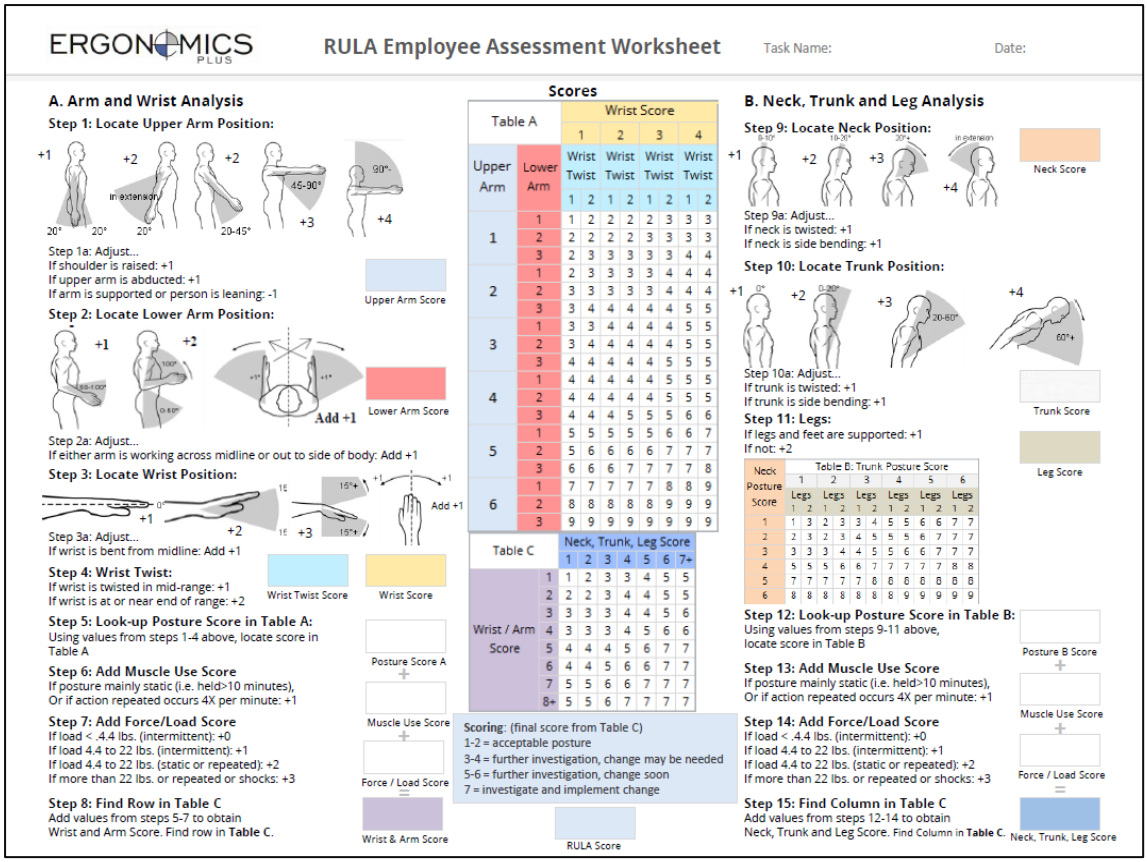

Figure 8. RULA score sheet (retrieved from https://ergo-plus.com/rula-assessment-tool-guide/).

2.3.2 Psychophysiological risk assessment

Many methods for measuring mental workload have been utilized in ergonomics coming from the medical field (Table 2). Brookhuis in [91] has attributed it to three reasons. First, the changes in the work nature from being physical (e.g., posture and force exertion) to being cognitive (e.g., brain activity). Second, a large percentage of accidents in workplaces is due to the victims themselves. Third, he related most of the workplace accidents to inadequate data processing that comes from mental overload.

Mental overload and underload are reflected in heart rate parameters. The vision parameters (i.e., lower awareness and lower attention) can be used to distinguish between high and low mental loads. In addition, work accidents and mental workload can be associated with blood pressure and muscle fatigue (e.g., measured by the electroencephalogram).

2.3.2.1 Electromyography (EMG)

EMG is a sensor to measure muscle activities using electrical signals generated during muscle contractions.

There is two way to measure the muscle activity by EMG electrodes either by inserting needle electrodes in the muscle or by placing surface electrodes on the skin over the muscle. The needle electrodes usually utilized in medical applications. Surface EMG electrodes are used in ergonomic because of their small size that allows measurement during motion.

In ergonomics, the EMG is used to measure the muscle load, local muscle strain due to overload, muscle timing, and coordination. In most ergonomic applications, EMG measures are accompanied by other measures such as body posture, external load, and joint angles for a comprehensive interpretation.

The advantages of EMG can be noticeable in its ability to measure continuous data with a high temporal resolution and sense the muscle fatigue in the early stage. Yet, there are some limitations to the EMG measures. For example, only muscles underneath the skin can be measured using surface EMG, there should not be too many fat tissues between the skin and muscles, and careful calibration, instrumentation design, and data interpretation are needed.

2.4 Summary

In this chapter, a review of the literature that is related to this thesis was presented. This review revealed that the observational methods are more accurate and reliable than self-report methods in order to prevent physical risk factors of WMDs. In addition, to increase the accuracy and reliability of observation methods, the literature suggested integrating them with direct measurements and video observations rather than human observations. However, few studies investigate the validity of using wearable technologies and marker-less sensors for objective assessment of physical risk factors of WMDs. To the best of our knowledge, no study investigated the agreement between ergonomic risk assessment using wearable technology and that using a marker-based motion capture system as a gold-standard motion measurement system for manual material handling task evaluation. Note that the deployment of the latter system in workplaces for real-time evaluation is cumbersome, expensive, and hardly feasible. On the other hand, the studies that investigated the usability of a

marker-less optical sensor for ergonomic risk assessment for manual material handling tasks did not evaluate complex tasks and object-occlusion environments. Therefore, evaluation of WMDs risk factors using wearable technology and marker-less optical sensors is still technically challenging, and their accuracy and reliability are unknown. A new reliable system for in-field ergonomic risk assessment with proven accuracy and reliability can have a significant impact on preventing physical risk factors of WMDs, and enable objective ergonomic workplace modifications.

Chapter 3

Chapter 3 provides the methodology that has been followed in this thesis. The chapter was divided into six subsections, participants statistics, experiment protocol, data collection, join angles calculation, RULA tool implementation, and data analysis.

3. Method

3.1 Participants

Eleven non-disabled male individuals, age of 26±5, height of 170±5 cm, and weight of 70±5 kg with no history of back pain, musculoskeletal, or neuromuscular injuries participated in the experiments. All participants had provided written consent before involved in the study. Research Ethics Board approval was received from the local ethics committee.

3.2 Experiment Protocol

The study participants conducted five scenarios for two manual material handling tasks. Each scenario lasted about 90 seconds. This included six repetitions of each of scenarios 1, 2, and 3 and three repetitions for each of scenarios 4 and 5. As such, the total experimental time was about 10 minutes for each participant (Figures 9 and 10). The scenarios 4 and 5 were performed without using any physical objects (i.e., tables) because the Kinect sensor was not able to capture the motion due to the occlusion problem. Also, the manipulated box was not used in this study to minimize occlusion problem associated with the marker-less system. The dimensions of the tables used in scenarios 1, 2, and 4 were obtained from the NIOSH lifting equation manual [92]. In Scenario 1 (Packing), the participant simulated twisting 90° to pick up an object from the initial position (table 1: height of 30 inches) and place it over the final destination (table 2: height of 24 inches) without any significant control of the object. While in scenario 2 (Loading), the participant was required to bend and twist 45° to pick up an object from a cart (position 1: height of 15 inches) and put it on (table 2: height of 36 inches). Scenario 4 (Package inspection) involved symmetric movement in which the participant bent in the sagittal plane to 22 inches (height) (table 1: height of 22 inches) to pick up a box and placed it on (table 2: height of 59 inches) at head height. The scenarios associated with task 2 were i) picking an object from the ground and place it on the table with a height of 36 inches (scenario 3 [93]), and ii) reaching an object from

a position above the head (height of 75 inches) (scenario 5). In all tasks' scenarios, the participants were not allowed to move the feet on the ground.

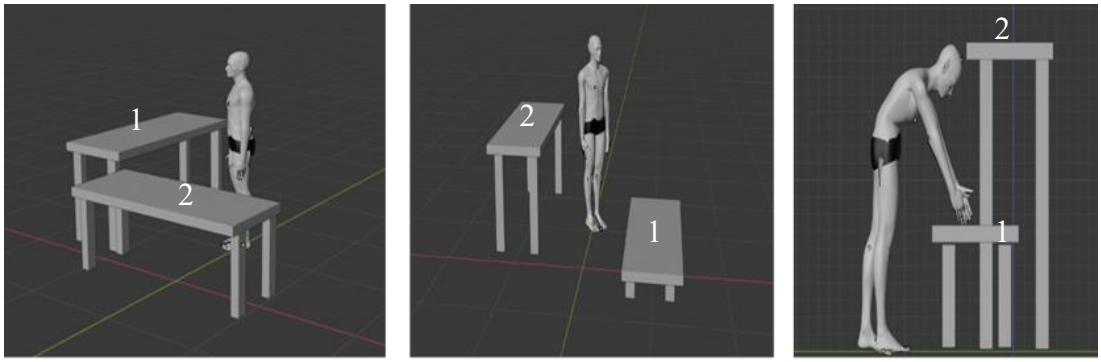

Figure 9. Task 1 consists from three scenarios (a) Scenario 1, (b) Scenario 2, and (c) Scenario 4.

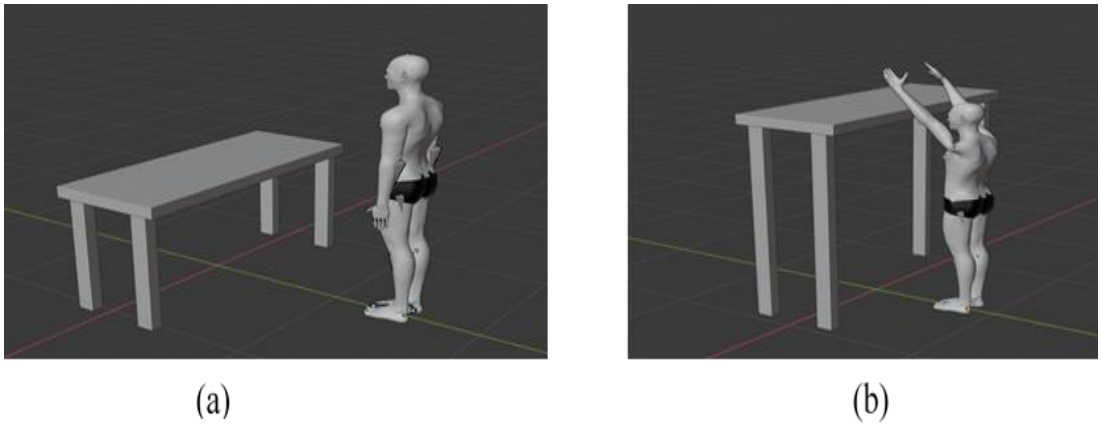

Figure 10. Task 2 consists of (a) Scenario 3, and (b) Scenario 5.

3.3 Data collection

Twenty-seven reflective markers (10 mm diameter) were mounted on the anatomical landmarks of each participant's body (Figure 2), representing a fifteen-segment marker-based model of the body. Eight motion capture cameras (Vicon, Oxford, UK) recorded the trajectory of the markers at a sampling rate of 100 Hz. Synchronously with the motion cameras, seventeen IMUs (Xsens, Netherlands) along with (Microsoft Kinect

V2, USA) was used to record the motion of the participant at a sampling frequency of 60, and 30 Hz respectively. Each IMU included a tri-axial accelerometer (range: ±16 g), a tri-axial gyroscope (range: ±2000 deg/s), and a tri-axial magnetometer (range: ±1.9 Gauss) and was attached to body segments using double-sided medical tape. The Kinect Sensor was placed in front of the participant three meters away and 0.69 meters high as recommended by Microsoft. Due to the irregularity in the Kinect sampling frequency (i.e., fluctuated between 30 and 29 Hz), offline spline interpolation was utilized to maintain a regular sampling frequency. Also, both Kinect and IMUs sampling frequency were resampled to attain identical sampling frequency with Vicon cameras at 100 Hz.

Customized software was created to acquire Kinect data and to synchronize data collection of Kinect, IMUs, and Vicon cameras. In this regard, Open source Adafruit Metro Mini 328 (Arduino-Compatible - 5V 16MHz mini) chip was used to send a 5-volt signal from a laptop to trigger the process (Figure 11), see section 3.3.2 for more details).

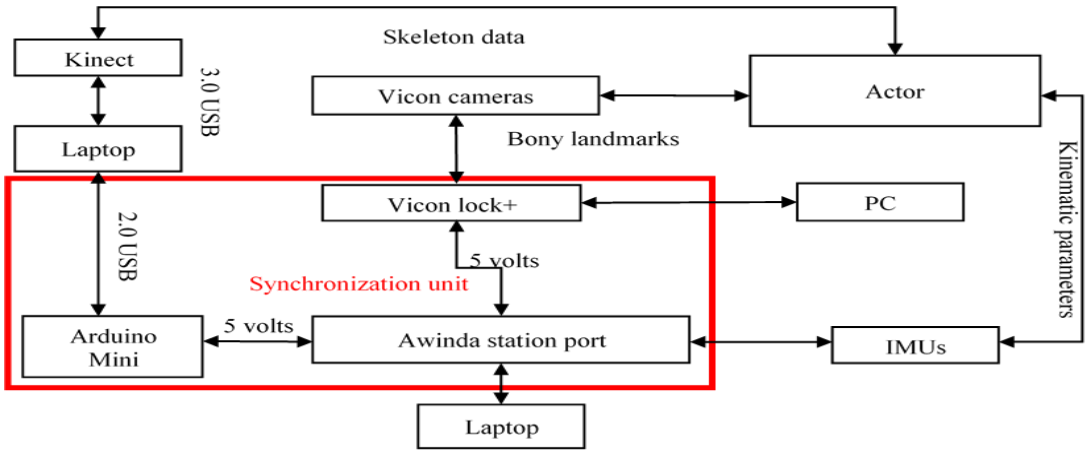

Figure 11. Data collection diagram. The synchronization unit consists of Arduino Mini board (connected the Kinect), IMU-based system synchronization port (Awinda station), and marker-based system synchronization device (Vicon lock+)

3.3.1 Marker-based Kinematic model (reference)

In order to achieve three identical kinematic models, the IMU-based model and marker-based model were reconstructed to be close to the Kinect model in terms of

joints number and position. The reflective markers were placed over the bony landmarks to obtain the location of the body segments center, as shown in Table 4.

As it is known, the hip joint center cannot be determined easily since it is not a palpable bony landmark. Therefore, many studies have proposed a virtual hip joint center using regression estimation [94]. The method presented in [94] was used to find the hip joint center position in the pelvis LCS. For this purpose, markers were placed on the anterior superior iliac spines (ASIS), Posterior superior iliac spines (PSIS), and Femoral Lateral Epicondyle bony landmarks (Figure 12).

Table 4. Bony landmarks for reflective markers positioning, and segment's origin.

Body part	Anatomical landmarks	Segment origin
Head	Right Auricularis (RA), and left Auricularis (LA)	Midpoint of RA and LA
Neck	C7	C7
Left shoulder	Left Acromion (LA)	LA
Right shoulder	Right Acromion (RA)	RA
Left elbow	Left Lateral Humeral Epicondyle (LLHE), Left Medial Humeral Epicondyle (LMHE)	Midpoint of LLHE and LMHE
Right elbow	Right Lateral Humeral Epicondyle (LLHE), Right Medial Humeral Epicondyle (LMHE)	Midpoint of RLHE and RMHE
Left wrist	Left Radial Styloid (LRS), Left Ulnar Styloid (LUS)	Midpoint of LRS and LUS
Right wrist	Right Radial Styloid (RRS), Right Ulnar Styloid (RUS)	Midpoint of RRS and RUS
Left Knee	Left Femoral Lateral Epicondyle (LLE), Left Femoral Medial Epicondyle (LME)	Midpoint of LLE and LME
Right Knee	Right Femoral Lateral Epicondyle (RLE), Right Femoral Medial Epicondyle (RME)	Midpoint of RLE and RME
Left ankle	Left Lateral Malleolus (LLM), Left Medial Malleolus (LMM)	Midpoint of LLM and LMM
Right ankle	Right Lateral Malleolus (RLM), Right Medial Malleolus (RMM)	Midpoint of RLM and RMM

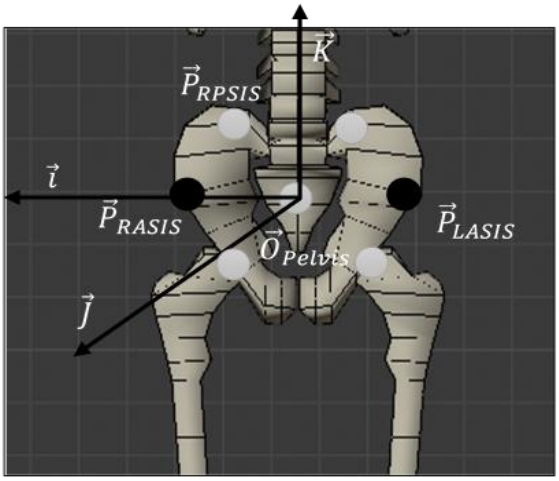

Figure 12. Anatomical landmarks for the origin and axes of Pelvis LCS.

The origin of the Pelvis LCS was calculated as the midpoint between RASIS and LASIS markers position.

$$\vec{O}_{pelvis} = 0.5(\vec{P}_{RASIS} + \vec{P}_{RASIS}) \quad \text{(Eq. 3.1)}$$

The x-axis ($\vec{\imath}$) of the Pelvis LCS was defined as the vector passes the Pelvis origin and RASIS position.

$$\vec{\imath} = \frac{\vec{P}_{RASIS} - \vec{O}_{pelvis}}{|\vec{P}_{RASIS} - \vec{O}_{pelvis}|} \quad \text{(Eq. 3.2)}$$

Then an auxiliary vector was created the midpoint between RPSIS and LPSIS locations to $\vec{O}_{pelvis}$.

$$\vec{v} = \frac{\vec{O}_{pelvis} - 0.5(\vec{P}_{RPSIS} + \vec{P}_{LPSIS})}{|\vec{O}_{pelvis} - 0.5(\vec{P}_{RPSIS} + \vec{P}_{LPSIS})|} \quad \text{(Eq. 3.3)}$$

Using the cross product, the y-axis and z-axis of the Pelvis LCS ($\vec{k}$ and $\vec{\jmath}$) were calculated based on the right-hand rule.

$$\vec{k} = \frac{\vec{\imath} \times \vec{v}}{|\vec{\imath} \times \vec{v}|} \quad \text{(Eq. 3.4)}$$

$$\vec{j} = \vec{k} \times \vec{\imath} \quad \text{(Eq. 3.5)}$$

The rotation matrix from Pelvis LCS to GCS was obtained as follows:

$$R_{Pelvis}^{GCS} = \begin{bmatrix} \vec{\imath}_X & \vec{\imath}_Y & \vec{\imath}_z \\ \vec{J}_X & \vec{J}_Y & \vec{J}_z \\ \vec{k}_X & \vec{k}_Y & \vec{k}_z \end{bmatrix}^T \quad \text{(Eq. 3.6)}$$

The position of the right hip joint center in the Pelvis LCS [94] is obtained using the following equation:

$$\vec{P}_{Rhip}^{Pelvis} = \begin{bmatrix} 0.36 * \left|\vec{P}_{RASIS} - \vec{P}_{LASIS}\right| \\ -0.19 * \left|\vec{P}_{RASIS} - \vec{P}_{LASIS}\right| \\ -0.30 * \left|\vec{P}_{RASIS} - \vec{P}_{LASIS}\right| \end{bmatrix} \quad \text{(Eq. 3.7)}$$

The position of the left hip joint center was obtained by multiplying the first row in $\vec{P}_{Rhip}^{Pelvis}$ by -1. In addition, to express the hip joint center in the GCS, Eq. 2.1 was applied as follows:

$$\vec{P}_{Rhip}^{GCS} = R_{Pelvis}^{GCS} * \vec{P}_{Rhip}^{Pelvis} + \vec{O}_{Pelvis}^{GCS} \quad \text{(Eq. 3.8)}$$

3.3.2 The kinematic model for the marker-less system

The Kinect Skeletal data were extracted using the official Microsoft software development kit (SDK) (Microsoft, USA). Skeletal data were attained from the dynamic link library (DLL) ‘‘Microsoft.Research.Kinect.dll’’ version 2.0.0.0 utilizing the .NET framework and customized software built in C# (Figure 13). The skeletal data were obtained by depth image processing algorithms that calculated the 3D positions of the human skeleton joints in the Kinect field of view. The algorithms are complex, and use matrix transforms and machine learning techniques.

Kinect V2 skeleton consists of twenty-five joints and exceeds that of Kinect V1 by five joints, as mentioned in Table 1. These joints are shown in (Figure 17). The first step in acquiring the Kinect skeletal data is to use either polling retrieval method or events

method (see M. Rahman [31] for more details). The latter was used in this study because it required a short code and is more common [95]. An event called *FrameArrived* is triggered whenever body data or (skeleton data in Kinect V1) are available to access from the *BodyFrame* Source of the *KinectSensor* class. Each frame of the *BodyFrame* Source creates a collection of *bodies* object up to six tracking bodies. Each *body* object has data that contain the body joints location. Each joint had a name (e.g., head, spin shoulder, and spine base) and a 3D vector. Secondly, the collected body joints are streamed and stored in a text file using the *StreamWriter* class for offline data analysis.

Right after conducting the standard laboratory coordinates calibration for the (Vicon MX with Nexus V1.5.2) system, the Microsoft Kinect coordinates were aligned with the laboratory coordinates by placing a plate with four reflected markers. These four markers were captured by both systems to reconstruct the plate orientation with respect to both systems coordinate system and plug them in (Eq. 3.9) to find the Kinect orientation with respect to the GCS (i.e., the laboratory coordinate system).

$$R_{CS_{Kinect}}^{GCS} = R_{plate}^{GCS} * {R_{plate}^{CS_{Kinect}}}^{T} \quad \text{(Eq. 3.9)}$$

where ${R_{plate}^{CS_{Kinect}}}^{T}$ and R_{plate}^{GCS} represent the plate rotation matrix in Kinect coordinate system and GCS, respectively.

Since Kinect was not able to recognize the reflected markers; therefore, the screws used to fix the markers on the plate were captured. As mentioned above, the Kinect depth image contains 3D information of the scene. Similar to the skeletal data, depth image used *FrameArrived* event to access the *DepthFrame* Source whenever the Kinect sensor is open. The depth image is available in 16-bit ushort values representing millimeter distances from the Kinect's coordinate system. In order to obtain the distance out of the depth image pixels, first, all pixels are stored in [512X424] array. Then by clicking over the targeted point in the Gray8 depth image the x and y coordinates of the targeted point are obtained and plugged in depth pixels array:

$$index = (x + y * 424) \quad \text{(Eq. 3.10)}$$

$$depthpixels = [index] \quad \text{(Eq. 3.11)}$$

Figure 13. Customized software to collect and visualize the marker-less system (Kinect V2). The software presents the colored image (on the left-hand side) and the depth image (on the right-hand side). The toolbar in the left shows the start and stop buttons, the sampling frequency, number of frames captured, and the Arduino board status. The horizontal box shows the position of any point in the images in (X, Y, Z) with respect to the Kinect coordination system. The four points in the image are the marker used to calibrate Kinect.

The "Microsoft.Research.Kinect.dll'' library contains the *coordinatemapper class that* includes the *MapDepthPointToCameraSpace* method. This method is used to perform another transformation to the values obtained from *depthpixels* array to spatial points (X, Y, Z) with respect to the Kinect coordinate system. Figure 14 depicts Kinect and marker-based models before and after the calibration of the Kinect coordinate system in the GCS.

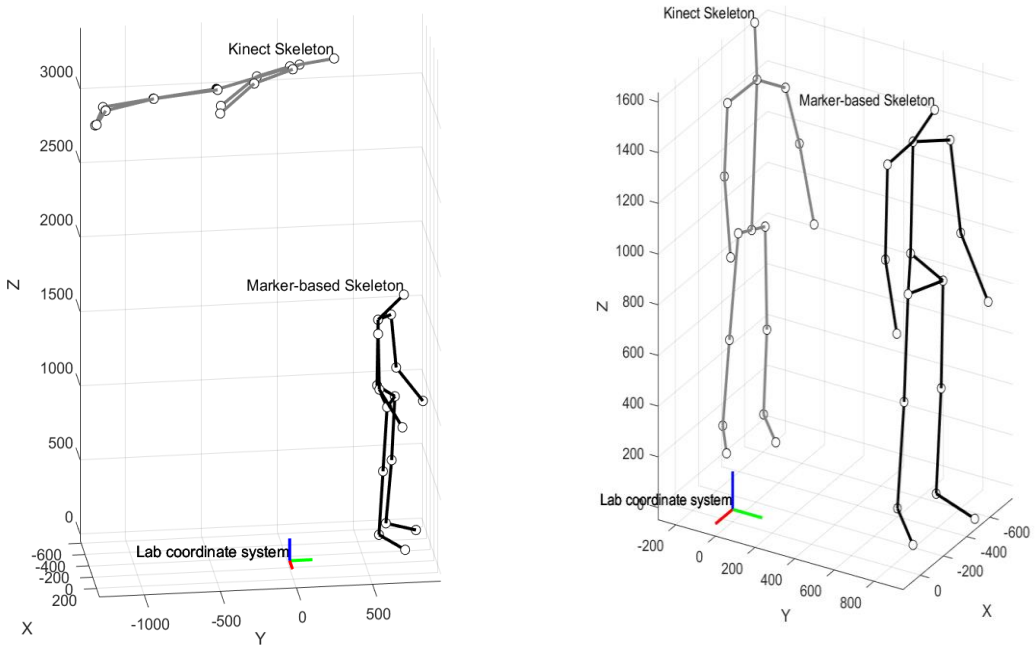

Figure 14. (a) Kinect and marker-based skeletons before calibration. (b) Kinect and marker-based skeletons after calibration. Both stick figures with respect to the lab coordinate system.

Using the depth image to capture the screws (on the back of the reflective markers' plate) from 2±0.5 meters was challenging. Therefore, the same method was used but with the color image, where the color image array size was [1920 x 1080], and the index changed to$(x + y * 1080)$. Also, instead of using the *MapDepthPointToCameraSpace* method, the *MapColorFrameToCameraSpace* method was used with the color image.

When the Kinect skeleton or body data are available, and a participant is detected, a method is called in the *KinectSensor* class to open a serial communication interface between Adafruit Metro Mini 328 and the laptop and send a 5-volt trigger signal through USB 2.0 cable. The trigger signal is received by the Xsens Awinda Station port to initiate the data collection of IMU-based and marker-based systems. In addition, when the motion tracking process is ended, another 5-volt signal is generated to stop the synchronization process.

3.3.3 IMU-based kinematic model

The *Xsens-MVN Analyze 2019* software package was utilized to create the IMU-based kinematic model. The MVN hardware is composed of the Xsens' IMUs and its wireless communication technology. Therefore, it is portable and not confined to the lab uses and can be used in workplaces or offices for ergonomic assessment. By using advanced data analysis algorithms, the MVN system provides various kinematic parameters of a 23-segment body model, such as segment orientation, angular velocity, and angular acceleration, and joint center position, velocity, and acceleration. The 3D joint angles of 22 joints are provided as well. Moreover, the magnetic field and the 3D acceleration data of 17 IMUs are available.

The system can view and record real-time tracking sessions. For offline data analysis and editing, data can be exported in various formats (e.g., BVH, C3D, FBX, and MVNX). The BVH extension contains data (joint angles only) in ASCII format that can be imported by different animation applications (e.g., Autodesk Motion Builder and Autodesk 3ds Max). The C3D extension has the bony landmarks of the body that can be used in motion capture systems. The FBX extension file consists of the segment center position and orientation of the 23 segments. This extension provides access to AutoCAD software. The last extension (MVNX) is the most useful one since all data are available in this extension from the segment position to the body center of mass. The MVNX file is readable be tremendous software programs (e.g., Matlab and Excel).

3.3.3.1 System calibration

After the body configuration is set (i.e., full body, lower body, or upper body tracking configuration), the scenario, body dimensions, and segment calibration were set in the following order. First, the system has different scenarios (Single-Level, Multi-Level, No-Level, and Soft-Floor) relying on the measurement type, and they define the measurement's accuracy and post-processing requirements. A Single-Level is selected when the participant walks on level terrain. A Multi-Level is selected when the participant climbs stairs. A No-Level scenario is selected when the participant is in a seated position. Finally, the Soft-Floor scenario is selected when the participant walks on grass or soft carpet. Second, the body dimensions entry consists of different anthropometric measurements such as body height, arm span, and ankle height, etc. These measurements are performed manually using a meter tape or other measurement

tools. For example, the body height is defined as the distance from the ground to the top of the head in the upright standing, more details about the body measurements are available in [96]. Finally, the segment calibration is conducted to align the IMU with the participant segments, which is important to be done with care and attention to have the best outcome. In the calibration, the participant is asked to stand in N-Pose for a few seconds, and then walk forward and back in the normal style. Before the calibration results are applied, the participant stands in N-Pose at the position from where the calibration starts to set the X-axis pointing forward and to define the coordinate system at the participant right heel.

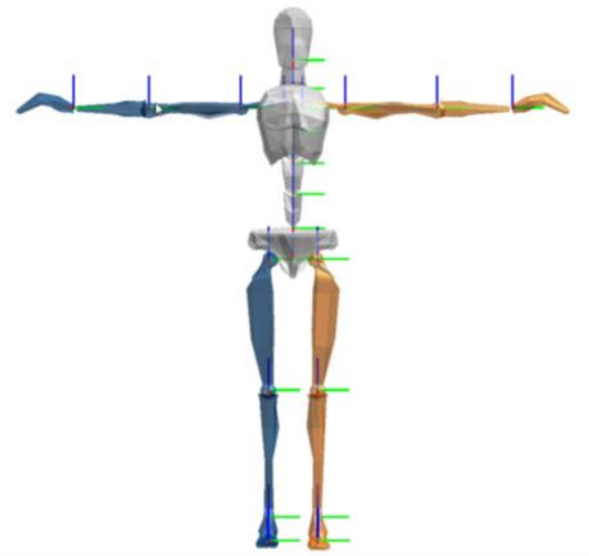

Figure 15. Xsens MVN model in T-Pose (adopted from [96].)

3.3.3.2 IMU-based model reconstruction

By using a Single-Level scenario and full-body configuration, the tracking sessions were performed, and the MVNX files were exported containing different kinematic parameters. Kinect parameters were also obtained simultaneously. Also, the positions of different anatomical landmarks positions were available with respect to the segment LCS. To get a similar model to both Kinect and marker-based models, these anatomical landmark positions were obtained with respect to GCS (of the MVN system) using the orientation and position of the segment in which the anatomical landmarks located. In Figure 3, the (X_g, Y_g, Z_g) coordinates represent the MVN system GCS, and the (X_l, Y_l, Z_l) coordinates represent the segment LCS and the vector $\vec{P}_a^l$ represent the anatomical

landmark position in the segment LCS. After obtaining all the required anatomical landmarks, the same definition as section 3.3.1 was applied to reconstruct the IMU-based model.

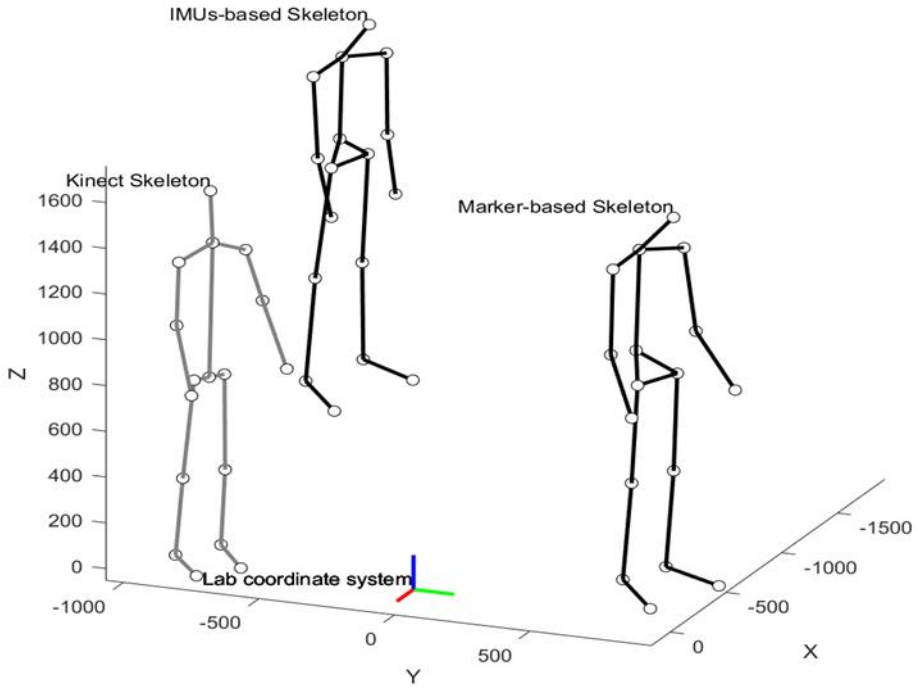

Figure 16. The three systems stick figures with respect to the lab coordinate system (GCS).

Similar to Kinect, the Xsens MVN system has its own coordinate system; therefore, to represent the IMU-based model in the GCS, all joints locations were multiplied by a rotation matrix. The rotation matrix was obtained using any of the 23 segment orientation provided by the Xsens MVN system and the marker-based system according to (Eq. 3.1) where R_{plate}^{GCS} is replaced with $R_{any\ segment}^{GCS}$ and $R_{plate}^{CS_{Kinect}}$ is replaced with$R_{any\ segemnt}^{CS_{MVN}}$.

3.4 Joint angles calculation

3.4.1 2D joint angles

The sagittal, frontal, and transverse planes of the body were defined to locate the segments' position required for the RULA assessment tool [32] (Figure 17). The sagittal plane was perpendicular to the line connecting right shoulder (4) and left shoulder (5) (Shoulder vector). The frontal plane was parallel to the Shoulder vector and passed through the Trunk vector, the line connecting the spine base (3) and spine shoulder (2). The transverse (horizontal) plane was the ground.

The neck flexion/extension angle, neck lateral bending angle, trunk flexion/extension angle, trunk lateral bending angle, and trunk rotation angle were calculated to obtain the neck and trunk scores in the RULA assessment tool. The neck flexion/extension angle was the angle between the projection of the line connecting head and spine shoulder points (1 and 2) (Neck vector) in the sagittal plane and the projection of the Trunk vector in the same plane. The neck lateral bending was the angle between the Neck vector and the Shoulder vector [32]. The trunk flexion/extension was defined by the angle measured between the Trunk vector and the vertical direction [32]. The trunk lateral bending angle was measured between the projections of the Shoulder vector and Hip vector in the frontal plane. Hip vector was defined as a vector passing through the right and left hips joint centers (10 and 11). The trunk rotation was defined as the angle between the projections of the Shoulder vector and the Hip vector in the transverse plane.

The upper arm flexion/extension angle, upper arm adduction/abduction angle, and elbow angle were calculated to obtain the upper limb score in the RULA assessment tool. The upper arm flexion/extension was the angle between the projections of the Trunk vector and the Upper-arm vector in the sagittal plane. The latter vector was defined as a vector directed from the shoulders (4 or 5) to the elbows (6 or 7). The upper arm adduction/abduction was the angle made between the projection of the Upper-arm vector in the frontal plane and the Trunk vector. The elbow angle was the angle between the Upper-arm vector and the Lower-arm vector that passes through the elbows (6 or 7) to the wrists (8 or 9). In addition, the position of the lower arm was evaluated using the angle between the Shoulder vector and the Lower-arm vector projected into the transverse plane.

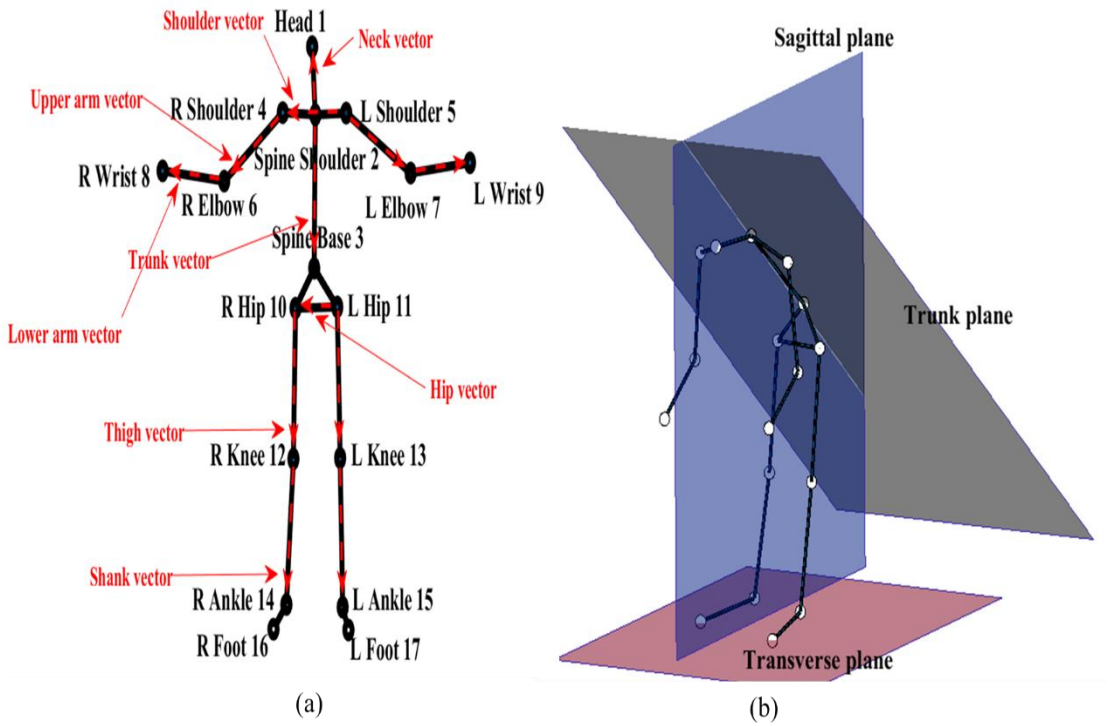

Figure 17. Illustration of (a) the joints center positions used in (2D joint angles calculation), and (b) Body planes. (b) Depicts the three anatomical planes used for 2D joint angles calculation: sagittal, frontal, and transverse planes.

The projection of a vector ($\vec{a}$) into a plane with normal vector ($\vec{n}$) and the angle (θ) between two vectors ($\vec{a}$) and ($\vec{b}$) were calculated as follows:

$$Proj_{plane}(\vec{a}) = \vec{a} - \frac{\vec{a}.\vec{n}}{\|\vec{n}\|^2}\vec{n} \qquad \text{(Eq. 3.12)}$$

$$\cos\theta = \frac{\vec{a}.\vec{b}}{\|\vec{a}.\|\|\vec{b}\|} \qquad \text{(Eq. 3.13)}$$

3.4.2 3D joint angles

To evaluate the impact of joint angles definition on the RULA scores calculation, 3D joint angles were obtained based on the Cardan angle convention in addition to the

angles obtained between the projected vectors. In order to calculate 3D joint angles, a segmental biomechanical model was used in this study. This model (hereafter referred to as 3D model) was based on anatomical landmarks as in the ISB recommendations [97]-[98]. For head and trunk segments we were not able to follow the ISB recommendations, because the head segment, was not defined by the ISB recommendations, and the T8, needed for trunk segment definition was missed in most of the trials. Therefore, the midpoint between C7 and Incisura Jugularis (IJ) and right and left Auricularis anatomical landmarks were used to identify the head segment. Also, C7, IJ, and Processus Xiphoideus (PX) were used to define the trunk segment. Moreover, the hip joint center of rotation was calculated as in section 3.3.1. Anatomical coordinate systems were built according to the same ISB recommendations.

3.5 RULA score implementation

After calculating the joint angles during each scenario, the RULA score was calculated, RULA parameters were set as in Table 5. The RULA score for each scenario was calculated for each frame. For those angles (in the RULA sheet adjustments), that have no defined thresholds, 20° was set as in [62].

Table 5. Shows the RULA segment position and its corresponded joint angle

RULA segment position	Joint angle
Upper arm position	Upper arm flexion/extension
	Upper arm adduction/abduction
	Shoulder adduction/abduction*
Lower arm position	Elbow flexion/extension
	Upper arm rotation
Wrist position	Set manually
Neck position	Neck flexion/extension
	Neck lateral bending
Trunk position	Trunk flexion/extension
	Trunk adduction/abduction
	Trunk rotation
Muscle and Force	Set manually

*This angle was used in both 2D and 3D calculations.

3.6 Data analysis

Data from all systems were filtered using a 3rd-order one-dimensional median filter. The measurement reliability of all trials for the Microsoft Kinect, IMU-based system, and the marker-based system was quantified using the intra-class correlation coefficient ($ICC_{2,1}$). The $ICC_{2,1}$ coefficients were calculated in a 2-way analysis of variance based on the absolute agreement as in [52]. The raters' agreement was identified by calculating the proportion agreement index and Cohen's Kappa coefficient as in [32]. The variation of RMSE was tested using a Multiple-sample test for equal variances (Bartlett test) at the significance level: 5%. The Kruskal-Wallis test used to test that if joint angles RMSEs come from the same distribution at a significance level of 5%. Also, a post-hoc multiple comparison test was used. A non-parametric statistical hypothesis test (Wilcoxon signed-rank test) was used to compare the right and left sides (significance level: 5%).

Chapter 4

This chapter provides the results obtained in this research. First, the results of the 3D joint angles for the IMU-based system, then the 2D joint angles of the same system, are presented. Finally, the results of the 2D joint angles of the marker-less system are presented.

4. Results

4.1 IMU-based system model

4.1.1 3D joint angles

The root mean square error (RMSE) of the joint angles (calculated using the method described in section 3.4.2) is provided for both body sides for scenarios 1, 4, and 5 between the IMU-based system model and marker-based system model (as reference) in Figures 18 to 20. In all scenarios, the median of RMSE was close to or below 10° for trunk and neck angles, except for neck flexion/extension in scenarios 1, 4 and 5 (16.4°, 20.4° and 24.6°, respectively), and trunk flexion/extension in scenario 5 (11.3°). The Bartlett test indicated that the null hypothesis of equal variances across the different joint angles is rejected at p-value < 0.05 for all scenarios. The Kruskal-Wallis test also rejected the null hypothesis for all scenarios. The post-hoc multiple comparison test indicated significant differences among the RMSE median of joint angles in all scenarios.

In scenario 1, we found that both right and left elbow adduction/abduction were significantly larger than other joint angles with RMSE medians of 27.9° and 25.1°, respectively. At the same time, the left knee rotation was significantly smaller than other joint angles (RMSE median of 0.5°) (Figure 18).

In scenario 4, both right elbow flexion/extension and elbow adduction/abduction were significantly larger than other joint angles with RMSE medians of 24.1° and 25.0°, respectively. Similar to scenario 1, both right and left knee rotation showed significantly smaller RMSE median compared to other joint angles with values of 1.9° and1.1°, respectively (Figure 19).

In scenario 5, the right elbow flexion/extension was significantly larger than other joint angles with an RMSE median of 26.6°. In contrast, the RMSE median of right and left

knee rotation angles were significantly smaller than other joint angles with values of 0.3˚ and 0.2˚, respectively (Figure 20).

In scenario 1, the right upper arm adduction/abduction and rotation angles had a significantly smaller RMSE median than the left side. In addition, the elbow flexion/extension and knee adduction/abduction angles showed a significantly smaller RMSE median on the left side than the right side (Figure 18). In scenario 4, elbow flexion/extension, elbow adduction/abduction, and knee rotation showed a significantly larger RMSE median on the right side than the left side. Whereas, the left elbow rotation and left upper arm adduction/abduction had a lager RMSE median (Figure 19). In scenario 5, the right elbow flexion/extension and right elbow adduction/abduction angles showed a significantly larger RMSE median than the left side. In contrast, the elbow rotation and upper arm adduction/abduction on the left side were significantly larger than the right side (Figure 20).

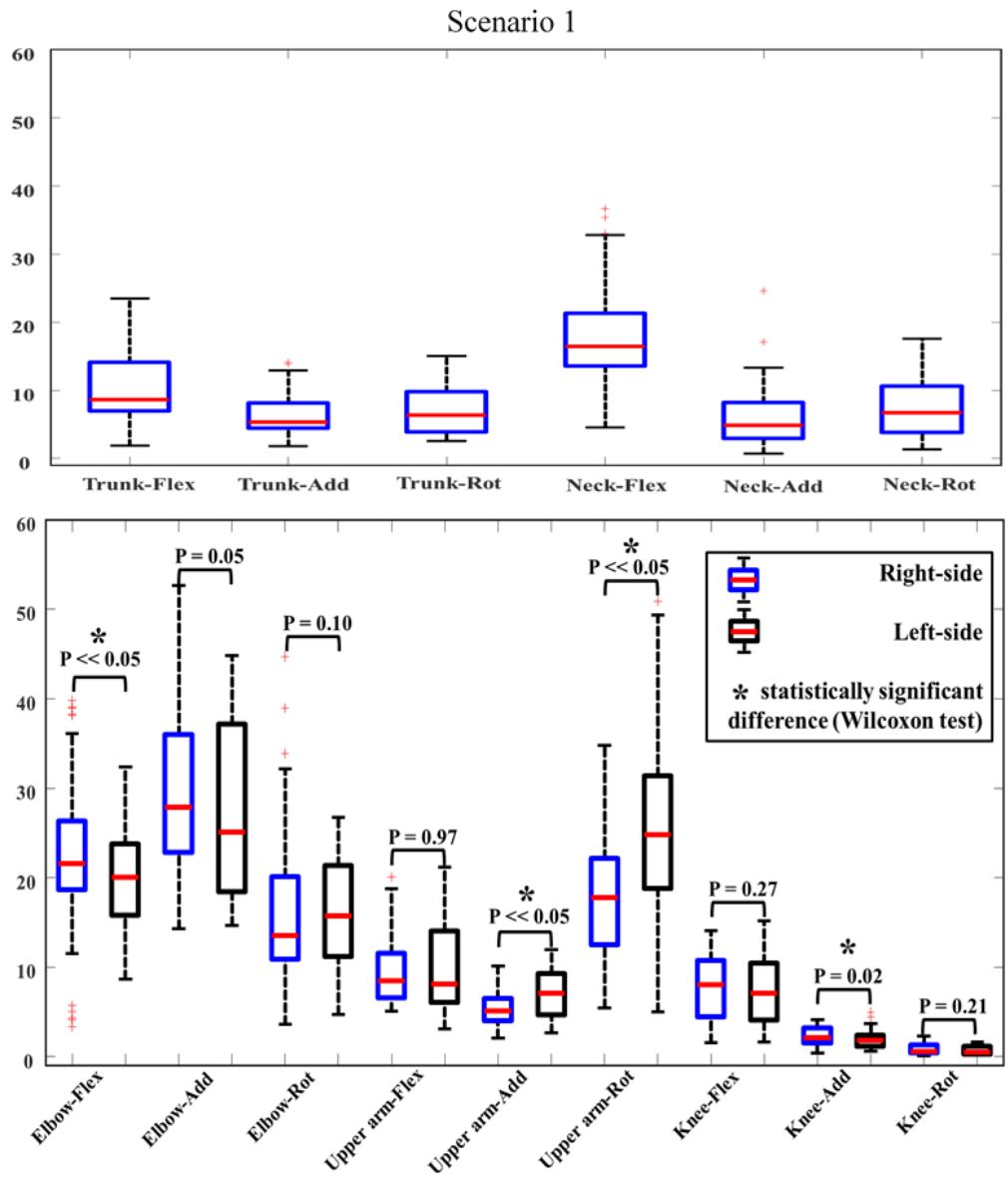

Figure 18. Scenario 1: RMSE of the joint angles (3D joint angles) obtained by the IMU-based system compared to those obtained by the marker-based system. The results are expressed in degrees, and each boxplot represents the data from the study participants.

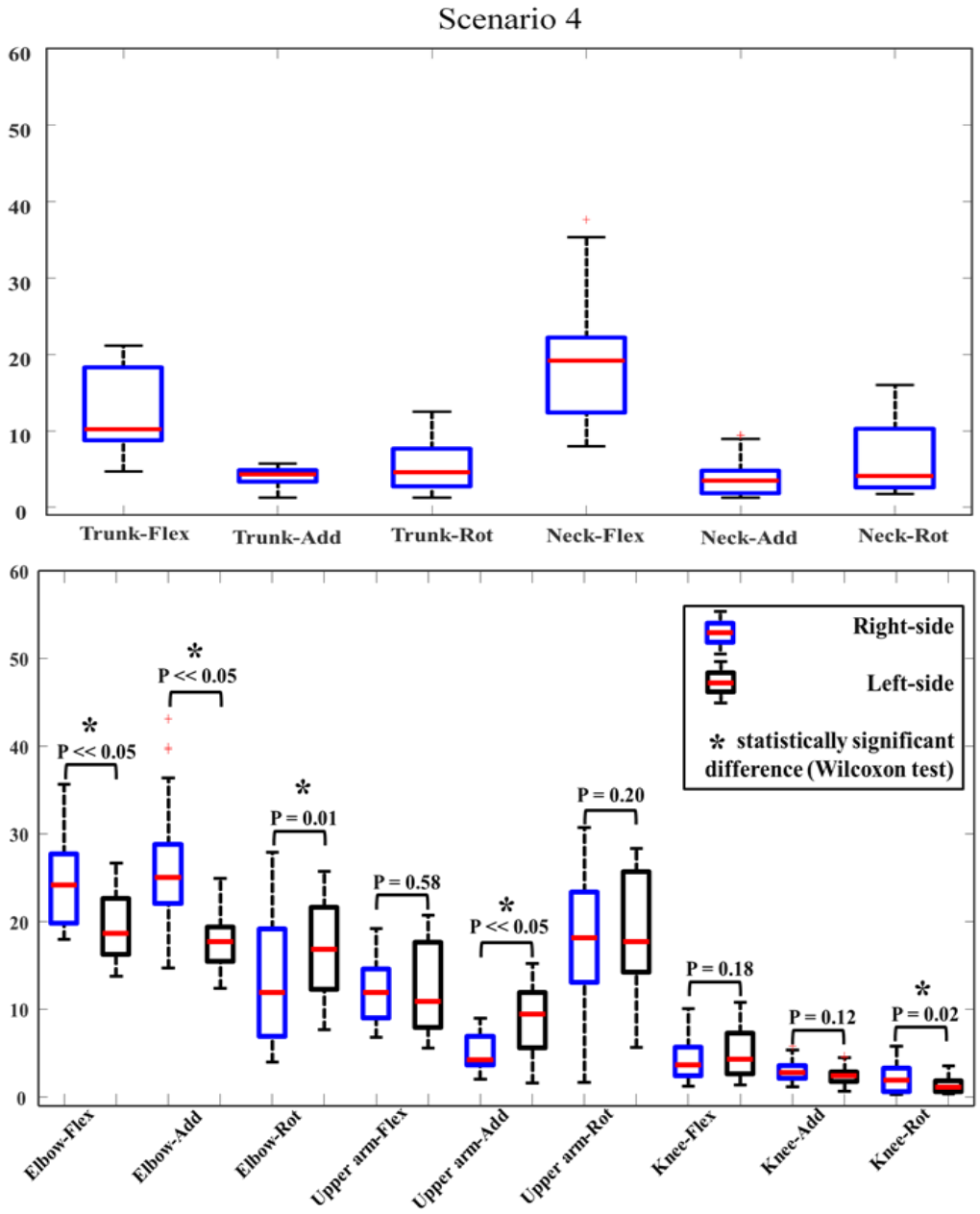

Figure 19. Scenario 4: RMSE of the joint angles (3D joint angles) obtained by the IMU-based system compared to those obtained by the marker-based system. The results are expressed in degrees, and each boxplot represents the data from the study participants.

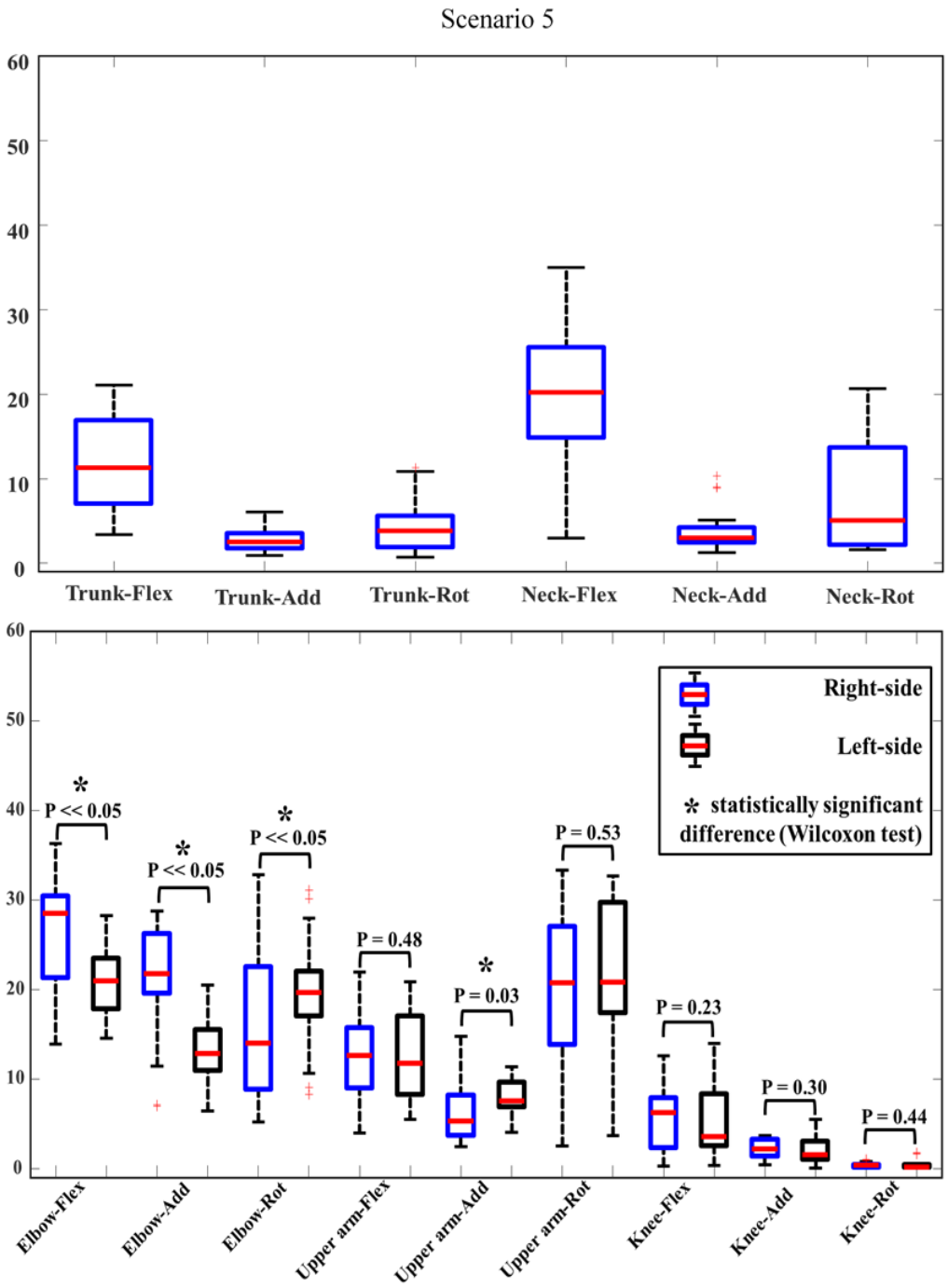

Figure 20. Scenario 5: RMSE of the joint angles (3D joint angles) obtained by the IMU-based system compared to those obtained by the marker-based system. The results are expressed in degrees, and each boxplot represents the data from the study participants.

Table 6. Proportion agreement index Po, linear weighted Cohen's kappa coefficient, and Z-test results for RULA scores obtained by the IMU-based model and Marker-based model using (3D joint angles). The results are presented in 50^{th} (25^{th}, 75^{th}) percentile among the participants.

	Body Side	P_o	Cohen's kappa	Agreement (Landis and Koch scale)	z (k/sqrt (var))	p value	Null hypothesis
Scenario 1	Right side	0.72(0.66,0.82)	0.41(0.28,0.58)	Moderate	14.2(7.8,21.2)	< 0.001	Rejected
	Left side	0.76(0.66, 0.81)	0.45(0.23,0.67)	Moderate	14.7(7.7,21.1)	< 0.001	Rejected
Scenario 4	Right side	0.82(0.80, 0.87)	0.55(0.53,0.69)	Moderate	20.4(18.0,29.3)	< 0.001	Rejected
	Left side	0.82(0.78,0.88)	0.55(0.49, 0.70)	Moderate	20.4(16.8 ,32.0)	< 0.001	Rejected
Scenario 5	Right side	0.89(0.71, 0.98)	0.63(0.25, 0.89)	Substantial	18.0(5.9,34.2)	< 0.001	Rejected
	Left side	0.80(0.68,0.95)	0.58(0.24,0.82)	Moderate	21.0(5.5, 32.8)	< 0.001	Rejected

The RULA scores obtained by both the IMU-based system and marker-based system were compared on a sample-to-sample basis using the proportion agreement index and Cohen's kappa coefficient (Table 6). According to the Landis and Koch scale [99], the results showed a "moderate" agreement between the two systems in all scenarios, except for the right body side in scenario 5 showed a "substantial" agreement. To show the significance of the results, the Z-test was used to test the null hypothesis whether the probability of the agreement between the two systems was accidental. This null hypothesis ($p < 0.05$) was rejected in all scenarios and for both right and left body sides. The results presented in Table 8 showed the ICC inter-participant agreement for each system. Using 3D joint angles calculation for RULA evaluation, both IMU-based and Marker-based systems showed an "excellent" agreement in the RULA scores median between participants for all scenarios, according to Cicchetti [100] guidelines for interpretation for ICC.

4.1.2 2D joint angles

Similarly, the RMSEs of the joint angles (calculated using the method described in section 3.4.1) between the IMU-based system model and marker-based system model (as reference) for both body sides for scenarios 1 to 5 are depicted in Figures 21 to 25. In all scenarios, the RMES median was below or close to 10° for trunk and neck angles. The Bartlett test indicated that the null hypothesis of equal variances across the different joint angles is rejected at p-value < 0.05 in all scenarios. The Kruskal-Wallis test rejected the null hypothesis for all scenarios. The post-hoc multiple comparison test indicated significant differences among the RMSE median of joint angles for all scenarios. In scenario 1, both elbow flexion/extension (right and left), and upper arm adduction/abduction (right and left) had an RMSE median significantly larger than other joint angles with values of (24.4° and 22.6°), and (16.3° and 22.6°), respectively. Also, the left upper arm flexion/extension was noticed having the smallest RMSE median (median: 3.2°) (Figure 21).

In scenario 2, the RMSE median of right and left elbow flexion/extension was significantly larger compared to other joint angles with medians of 24.9° and 23.1°, respectively. Also, the right knee flexion/extension was the smallest with an RMSE median of 3.2° (Figure 22).

In the same way, in scenario 3, the right and left elbow flexion/extension showed a significantly larger RMSE median compared to other angles (24.8° and 22.7°). Also, the

RMSE median of trunk adduction/abduction, and trunk rotation angles were significantly smaller than other joint angles with values of 2.0° and 2.4°, respectively (Figure 23).

In scenario 4, likewise, right and left elbow flexion/extension showed a significantly larger RMSE median compared to other angles (25.0° and 23.5°), respectively. Also, the RMSE median of trunk adduction/abduction, and trunk rotation angles were significantly smaller than other joint angles with medians of 2.6° and 3.1°, respectively (Figure 24). In addition, in scenario 5, right and left elbow flexion/extension had the largest RMSE median (24.3° and 23.2°) respectively, while the smallest RMSE median was noticed in the trunk adduction/abduction and trunk rotation with medians of 1.3° and 1.5°, respectively (Figure 25).

In scenario 1, the right elbow flexion/extension and right shoulder adduction/abduction were significantly larger RMSE median than the left side, while upper arm adduction/abduction and rotation angles showed a significantly smaller RMSE median in the right side than the left side (Figure 21). In scenario 2, the shoulder adduction/abduction and elbow flexion/extension showed a significantly larger RMSE median on the right side than the left side. Also, the knee flexion/extension and upper arm rotation had a significantly large RMSE median on the left side (Figure 22). In scenario 3, elbow, upper arm, and knee flexion/extension angles showed a significantly larger RMSE median in the right side than the left side, while in the shoulder adduction/abduction, the significantly larger RMSE median was in the left side (Figure 23). In scenario 4, the right elbow flexion/extension, and shoulder adduction/abduction angles showed a significantly larger RMSE median in the right side. Also, the upper arm rotation had a significantly larger RMSE median on the left side (Figure 24). In scenario 5, the elbow and upper arm flexion/extension on the right side had a significantly larger RMSE median than the left side, whereas the upper arm rotation angle RMSE median was significantly larger on the left side (Figure 25).

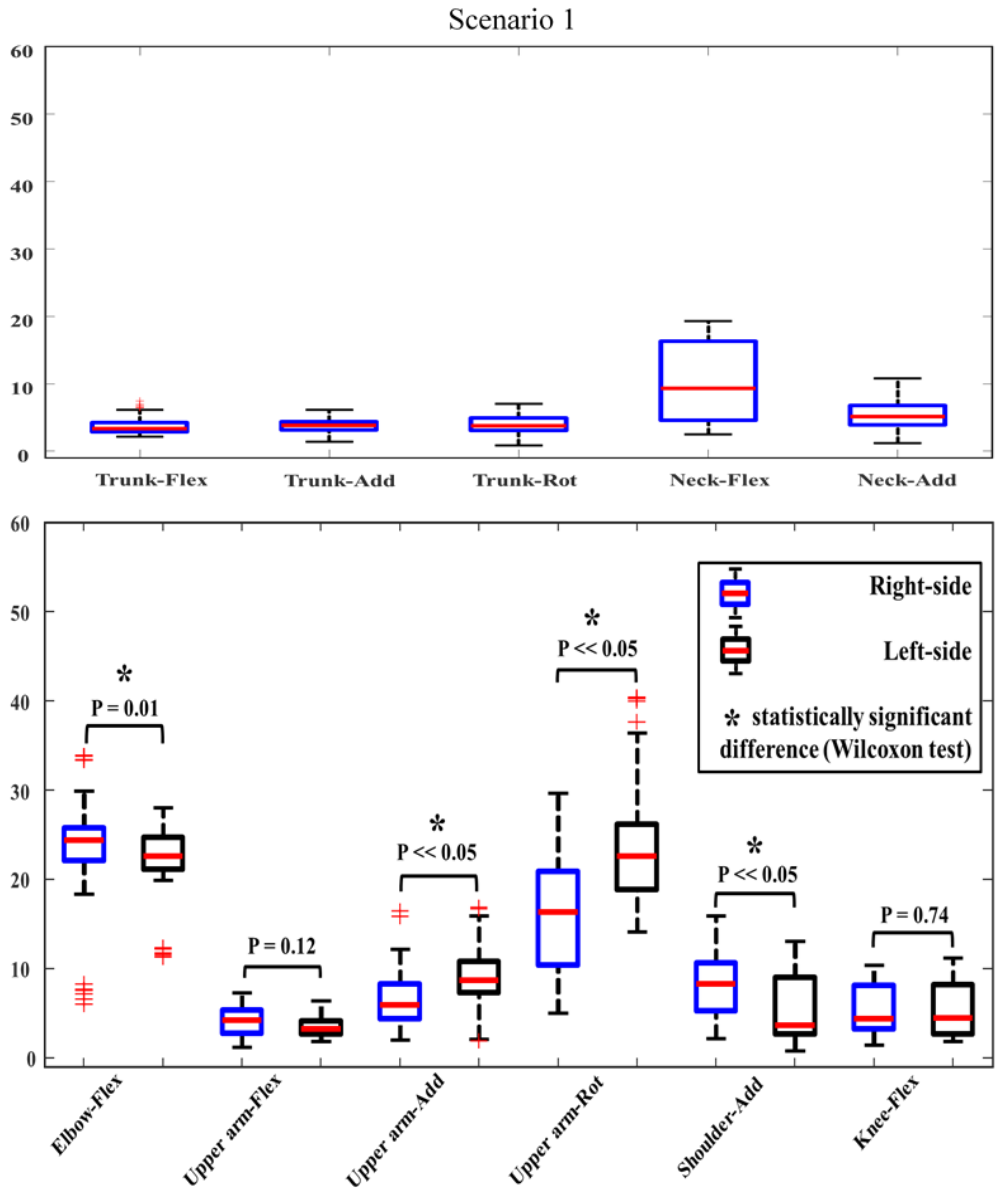

Figure 21. Scenario 1: RMSE of the joint angles (2D joint angles) obtained by the IMU-based system compared to those obtained by the marker-based system. The results are expressed in degrees, and each boxplot represents the data from the study participants.

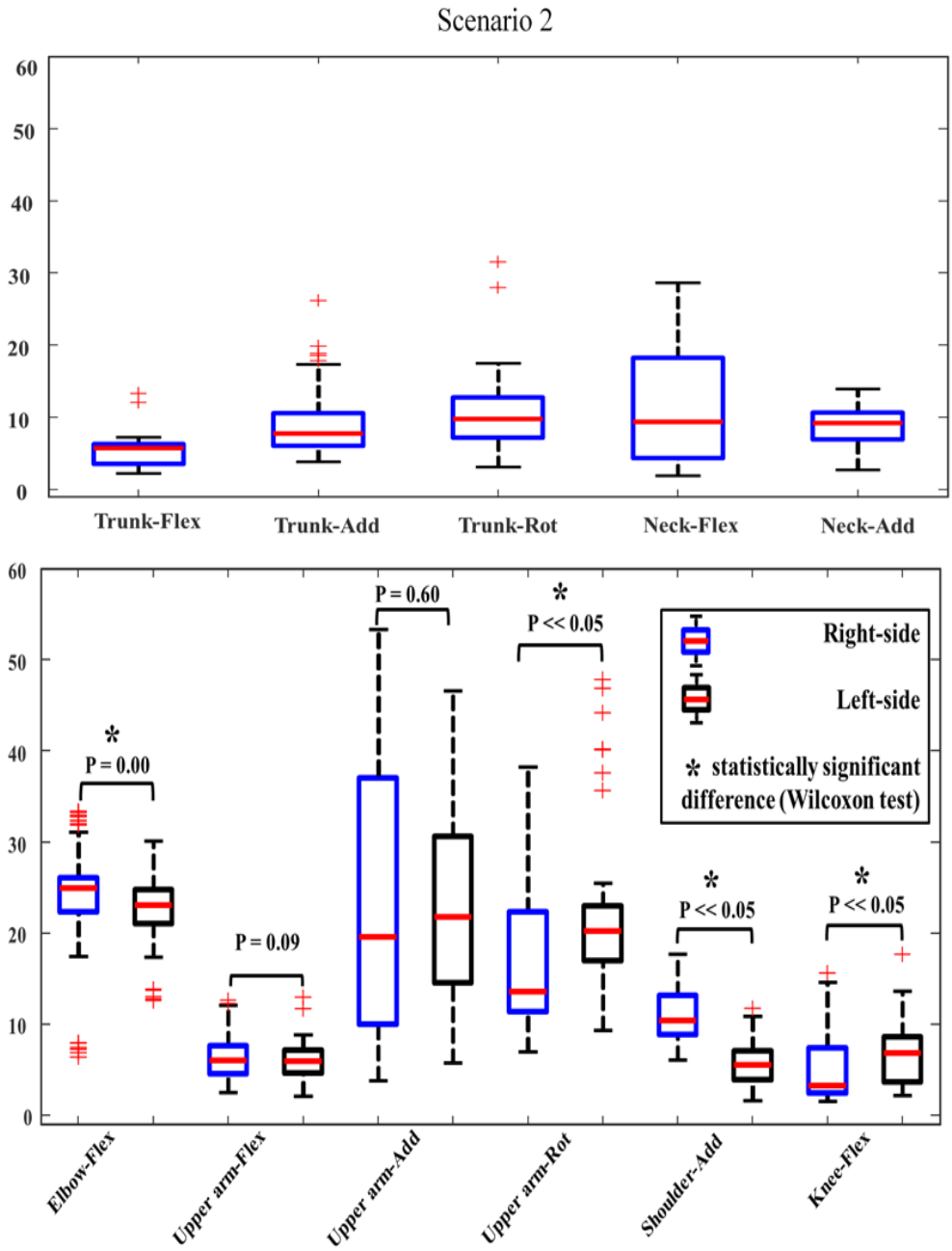

Figure 22. Scenario 2: RMSE of the joint angles (2D joint angles) obtained by the IMU-based system compared to those obtained by the marker-based system. The results are expressed in degrees, and each boxplot represents the data from the study participants.

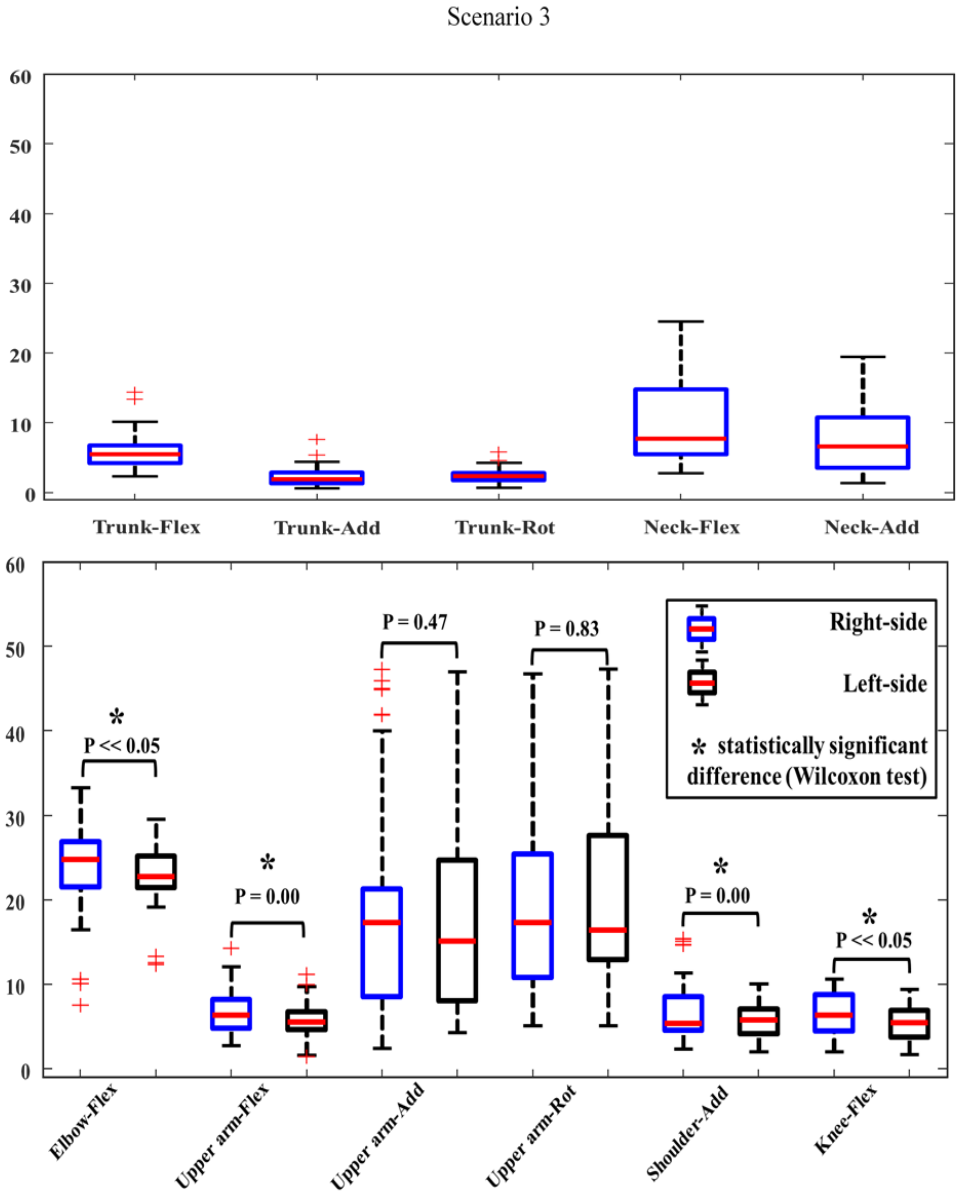

Figure 23. Scenario 3: RMSE of the joint angles (2D joint angles) obtained by the IMU-based system compared to those obtained by the marker-based system. The results are expressed in degrees and each boxplot represents the data from the study participants.

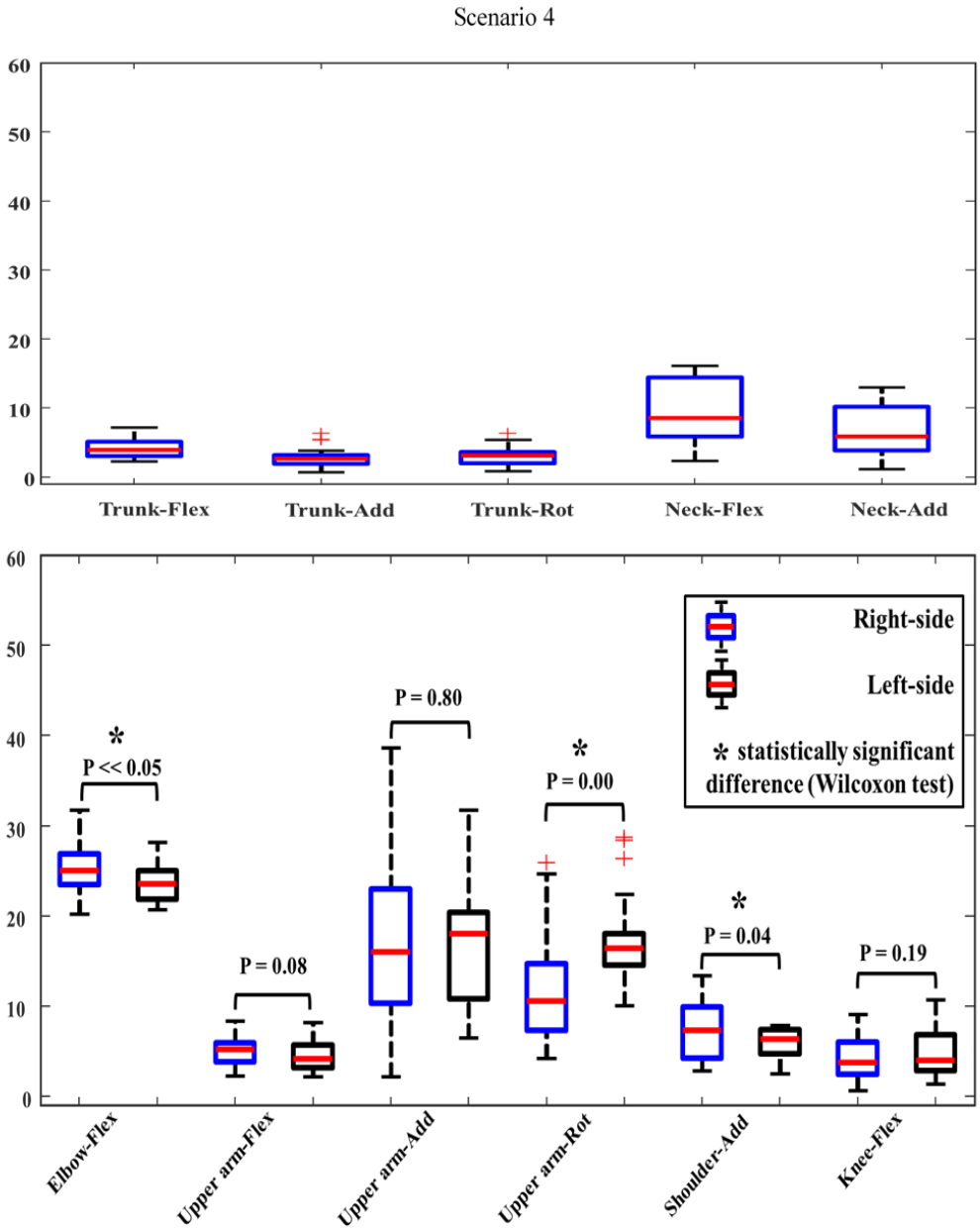

Figure 24. Scenario 4: RMSE of the joint angles (2D joint angles) obtained by the IMU-based system compared to those obtained by the marker-based system. The results are expressed in degrees, and each boxplot represents the data from the study participants.

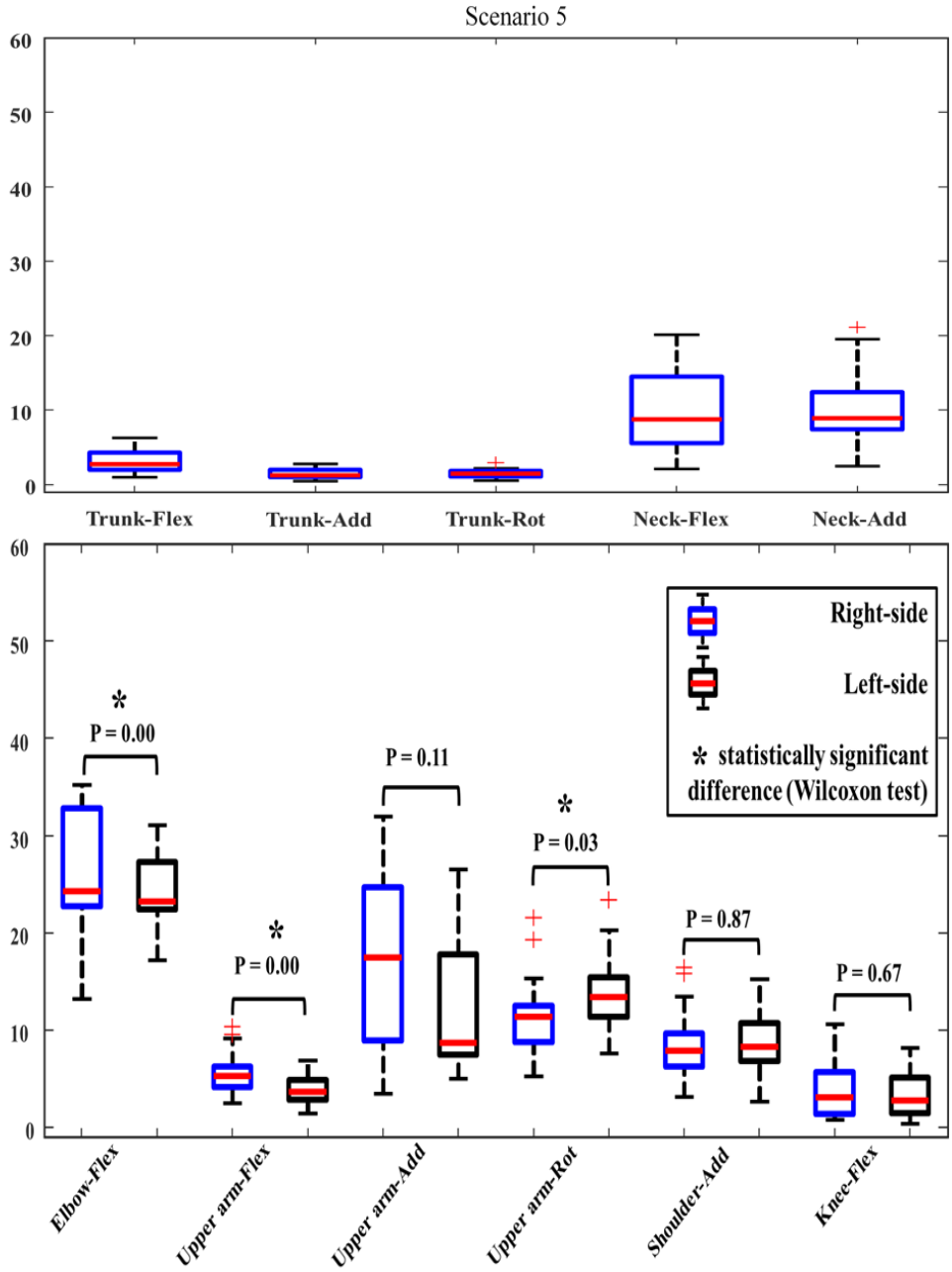

Figure 25. Scenario 5: RMSE of the joint angles (2D joint angles) obtained by the IMU-based system compared to those obtained by the marker-based system. The results are expressed in degrees and each boxplot represents the data from the study participants.

Table 7. Proportion agreement index Po, linear weighted Cohen's kappa coefficient, and Z-test results for RULA scores obtained by the IMU-based model and Marker-based model using (2D joint angles). The results are presented in 50^{th} (25^{th}, 75^{th}) percentile among the participants.

	Body Side	P_o	Cohen's kappa	Agreement (Landis and Koch scale)	z (k/sqrt (var))	p value	Null hypothesis
Scenario 1	Right side	0.89(0.84,0.98)	0.65 (0.55,0.93)	Substantial	26.8(18.8,39.0)	< 0.001	Rejected
	Left side	0.92(0.86, 0.99)	0.75(0.56,0.95)	Substantial	30.6(18.4,39.8)	< 0.001	Rejected
Scenario 2	Right side	0.89(0.82,0.92)	0.73 (0.59,0.82)	Substantial	32.9 (23.0,42.6)	< 0.001	Rejected
	Left side	0.85(0.80, 0.89)	0.66 (0.53,0.75)	Substantial	27.0(19.4,35.1)	< 0.001	Rejected
Scenario 3	Right side	0.88(0.83, 0.92)	0.67 (0.56,0.77)	Substantial	26.6 (19.6,34.3)	< 0.001	Rejected
	Left side	0.87(0.80, 0.92)	0.61(0.44,0.77)	Substantial	23.2(14.2,35.0)	< 0.001	Rejected
Scenario 4	Right side	0.89(0.79, 0.95)	0.65(0.40,0.85)	Substantial	25.7(12.0,36.9)	< 0.001	Rejected
	Left side	0.88(0.81,0.93)	0.64 (0.48, 0.80)	Substantial	24.6(13.6,36.1)	< 0.001	Rejected
Scenario 5	Right side	0.89(0.80, 0.99)	0.70(0.61, 0.98)	Substantial	27.7(17.2,38.2)	< 0.001	Rejected
	Left side	0.91(0.80,0.98)	0.66(0.58,0.94)	Substantial	23.1(17.1, 39.7)	< 0.001	Rejected

The RULA scores obtained by both the IMU-based system and marker-based system were compared on a sample-to-sample basis using the proportion agreement index and Cohen's kappa coefficient (Table 7). According to the Landis and Koch scale [99], the results showed a "substantial" agreement between the two systems in all scenarios. To show the significance of the results, the Z-test was used to test the null hypothesis whether the probability of the agreement between the two systems was accidental. This null hypothesis ($p < 0.05$) was rejected in all scenarios and for both right and left body sides. The results presented in Table 8 showed the ICC inter-participant agreement for each system. Using 2D joint angles calculation for RULA evaluation, the IMU-based showed an "excellent" agreement in the RULA scores median between participants for all scenarios except scenario 2 left side showed a "good" agreement. In contrast, the marker-based systems showed an "excellent" agreement in the RULA scores median between participants for all scenarios, according to Cicchetti [100] guidelines for interpretation for ICC.

Table 8. Intraclass correlation coefficient (ICC) (lower/upper bound of 95% confidence interval [CI] in parentheses) of RULA scores median scores of 5 manual handling scenarios for all participants.

	Body side	Marker-based system 2D	Marker-based system 3D	IMU-based system 2D	IMU-based system 3D	Kinect
		$ICC_{2,1}$ (95% CI)	$ICC_{2,1}$ (95% CI)	$ICC_{2,1}$ (95% CI)	$ICC_{2,1}$ (95% CI)	$ICC_{2,1}$ (95% CI)
Scenario 1	Right side	0.77(0.47,0.93)	0.88(0.72,0.97)	0.87(0.70,0.96)	0.82(0.55,0.95)	0.91(0.75,0.98)
	Left side	0.90(0.77,0.97)	0.92(0.81,0.98)	0.93(0.84,0.98)	0.89(0.75,0.97)	0.91(0.75,0.98)
Scenario 2	Right side	0.82(0.60,0.95)	NA	0.81(0.58,0.94)	NA	0.58(-0.1,0.89)
	Left side	0.85(0.66,0.95)	NA	0.70(0.30,0.91)	NA	0.58(-0.1,0.89)
Scenario 3	Right side	0.96(0.90,0.99)	NA	0.86(0.67,0.96)	NA	0.66(0.18,0.92)
	Left side	0.92(0.83,0.98)	NA	0.84(0.63,0.95)	NA	0.66(0.18,0.92)
Scenario 4	Right side	0.85(0.59,0.96)	0.81(0.43,0.95)	0.92(0.87,0.99)	0.91(0.72,0.98)	0.87(0.63,0.96)
	Left side	0.95(0.77,0.98)	0.86(0.56,0.96)	0.95(0.77,0.98)	0.82(0.48,0.95)	0.87(0.63,0.96)
Scenario 5	Right side	0.95(0.65,0.96)	0.89(0.64,0.97)	0.95(0.65,0.96)	0.90(0.69,0.98)	0.79(0.43,0.94)
	Left side	0.87(0.85,0.98)	0.86(0.57,0.97)	0.87(0.85,0.98)	0.94(0.83,0.99)	0.79(0.43,0.94)

$ICC_{2,1}$: Type 2,1 intraclass correlation coefficient; 95% CI: 95% confidence interval

Table 9. Intraclass correlation coefficient (ICC) interpretation based on Cicchetti (1994)

ICC coefficient	interpretation
Less than 0.40	poor
0.40 <ICC<0.59	fair
0.60<ICC<0.74	good
0.75<ICC<1.00	excellent

4.2 Marker-less system model

Figures 26 to 30 show the RMSEs median of the joint angles (calculated using the method describes in section 3.4.1) obtained by the marker-less system compared to those the marker-based model (as reference) for both body sides for all scenarios. On the contrary, to the IMU-based model, all scenarios had a median of RMSE above 10° for trunk and neck, except for trunk adduction/abduction and rotation angles in scenarios 3, 4, and 5. In addition, the RMSE median of trunk flexion/extension was below 10° in scenario 5. The Bartlett test indicated that the null hypothesis of equal variances across the different joint angles is rejected at p-value < 0.05 for all scenarios. The Kruskal-Wallis test rejected the null hypothesis for all scenarios. The post-hoc multiple comparison test indicated significant differences among the RMSE median of joint angles in all scenarios. In scenario 1, the RMSE median of neck flexion/extension was significantly larger than other joint angles with a median of 29.6°. At the same time, the RMSE median of left trunk adduction/abduction was significantly smaller than other joint angles (median: 7.0°) (Figure 26).

In scenario 2, the right and left upper arm adduction/abduction, and trunk adduction/abduction RMSE median were significantly larger compared to other joint angles with medians of 30.0° and 33.8° and 28.5°, respectively. The right and left shoulder adduction/abduction showed significantly smaller RMSE median compared to other joint angles with medians of 10.0° and 9.5°, respectively (Figure 27).

In scenario 3, the neck adduction/abduction, right and left upper arm adduction/abduction, and right and left knee flexion/extension were significantly larger than other joint angles with medians of 25.8°, (36.6° and 33.1°), and (25.4° and 25.6°) respectively. Also, the RMSE median of trunk adduction/abduction, and trunk rotation angles were significantly smaller than other joint angles with medians of 5.5° and 6.0°, respectively (Figure 28).

In scenario 4, the right and left upper arm adduction/abduction had a significantly larger RMSE median than other angles with medians of 38.1°, and 39.6° respectively, while the trunk adduction/abduction and trunk rotation showed significantly small RMSE medians, 2.7°, and 2.9°, respectively (Figure 29). In the last scenario (scenario 5), the largest RMSE was noticed in the right and left upper arm flexion/extension and adduction/abduction with medians of (28.7° and 29.6°), and (33.2° and 31.2°) respectively. Also, the trunk flexion/extension, adduction/abduction, and rotation had the smallest RMES median 3.1°, 1.9°, and 2.0°, respectively (Figure 30).

In scenario 1, the right upper arm adduction/abduction had a significantly smaller RMSE median than the left side, while the knee flexion/extension angle showed a significantly smaller RMSE median on the left side than the right side (Figure 26). In scenario 2, all upper arm joint angles, and knee flexion/extension showed a significantly larger RMSE median on the left side than the right side (Figure 27). In scenario 3, no significant difference was observed between the right and left sides (Figure 28). In scenario 4, the right upper arm flexion/extension angles showed a significantly smaller RMSE median than the left side (Figure 29). In scenario 5, the right side in the upper arm adduction/abduction was significantly larger than the left side (Figure 30).

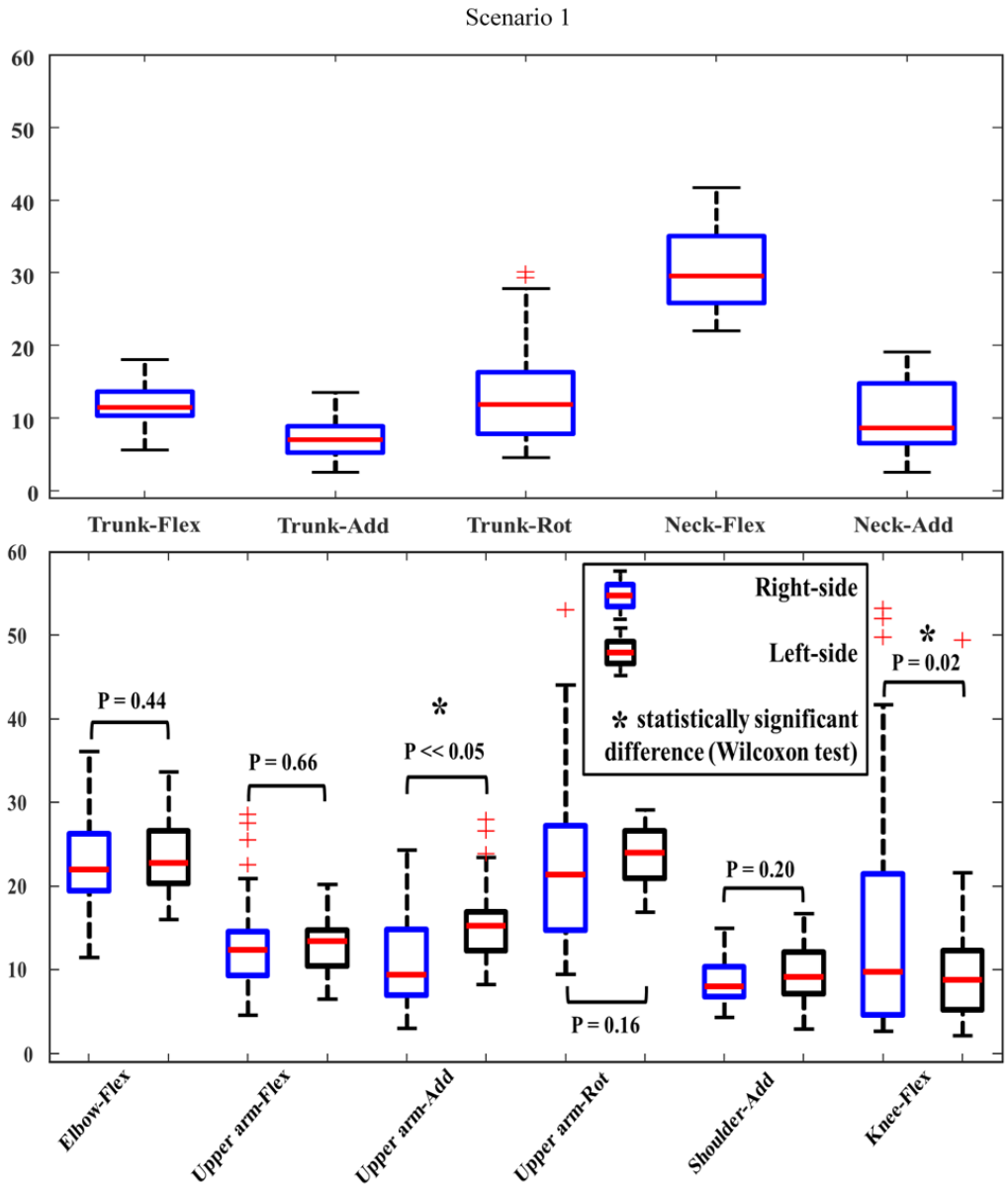

Figure 26. Scenario 1: RMSE of the joint angles (2D joint angles) obtained by marker-less system compared to those obtained by the marker-based system. The results are expressed in degrees and each boxplot represents the data from the study participants.

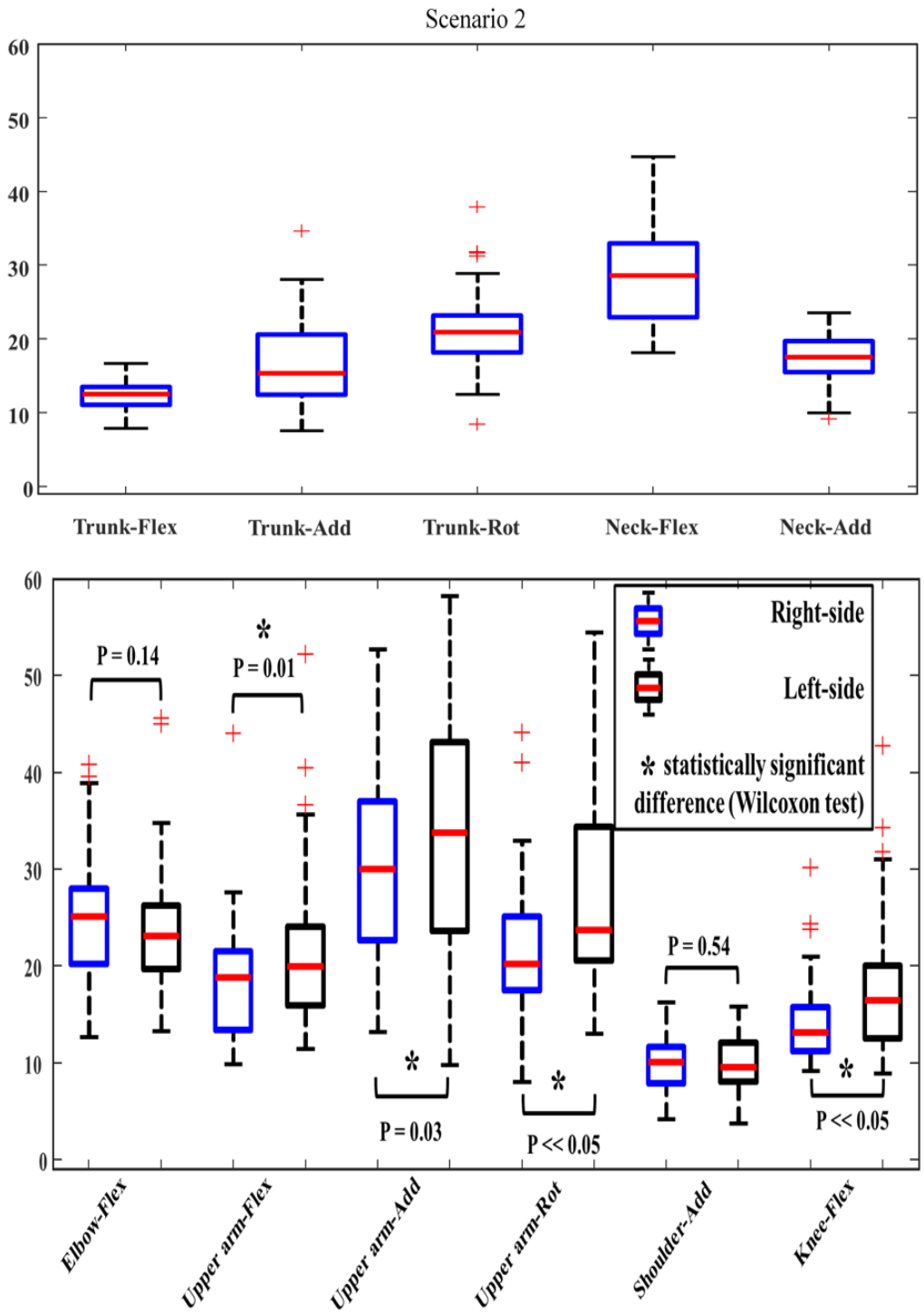

Figure 27. Scenario 2: RMSE of the joint angles (2D joint angles) obtained by the marker-less system compared to those obtained by the marker-based system. The results are expressed in degrees, and each boxplot represents the data from the study participants.

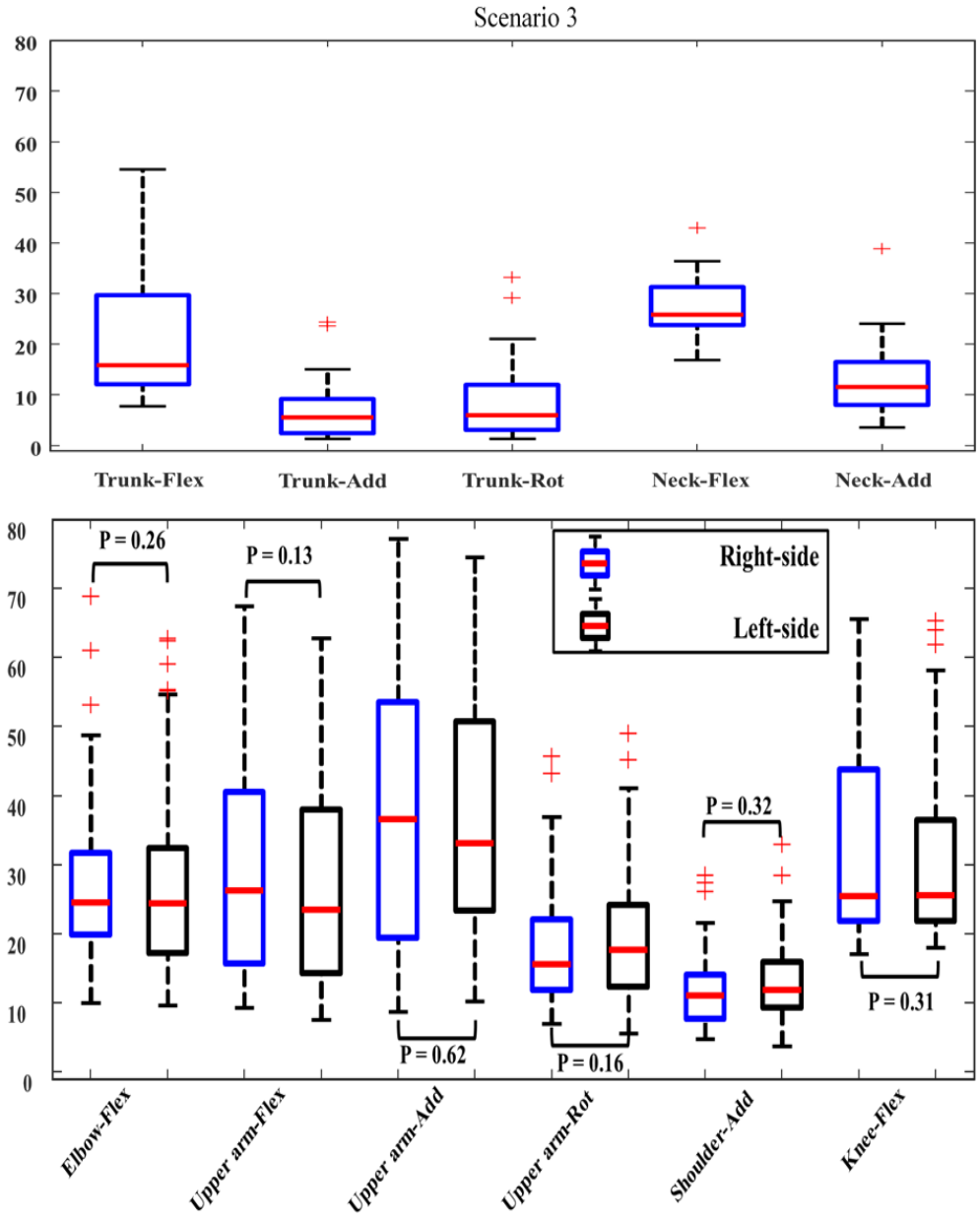

Figure 28. Scenario 3: RMSE of the joint angles (2D joint angles) obtained by marker-less system compared to those obtained by the marker-based system. The results are expressed in degrees and each boxplot represents the data from the study participants.

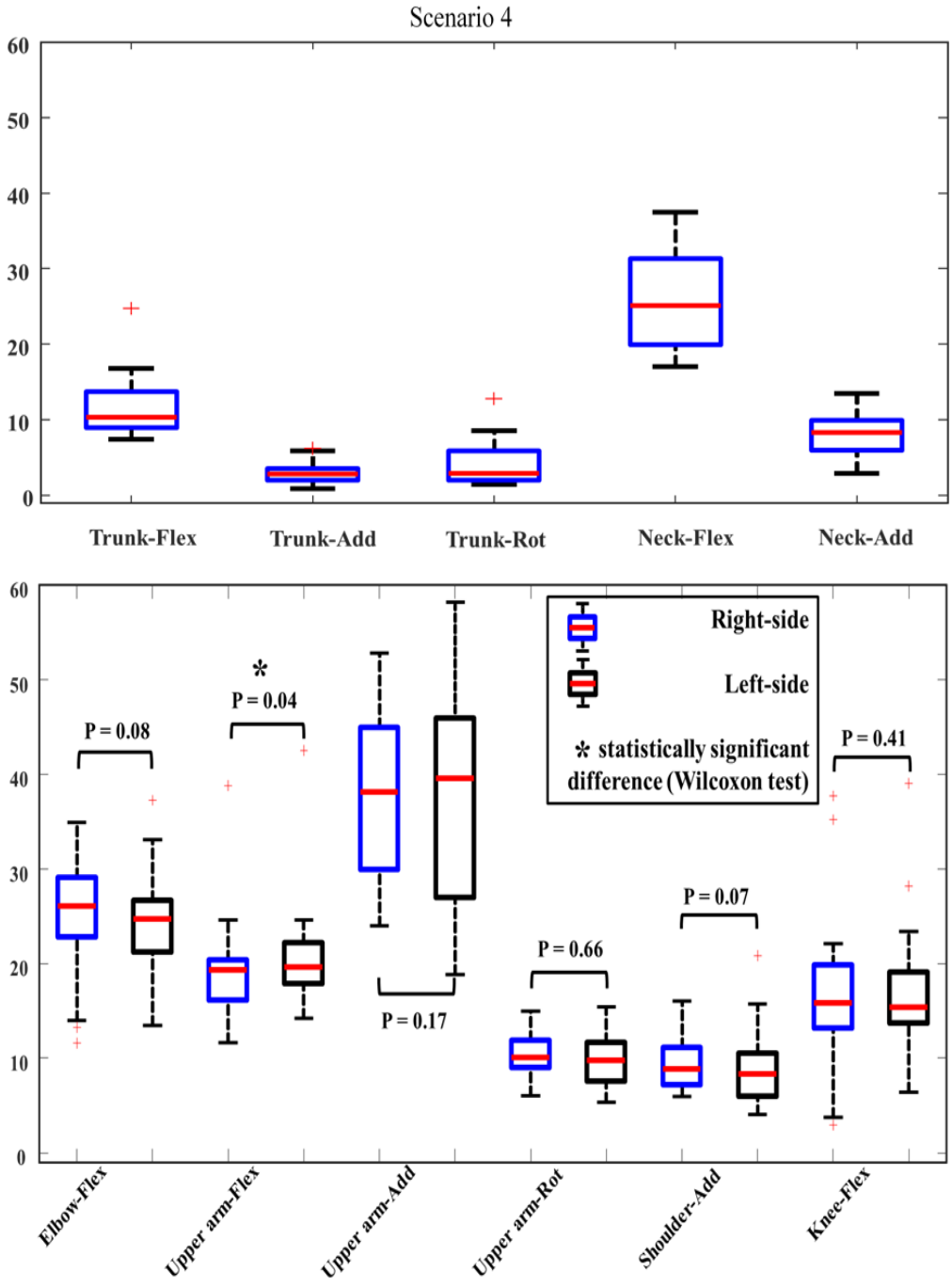

Figure 29. Scenario 4**:** RMSE of the joint angles (2D joint angles) obtained by the marker-less system compared to those obtained by the marker-based system. The results are expressed in degrees, and each boxplot represents the data from the study participants.

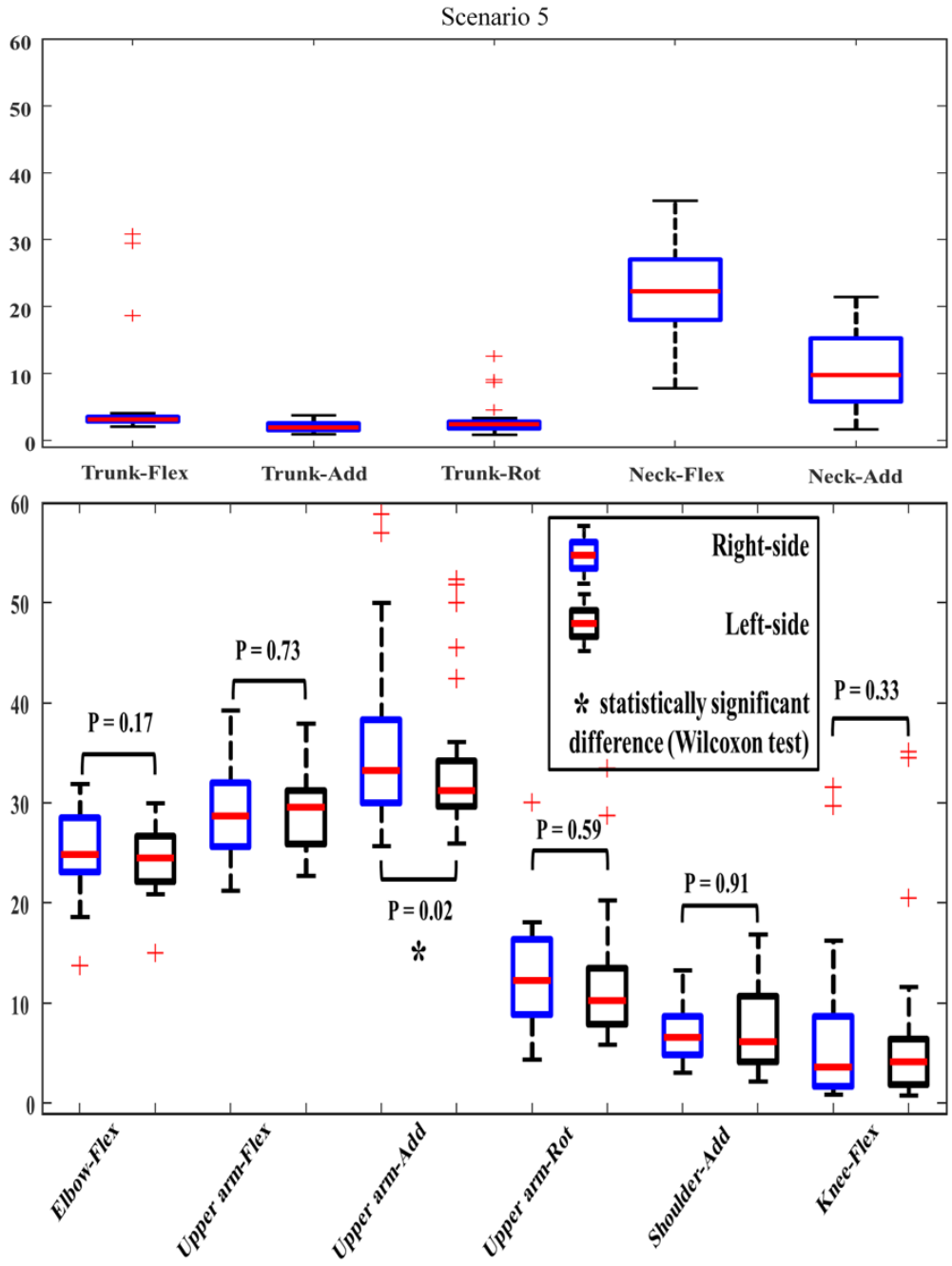

Figure 30. Scenario 5: RMSE of the joint angles (2D joint angles) obtained by the marker-less system compared to those obtained by the marker-based system. The results are expressed in degrees, and each boxplot represents the data from the study participants.

Table 10. Proportion agreement index Po, linear weighted Cohen's kappa coefficient, and Z-test results for RULA scores obtained by marker-less model and Marker-based model using (2D joint angles). The results are presented in 50^{th} (25^{th}, 75^{th}) percentile among the participants.

	Body Side	P_o	Cohen's kappa	Agreement (Landis and Koch scale)	z (k/sqrt (var))	p value	Null hypothesis
Scenario 1	Right side	0.82(0.75,0.87)	0.24(0.0,0.51)	Fair	6.1(0.0,13.6)	< 0.001	Rejected
	Left side	0.78(0.67,0.84)	0.22(0.0,0.51)	Fair	5.5(0.8,18.4)	< 0.001	Rejected
Scenario 2	Right side	0.80(0.75,0.86)	0.58(0.46,0.67)	Moderate	20.6(15.5,26.1)	< 0.001	Rejected
	Left side	0.77(0.71,0.84)	0.48(0.38,0.61)	Moderate	17.5(12.2,24.9)	< 0.001	Rejected
Scenario 3	Right side	0.84(0.80,0.88)	0.56(0.43,0.63)	Moderate	18.4(11.9,27.6)	< 0.001	Rejected
	Left side	0.83(0.80,0.89)	0.56(0.45,0.69)	Moderate	23.9(16.1,30.8)	< 0.001	Rejected
Scenario 4	Right side	0.81(0.71,0.85)	0.38(0.23,0.51)	Fair	14.6(2.6,21.5)	< 0.001	Rejected
	Left side	0.79(0.71,0.85)	0.41(0.25,0.50)	Moderate	16.1(9.9,22.1)	< 0.001	Rejected
Scenario 5	Right side	0.94(0.82,0.95)	0.57(0.51,0.79)	Moderate	32.0(21.9,35.5)	< 0.001	Rejected
	Left side	0.80(0.75,0.92)	0.55(0.50,0.77)	Moderate	18.2(13.4,31.1)	< 0.001	Rejected

The RULA scores obtained by both the IMU-based system and marker-based system were compared on a sample-to-sample basis using the proportion agreement index and Cohen's kappa coefficient (Table 10). According to the Landis and Koch scale [99], the results showed a "moderate" agreement between the two systems in scenarios 2, 3, 5 and left side of scenario 4, while scenario 1 and right side of scenario 4 showed "fair" agreement. To show the significance of the results, the Z-test was used to test the null hypothesis whether the probability of the agreement between the two systems was accidental. This null hypothesis ($p < 0.05$) was rejected in all scenarios and for both right and left body sides. The results presented in Table 8 showed the ICC inter-participant agreement for each system. Using 2D joint angles calculation for RULA evaluation, the marker-less system showed an "excellent" agreement for scenarios 1, 4, and 5, "fair" agreement in scenario 2, and "good" in scenario 3 in the RULA scores median between participants according to Cicchetti [100] guidelines for interpretation for ICC.

Chapter 5

This chapter discusses the results of the IMU-based system for in-field body motion tracking and RULA assessment tool evaluation in sections 5.1 and 5.2. Sections 5.3 and 5.4 discuss the results of the marker-less system for in-field body motion tracking and RULA assessment tool evaluation. Sections 5.5 and 5.6 discuss the limitations of the study and the conclusion and future work.

5. Discussion and Conclusions

5.1 IMU-based system for in-field body motion assessment

We investigated the accuracy of a commercial IMU system for RULA score measurement against the marker-based motion-capture system for manual material handling tasks. The RULA ergonomic assessment method was used in this study because it is designed for sedentary tasks and for the risk factor of posture-related WMDs. For this purpose, the angular position of body segments was identified using vector convention and their projection into different planes on the one hand (2D joint angles). At the same time, the 3D joint angles were calculated by using the joint coordinate system (JCS) convention. In the IMU-based system, the RMSE of joint angles was high on upper and lower arms adduction/abduction, also in the elbow flexion/extension angles in all scenarios, mainly due to their high range of motion. In upper arm joint angles, the projection of vectors contributed to the majority of the error in the 2D models since the marker-based model overestimates the joint angles for some of the participants due to the markers placement and the anthropometric differences between the participants especially in high range motion in these limbs. However, the error in the elbow joint angles was mainly to the offset between systems and almost around 20° in all scenarios and participants. Robert-Lachaine et al. [101] investigated the differences between the body joint angles obtained by the Xsens IMUs MVN system and those obtained by a marker-based system and showed that the IMUs and markers displacement over skin during manual material handling tasks might affect the calculation of joint angles. They also showed that the IMUs calibration process and the anthropometric measurements could contribute to the observed offset errors. They reported RMSE values of 40.2° on the upper arm adduction/abduction, which were larger than the largest RMSE median of the same angle (3D joint angles) presented in our study

9.5° for the left side. This large difference could be attributed to the fact that their study measured the glenohumeral joint to represent the upper arm joint center position. Also, in 2D joint angles, the largest upper adduction/abduction RMSE median in our study (21.28°) was smaller than the error in the study of Robert-Lachaine et al., which can be due to the difference between the angle calculation methods. The duration of the tasks in their study was long (about 32 minutes) that could also increase the error. Conversely, the largest elbow flexion/extension (3D joint angles) RMSE median in our study, was larger (26.6°) than the RMSE in their study (6.2°). Also, the largest (2D joint angles) elbow flexion/extension RMSE median was (25.0°). This error mainly resulted from the offset between the IMU-based system used in our study and the marker-based system. Robert-Lachaine et al. concluded that the task complexity (i.e., range of motion, and the duration of the task) contributed to the error.

5.2 IMU-based system for in-field assessment of RULA score

A few studies [28]-[29]-[102] calculated RULA scores for ergonomic risk assessment using IMU-based systems based on a biomechanical model with different degrees of freedom. However, neither of them compared the results with a marker-based system as a reference to demonstrate the level of agreement between the RLA. The results in Tables 6 and 7 show that the IMU-based system was able to obtain a RULA score with moderate and substantial agreement with the marker-based system when the 3D joint angles and 2D joint angles conventions were used. The absolute differences between Cohen's Kappa coefficient obtained for the right and left body sides were due to the asymmetry in the tasks. In [28], the authors reported that their IMU-based system had 94.79% accuracy compared to a subjective observation during grocery tasks. In our study, the agreement between the IMU-based system and marker-based system was ranging from moderate to substantial.

5.3 Marker-less system for in-field body motion assessment

The accuracy and reliability of the marker-less system for ergonomic evaluation were investigated and compared with the marker-based system. The same joint angle convention (2D joint angles) used to obtain joint angles by the IMU-based system and by the marker-less system (Kinect). The marker-less system had a significant larger RMSE in most of the joint angles compared to IMU-based system (see Appendix B, FigureB14, and B18). The

error in Kinect results can be referred to the fact that the performance of Kinect depends on the depth image processing algorithm that can be affected by a couple of factors such as the existence of objects between the camera and the participant, and the lighting condition. In addition, as reported in [50], the reflective markers of the marker-based system and the plates used to attach the IMUs may influence the accuracy of the Kinect tracking algorithm. A study done in 2016 to validate a new method for correcting Kinect skeleton data, obtained the RMSE of the joint angles during short lifting and lowering tasks values between 5.2° and 18.3° for right elbow flexion/extension, shoulder flexion/extension, and shoulder adduction/abduction and between 7.2° and 26.7° for left elbow flexion/extension, shoulder flexion/extension, and shoulder adduction/abduction. Our results showed larger RMSE, which may be attributed to the joint angles calculation method, the algorithm used to correct Kinect data, and the complexity of the tested tasks in our study compared to that study. Good accuracy was obtained during rehabilitation movement by a physical therapist with mean error (ME) between 5.53° and 13.9° for knee, shoulder, and hip flexion/extension, and shoulder and hip adduction/abduction [54]. Another study by Wiedemann et al. [103] found the highest difference on the neck angle with the median of 8.46° and upper and lower bound of 30.22° and -11.06° respectively for all static postures. They observed the lowest median error on the left knee 0.26° for all postures. Their results are better than what is presented in the present study because they tested static postures and without occluded objects that retarder the Kinect view.

5.4 Marker-less system for in-field assessment of RULA score

The results in Table 10 reveal that marker-less system showed low agreement in the task scenarios that required a small range of motion, such as scenarios 1 and 4. It is because the measured joint angles by Kinect were not accurate around the thresholds used in the RULA definition, and thus Kinect was not able to detect a change in the RULA score. Therefore, a smaller RULA score was obtained by Kinect compared to what marker-based system obtained. In contrast, in scenarios with larger range of motion, such as scenarios 2 and 3, the maximum thresholds were reached by both systems in most of the frames a moderate agreement was observed (see Appendix B, FigureB11, and B12). This could be due to the jittering in the Kinect joints, and the occurred self-occlusion. In scenario 5 where most of the motion was in the arms, the agreement was very high, and the range of motion was

beyond angle thresholds used by RULA. However, the ICC agreement of RULA scores median was moderate to excellent (Table 8) and similar to that of IMU-based and marker-based system. However, the lower and upper bound were various. A glance at the results of the Kinect and IMU-based system showed that the IMU-based system provided more stable measures than Kinect for continuous measurements. Another study [30] reported a perfect agreement between Kinect and a marker-based system for all postures tested, where in the present study; we observed a moderate agreement. The reason might be that they tested static postures adopted by one actor and without occluded objects.

5.5 Limitations of the study

First, RULA mothed is not a perfectly precise assessment tool since the users should enter many thresholds. In addition, the RULA method does not consider the lumbar zone, which should be considered for a comprehensive evaluation [27]. We did not consider the muscle use and weight. Also, the wrist joint angles were entered manually due to limited kinematic data obtained from the Kinect and marker-based system.

The IMUs inherently suffer from drift and magnetic disturbance, which may be overcome by integrating them with video-based systems. As mentioned, the occlusion due to objects was the main limitation of both Kinect and marker-based system. Particularly, the results obtained by the Kinect sensor with affected by both body self-occlusions and environment objects occlusions.

Finally, we tested these systems in a laboratory set-up with controlled lighting conditions with 11 male participants. This is the best working condition for the Skeleton Tracking algorithm for Kinect V2, and the results in an out-of-lab environment might be different.

5.6. Conclusions and future works

This study aimed to evaluate the validity of a marker-less system (Kinect) and IMU-based system as an in-field assessment tool for posture-based ergonomic risk assessment (based on RULA score). Both systems were used to calculate joint angles using a vector convention presented in [30], and we compared them to a marker-based motion-capture system (Vicon, UK) as a reference. The results showed the high accuracy and robustness of the IMU-based system in ergonomic risk assessment for manual material handling tasks

and with a substantial agreement with the marker-based system for all task scenarios. Therefore, the IMU-based system can be recommended for ergonomic risk assessment in real workplaces where the marker-based systems are of limited use. The IMU sensors are affordable for many workplaces and can capture the motions and postures with sampling frequency up to 100 Hz, which is sufficient for providing feedback toward reducing the risk of WMDs in work environments. To this end, we recommend a 3D joint angles calculation approach instead of a 2D vector convention in order to obtain more accurate joint angles and thus RULA scores.

The marker-less system (e.g., Kinect) have advantageous characteristics for many applications of in-field motion assessments, such as the acceptable sampling rate (30 Hz), low cost, and being marker-less. Yet, we observed that the Kinect sensor showed lower accuracy for all tested task scenarios compared to the IMU-based system. In addition, the agreement between Kinect and marker-based systems in obtaining the RULA score ranged from “fair” to “moderate,” unlike the IMU-based system. It means that the performance of this marker-less system (Kinect) for ergonomic risk assessment is not stable and depends on many conditions similar to many vision-based systems, such as occlusion, lighting conditions, environment, etc. In order to increase the accuracy and robustness of the marker-less system for reliable, ergonomic risk assessment, updated data processing methods could be used as in [60]-[104]. Finally, we investigated the validity of a marker-less system and an IMU-based system in five common manual material handling task scenarios. Further investigation should be performed for other working scenarios.

References

[1] W. Karwowski and W.S. Marras, “Occupational Ergonomics”, Baton Rouge: CRC Press, 2003.

[2] Intenational Ergonomics Association, “IEA Triennial Report,” 2003.

[3] The Workers' Compensation Board – Alberta, “Office Ergonomics,” pp. 2-33, 2007.

[4] Canadian Community Health Survey (CCHS), “Injuries at work,” 2013.

[5] P. Plantard, E. Auvinet, A.L. Pierres and F. Multon, "Pose estimation with a kinect for ergonomic studies: Evaluation of the accuracy using a virtual mannequin," Sensors (Basel, Switzerland), vol. 15, pp. 1785-1803, 2015.

[6] Daniel P Pope, Alan J Silman, Nicola M Cherry, Christina Pritchard and Gary J Macfarlane, "Validity of a self-completed questionnaire measuring the physical demands of work," Scandinavian Journal of Work, Environment & Health, vol. 24, pp. 376-385, 1998.

[7] Eira Viikari-Juntura, Sirpa Rauas, Rami Martikainen, Eeva Kuosma, Hilkka Riihimäki, Esa-Pekka Takala and Kari Saarenmaa, "Validity of self-reported physical work load in epidemiologic studies on musculoskeletal disorders," Scandinavian Journal of Work, Environment & Health, vol. 22, pp. 251-259,1996.

[8] Istvan Balogh, Palle Ørbaek, Jörgen Winkel, Catarina Nordander, Kerstina Ohlsson and John Ektor-Andersen, "Questionnaire-based mechanical exposure indices for large population studies — reliability, internal consistency and predictive validity," Scandinavian Journal of Work, Environment & Health, vol. 27, pp. 41-48, 2001.

[9] P. Spielholz, B. Silverstein and M. Stuart, "Reproducibility of a self-report questionnaire for upper extremity musculoskeletal disorder risk factors," Applied Ergonomics, vol. 30, pp. 429-433, 1999.

[10] A. Choobineh, S.H. Tabatabaee and M. Behzadi, "Musculoskeletal Problems Among Workers of an Iranian Sugar-Producing Factory," International Journal of Occupational Safety and Ergonomics, vol. 15, pp. 419-424, 2009.

[11] V. Jockin, R.D. Arvey and M. McGue, "Perceived Victimization Moderates Self-Reports of Workplace Aggression and Conflict," Journal of Applied Psychology, vol. 86, pp. 1262-1269, 2001.

[12] C. Trask, K. Teschke, J. Village, Y. Chow, P. Johnson, N. Luong and M. Koehoorn, "Measuring low back injury risk factors in challenging work environments: An evaluation of cost and feasibility," American Journal of Industrial Medicine, vol. 50, pp. 687-696, 2007.

[13] G.C. David, "Ergonomic methods for assessing exposure to risk factors for work-related musculoskeletal disorders," Occupational Medicine (Oxford, England), vol. 55, pp. 190-199, 2005.

[14] P. Spielholz, B. Silverstein, M. Morgan, H. Checkoway and J. Kaufman, "Comparison of self-report, video observation and direct measurement methods for upper extremity musculoskeletal disorder physical risk factors," Ergonomics, vol. 44, pp. 588-613, 2001.

[15] G. Li and P. Buckle, "Current techniques for assessing physical exposure to work-related musculoskeletal risks, with emphasis on posture-based methods," Ergonomics, vol. 42, pp. 674, 1999.

[16] O. Karhu, P. Kansi and I. Kuorinka, "Correcting working postures in industry: A practical method for analysis," Applied Ergonomics, vol. 8, pp. 199-201, 1977.

[17] L. McAtamney and E. Nigel Corlett, "RULA: a survey method for the investigation of work-related upper limb disorders," Applied Ergonomics, vol. 24, pp. 91-99, 1993.

[18] Christina Wiktorin, Monica Mortimer, Lena Ekenvall, Åsa Kilbom and Ewa Wigaeus Hjelm, "HARBO, a simple computer-aided observation method for recording work postures," Scandinavian Journal of Work, Environment & Health, vol. 21, pp. 440-449, 1995.

[19] C. Fransson-Hall, R. Gloria, Å Kilbom, J. Winkel, L. Karlqvist and C. Wiktorin, "A portable ergonomic observation method (PEO) for computerized on-line recording of postures and manual handling," Applied Ergonomics, vol. 26, pp. 93-100, 1995.

[20] M.H.W. Frings-Dresen and P.P.F.M. Kuijer, "The TRAC-system: An observation method for analysing work demands at the workplace," Safety Science, vol. 21, pp. 163-165, 1995.

[21] P. Holzmann, "ARBAN—A new method for analysis of ergonomic effort," Applied Ergonomics, vol. 13, pp. 82-86, 1982.

[22] A.L.F. Rodacki and J.E. Vieira, "The effect of different supermarket checkout workstations on trunk kinematics of checkout operators," Revista Brasileira De Fisioterapia, vol. 14, pp. 38-44, 2010.

[23] W.S. Marras, F.A. Fathallah, R.J. Miller, S.W. Davis and G.A. Mirka, "Accuracy of a three-dimensional lumbar motion monitor for recording dynamic trunk motion characteristics," International Journal of Industrial Ergonomics, vol. 9, pp. 75-87, 1992.

[24] R.G. RADWIN and M.L. LIN, "An analytical method for characterizing repetitive motion and postural stress using spectral analysis," Ergonomics, vol. 36, pp. 379-389, 1993.

[25] J.A. Diego-Mas and J. Alcaide-Marzal, "Using Kinect™ sensor in observational methods for assessing postures at work," Applied Ergonomics, vol. 45, pp. 976-985, 2014.

[26] R. Alberto, F. Draicchio, T. Varrecchia, A. Silvetti and S. Iavicoli, "Wearable Monitoring Devices for Biomechanical Risk Assessment at Work: Current Status and Future Challenges—A Systematic Review," International Journal of Environmental Research and Public Health, vol. 15, pp. 2001, 2018.

[27] D. Battini, A. Persona and F. Sgarbossa, "Innovative real-time system to integrate ergonomic evaluations into warehouse design and management," Computers & Industrial Engineering, vol. 77, pp. 1-10, 2014.

[28] L. Peppoloni, A. Filippeschi, E. Ruffaldi and C.A. Avizzano, "A novel wearable system for the online assessment of risk for biomechanical load in repetitive efforts," International Journal of Industrial Ergonomics, vol. 52, pp. 1-11, 2016.

[29] N. Vignais, M. Miezal, G. Bleser, K. Mura, D. Gorecky and F. Marin, "Innovative system for real-time ergonomic feedback in industrial manufacturing," Applied Ergonomics, vol. 44, pp. 566-574, 2013.

[30] O. Wasenmüller and D. Stricker, "Comparison of kinect v1 and v2 depth images in terms of accuracy and precision," in Asian Conference on Computer Vision, pp. 34-45, 2016.

[31] M. Rahman, Beginning Microsoft Kinect for Windows SDK 2.0: Motion and Depth Sensing for Natural User Interfaces, Berkeley, CA: Apress L. P, 2017.

[32] V.M. Manghisi, A.E. Uva, M. Fiorentino, V. Bevilacqua, G.F. Trotta and G. Monno, "Real time RULA assessment using Kinect v2 sensor," Applied Ergonomics, vol. 65, pp. 481-491, 2017.

[33] V. Medved, Measurement of human locomotion, Boca Raton [u.a.]: Crc Press, 2000.

[34] L. Chiari, U.D. Croce, A. Leardini and A. Cappozzo, "Human movement analysis using stereophotogrammetry: Part 2: Instrumental errors," Gait & Posture, vol. 21, pp. 197-211, 2005.

[35] K.D. Taylor, F.M. Mottier, D.W. Simmons, W. Cohen, R. Pavlak, D.P. Cornell and G.B. Hankins, "An automated motion measurement system for clinical gait analysis," Journal of Biomechanics, vol. 15, pp. 505-516, 1982.

[36] G. Ferrigno, N.A. Borghese and A. Pedotti, "Pattern recognition in 3D automatic human motion analysis," ISPRS Journal of Photogrammetry and Remote Sensing, vol. 45, pp. 227-246, 1990.

[37] U. Della Croce, A. Leardini, L. Chiari and A. Cappozzo, "Human movement analysis using stereophotogrammetry: Part 4: assessment of anatomical landmark misplacement and its effects on joint kinematics," Gait Posture, vol. 21, pp. 226-237, 2005.

[38] A. Leardini, L. Chiari, U. Della Croce and A. Cappozzo, "Human movement analysis using stereophotogrammetry. Part 3. Soft tissue artifact assessment and compensation," Gait & Posture, vol. 21, pp. 212-225, 2005.

[39] S. Corazza, L. Mündermann, A. Chaudhari, T. Demattio, C. Cobelli and T. Andriacchi, "A Markerless Motion Capture System to Study Musculoskeletal

Biomechanics: Visual Hull and Simulated Annealing Approach," Ann Biomed Eng, vol. 34, pp. 1019-1029, 2006.

[40] A. Cappozzo, U. Della Croce, A. Leardini and L. Chiari, "Human movement analysis using stereophotogrammetry: Part 1: theoretical background," Gait & Posture, vol. 21, pp. 186-196, 2005.

[41] M.P. Kadaba, H.K. Ramakrishnan and M.E. Wootten, "Measurement of lower extremity kinematics during level walking," Journal of Orthopaedic Research: Official Publication of the Orthopaedic Research Society, vol. 8, pp. 383-392, 1990.

[42] J. Bray, "Markerless based human motion capture: a survey," Department Systems Engineering Brunel University, 2001.

[43] B. Bonnechère, B. Jansen, P. Salvia, H. Bouzahouene, L. Omelina, F. Moiseev, V. Sholukha, J. Cornelis, M. Rooze and S. Van Sint Jan, "Validity and reliability of the Kinect within functional assessment activities: Comparison with standard stereophotogrammetry," Gait & Posture, vol. 39, pp. 593-598, 2013.

[44] T.B. Moeslund and E. Granum, "A survey of computer vision-based human motion capture," Comput.Vision Image Understanding, vol. 81, pp. 231-268, 2001.

[45] P. Plantard, H. H. Shum and F. Multon, "Filtered pose graph for efficient kinect pose reconstruction," Multimed Tools Appl, vol. 76, pp. 4291-4312, 2017.

[46] M.K. Leung and Yee-Hong Yang, "First Sight: A human body outline labeling system," Tpami, vol. 17, pp. 359-377, 1995.

[47] X. Zhu and D. Ramanan, "Face detection, pose estimation, and landmark localization in the wild," in 2012 IEEE conference on computer vision and pattern recognition, pp. 2879-2886, 2012.

[48] K. Rohr, "Incremental recognition of pedestrians from image sequences," pp. 8-13, 1993.

[49] E. Di Bernardo, L. Goncalves and P. Perona, "Monocular tracking of the human arm in 3D: real-time implementation and experiments," vol.3, pp. 622-626, 1996.

[50] B. Müller, W. Ilg, M.A. Giese and N. Ludolph, "Validation of enhanced kinect sensor based motion capturing for gait assessment," PloS One, vol. 12, pp. e0175813, 2017.

[51] T.B. Moeslund, "Interacting with a virtual world through motion capture," in Virtual interaction: Interaction in virtual inhabited 3D worlds, Springer, pp. 221-234, 2001.

[52] R.A. Clark, Y. Pua, K. Fortin, C. Ritchie, K.E. Webster, L. Denehy and A.L. Bryant, "Validity of the Microsoft Kinect for assessment of postural control," Gait & Posture, vol. 36, pp. 372-377, 2012.

[53] R.A. Clark, Y. Pua, A.L. Bryant and M.A. Hunt, "Validity of the Microsoft Kinect for providing lateral trunk lean feedback during gait retraining," Gait Posture, vol. 38, pp. 1064-1066, 2013.

[54] A. Fernández-Baena, A. Susin and X. Lligadas, "Biomechanical Validation of Upper-Body and Lower-Body Joint Movements of Kinect Motion Capture Data for Rehabilitation Treatments," pp. 656-661, 2012.

[55] D.J. Geerse, H. Coolen and M. Roerdink, "Kinematic Validation of a Multi-Kinect v2 Instrumented 10-Meter Walkway for Quantitative Gait Assessments," PLoS One, vol. 10, pp. e0139913, 2015.

[56] S. Kaenchan, P. Mongkolnam, B. Watanapa and S. Sathienpong, "Automatic multiple Kinect cameras setting for simple walking posture analysis," pp. 245-249, 2013.

[57] S. Springer and G. Yogev Seligmann, "Validity of the kinect for gait assessment: A focused review," Sensors, vol. 16, pp. 194, 2016.

[58] A.N. Staranowicz, C. Ray and G. Mariottini, "Easy-to-use, general, and accurate multi-Kinect calibration and its application to gait monitoring for fall prediction," pp. 4994-4998, 2015.

[59] H. Haggag, M. Hossny, S. Nahavandi and D. Creighton, "Real Time Ergonomic Assessment for Assembly Operations Using Kinect," pp. 495-500, 2013.

[60] P. Paliyawan, C. Nukoolkit and P. Mongkolnam, "Prolonged sitting detection for office workers syndrome prevention using kinect," pp. 1-6, 2014.

[61] C.C. Martin, D.C. Burkert, K.R. Choi, N.B. Wieczorek, P.M. McGregor, R.A. Herrmann and P.A. Beling, "A real-time ergonomic monitoring system using the Microsoft Kinect," pp. 50-55, 2012.

[62] P. Plantard, H.P.H. Shum, A. Le Pierres and F. Multon, "Validation of an ergonomic assessment method using Kinect data in real workplace conditions," Applied Ergonomics, vol. 65, pp. 562-569, 2017.

[63] K.S. Tee, E. Low, H. Saim, W.N.W. Zakaria, S.B.M. Khialdin, H. Isa, M.I. Awad and C.F. Soon, "A study on the ergonomic assessment in the workplace," in AIP Conference Proceedings, pp. 020034, 2017.

[64] J. Steven Moore and A. Garg, "The Strain Index: A Proposed Method to Analyze Jobs For Risk of Distal Upper Extremity Disorders," American Industrial Hygiene Association Journal, vol. 56, pp. 443-458, 1995.

[65] D. Colombini, Risk Assessment and Management of Repetitive Movements and Exertions of Upper Limbs: Job Analysis, Ocra Risk Indicies, Prevention Strategies and Design Principles, Elsevier, 2002.

[66] X. Yan, A.R. Li, H. Li and H. Zhang, "Wearable IMU-based real-time motion warning system for construction workers' musculoskeletal disorders prevention," Automation in Construction, vol. 74, pp. 2-11,2017.

[67] Ping Li, R. Meziane, M.J.-. Otis, H. Ezzaidi and P. Cardou, "A Smart Safety Helmet using IMU and EEG sensors for worker fatigue detection," pp. 55-60, 2014.

[68] J. Chen, C.R. Ahn and S. Han, "Detecting the Hazards of Lifting and Carrying in Construction through a Coupled 3D Sensing and IMUs Sensing System," in Computing in Civil and Building Engineering, pp. 1110-1117, 2014.

[69] V.M. Ciriello and S.H. Snook, "Survey of manual handling tasks," International Journal of Industrial Ergonomics, vol. 23, pp. 149-156, 1999.

[70] J. Howard and L. Welsh, "Ergonomic Guidelines for Manual Material Handling," Columbia: National Institute for Occupational Safety and Health, 2007.

[71] P.G. Dempsey, "A survey of lifting and lowering tasks," Int.J.Ind.Ergonomics, vol. 31, pp. 11-16, 2003.

[72] V.M. Ciriello and S.H. Snook, "A Study of Size, Distance, Height, and Frequency Effects on Manual Handling Tasks," Human Factors: The Journal of the Human Factors and Ergonomics Society, vol. 25, pp. 473-483,1983.

[73] M.A. Wahyudi, W.A.P. Dania and R.L.R. Silalahi, "Work Posture Analysis of Manual Material Handling Using OWAS Method," Agriculture and Agricultural Science Procedia, vol. 3, pp. 195-199, 2015.

[74] J.O. Crawford, "The Nordic musculoskeletal questionnaire," Occupational Medicine, vol. 57, pp. 300-301, 2007.

[75] B.M. Deros, D.D.I. Daruis and I.M. Basir, "A Study on Ergonomic Awareness among Workers Performing Manual Material Handling Activities," Procedia - Social and Behavioral Sciences, vol. 195, pp. 1666-1673, 2015.

[76] Y. Torres and S. Viña, "Evaluation and redesign of manual material handling in a vaccine production centre's warehouse," Work (Reading, Mass.), vol. 41 Suppl 1, pp. 2487-2491, 2012.

[77] S.H. Snook, R.A. Campanelli and J.W. Hart, "A study of three preventive approaches to low back injury." Journal of Occupational Medicine: Official Publication of the Industrial Medical Association, vol. 20, pp. 478-481, 1978.

[78] W. Boucsein and R.W. Backs, "Engineering psychophysiology as a discipline: Historical and theoretical aspects," Engineering Psychophysiology.Issues and Applications, pp. 3-30, 2000.

[79] K. Kemmlert, "A method assigned for the identification of ergonomic hazards — PLIBEL," Applied Ergonomics, vol. 26, pp. 199-211, 1995.

[80] M. Göbel, "Electromyographic evaluation of sensory feedback for movement control," in Proceedings of the XIth International Ergonomics and Safety Conference, Zurich, 1996.

[81] T.R. WATERS, V. PUTZ-ANDERSON, A. GARG and L.J. FINE, "Revised NIOSH equation for the design and evaluation of manual lifting tasks," Ergonomics, vol. 36, pp. 749-776, 1993.

[82] D. De Waard, The measurement of drivers' mental workload, Groningen University, Traffic Research Center Netherlands, 1996.

[83] V.H. Hildebrandt, "The Dutch musculoskeletal questionnaire (DMQ)," in Handbook of Human Factors and Ergonomics Methods, CRC Press, pp. 65-73, 2004.

[84] D. Aeschbach, J.R. Matthews, T.T. Postolache, M.A. Jackson, H.A. Giesen and T.A. Wehr, "Dynamics of the human EEG during prolonged wakefulness: evidence for frequency-specific circadian and homeostatic influences, Neurosci.Lett. vol. 239, pp. 121-124, 1997.

[85] G. Li and P. Buckle, "Evaluating change in exposure to risk for musculoskeletal disorders—a practical tool," in Proceedings of the Human Factors and Ergonomics Society Annual Meeting, pp. 5-408, 2000.

[86] J.W. Belliveau, D.N. Kennedy, R.C. McKinstry, B.R. Buchbinder, R. Weisskoff, M.S. Cohen, J.M. Vevea, T.J. Brady and B.R. Rosen, "Functional mapping of the human visual cortex by magnetic resonance imaging," Science, vol. 254, pp. 716-719, 1991.

[87] R. Karasek, C. Brisson, N. Kawakami, I. Houtman, P. Bongers and B. Amick, "The Job Content Questionnaire (JCQ): an instrument for internationally comparative assessments of psychosocial job characteristics." J.Occup.Health Psychol., vol. 3, pp. 322, 1998.

[88] S. Hignett and L. McAtamney, "Rapid Entire Body Assessment (REBA)," Applied Ergonomics, vol. 31, pp. 201-205, 2000.

[89] D.E. Anderson and L.B. Frank, "A microprocessor system for ambulatory monitoring of respiration," Journal of Ambulatory Monitoring, vol. 3, pp. 11-20, 1990.

[90] D.F. Sittig, G.J. Kuperman and J. Fiskio, "Evaluating physician satisfaction regarding user interactions with an electronic medical record system." in Proceedings of the AMIA Symposium, pp. 400, 1999.

[91] N.A. Stanton, A. Hedge, K. Brookhuis, E. Salas and H.W. Hendrick, "Handbook of human factors and ergonomics methods," CRC press, 2004.

[92] T.R. Waters, V. Putz-Anderson and A. Garg, "Applications manual for the revised NIOSH lifting equation," 1994.

[93] R.B. Graham, P.A. Costigan, E.M. Sadler and J.M. Stevenson, "Local dynamic stability of the lifting kinematic chain," Gait & Posture, vol. 34, pp. 561-563, 2011.

[94] G.E. Robertson, G.E. Caldwell, J. Hamill, G. Kamen and S. Whittlesey, "Research methods in biomechanics," Human kinetics, 2013.

[95] J. Webb and J. Ashley, "Beginning Kinect Programming with the Microsoft Kinect SDK", Apress, 2012.

[96] Xsens MVN User Manual," Xsens Technologies B.V," pp. 1-172, 2018.

[97] G. Wu, Van der Helm, Frans CT, H.D. Veeger, M. Makhsous, P. Van Roy, C. Anglin, J. Nagels, A.R. Karduna, K. McQuade and X. Wang, "ISB recommendation on definitions of joint coordinate systems of various joints for the reporting of human joint motion—Part II: shoulder, elbow, wrist and hand," J.Biomech., vol. 38, pp. 981-992, 2005.

[98] G. Wu, S. Siegler, P. Allard, C. Kirtley, A. Leardini, D. Rosenbaum, M. Whittle, D. D D'Lima, L. Cristofolini and H. Witte, "ISB recommendation on definitions of joint coordinate system of various joints for the reporting of human joint motion—part I: ankle, hip, and spine," J.Biomech., vol. 35, pp. 543-548, 2002.

[99] J. Richard Landis and Gary G. Koch, "The Measurement of Observer Agreement for Categorical Data," Biometrics, vol. 33, pp. 159-174, Mar 1. 1977.

[100] D.V. Cicchetti, "Guidelines, criteria, and rules of thumb for evaluating normed and standardized assessment instruments in psychology," Psychological Assessment, vol. 6, pp. 284-290, 1994.

[101] X. Robert-Lachaine, H. Mecheri, C. Larue and A. Plamondon, "Validation of inertial measurement units with an optoelectronic system for whole-body motion analysis, Med.Biol.Eng.Comput, vol. 55, pp. 609-619, 2017.

[102] L. Peppoloni, A. Filippeschi and E. Ruffaldi, "Assessment of task ergonomics with an upper limb wearable device," in 22nd Mediterranean Conference on Control and Automation, pp. 340-345, 2014.

[103] L.G. Wiedemann, R. Planinc, I. Nemec and M. Kampel, "Performance evaluation of joint angles obtained by the Kinect v2," 2015.

[104] B. Bonnechère, V. Sholukha, F. Moiseev, M. Rooze and J.S. Van Sint, "From Kinect TM to anatomically-correct motion modelling: Preliminary results for human application," in Games for Health, Springer, pp. 15-26, 2013.

Appendices

Appendix A: 3D joint angles for the IMU-based system.

Table A1 presents the offset and the RMSE after removing the offset (the offset was calculated at the first 200 frames) for all joint angles and for all scenarios. Figure A1 to figure A6 presents joint angles obtained from the marker-based system and IMU-based system of the manual material handling. Figure A7 and Figure A8 present RULA scores obtained from the marker-based system and IMU-based system during the manual material handling scenarios.

Table A1. Offset and RMSE of the joint angles (3D angles) in the comparison between Marker-based system and IMU-based system presented in 50th (25th, 75th) percentile of the participants.

	Body side	Offset			RMSE		
		Scenario 1	Scenario 4	Scenario 5	Scenario 1	Scenario 4	Scenario 5
Neck Flex/Ext		14.0(11.3,17.1)	12.2(7.8,16.0)	11.7(8.0,17.7)	3.7(2.4,5.7)	7.3(5.8,10.1)	7.2(5.1,9.7)
Neck Lat Bend		3.6(1.1,7.8)	2.5(1.4,5.3)	2.3(1.7,5.6)	4.2(2.6,6.7)	2.0(0.9,2.7)	2.3(1.8,3.2)
Neck Rotation		6.3(2.0,10.2)	5.5(2.1,11.2)	3.8(1.8,13.4)	2.8(2.0,3.9)	2.2(1.6,3.2)	1.6(1.1,2.8)
Trunk Flex/Ext		8.0(5.7,13.3)	8.7(7.6,14.7)	8.6(6.0,15.9)	4.1(3.4,4.9)	5.4(5.0,6.6)	2.0(1.4,3.5)
Trunk Lat Bend		2.9(1.3,5.0)	3.2(2.0,3.9)	2.6(1.6,4.1)	4.6(3.3,6.0)	2.5(2.0,3.5)	1.7(1.2,2.3)
Trunk Rotation		5.4(2.2,7.5)	4.6(2.1,8.1)	4.2(1.0,5.9)	4.8(3.8,6.2)	3.4(2.2,4.1)	1.5(1.0,2.9)
Fore Arm Flex/Ext	Right	23.7(16.8,35.2)	23.7(17.7,37.1)	25.9(18.0,36.6)	4.5(3.6,8.3)	7.0(5.7,8.7)	8.3(6.6,12.0)
	Left	22.6(18.4,31.2)	22.5(20.0,30.6)	23.8(21.5,34.3)	6.4(3.8,10.3)	7.9(7.2,10.8)	9.9(8.4,11.3)
Fore Arm Add/Abd	Right	29.8(21.9,42.9)	25.8(21.5,41.3)	24.6(19.6,31.4)	7.2(4.6,9.9)	6.2(4.2,8.0)	7.8(5.7,11.4)
	Left	24.6(17.3,36.4)	20.1(14.2,26.4)	18.7(11.6,23.2)	8.0(6.6,11.1)	6.6(5.1,11.2)	10.9(4.8,16.2)
Fore Arm Rotation	Right	12.7(5.9,23.7)	8.3(2.7,15.7)	4.4(2.8,8.5)	6.8(4.8,12.5)	10.6(6.0,13.6)	9.2(6.5,14.1)
	Left	16.8(9.4,28.7)	11.7(9.4,16.9)	8.1(5.1,20.9)	8.9(5.4,13.3)	11.8(6.7,17.8)	18.5(9.6,23.0)
Upper Arm Flex/Ext	Right	7.1(2.9,10.6)	6.6(2.6,12.7)	7.3(3.5,11.7)	5.2(4.2,7.1)	8.0(6.0,11.1)	8.5(5.6,11.9)
	Left	7.2(2.9,10.6)	9.6(2.0,13.4)	8.1(5.1,11.8)	5.1(3.9,7.2)	7.4(5.9,11.3)	8.2(4.1,10.1)
Upper Arm Add/Abd	Right	2.5(1.5,4.7)	2.8(1.5,4.7)	2.9(1.5,5.2)	4.2(2.5,6.2)	4.1(3.3,5.5)	4.9(3.6,6.8)
	Left	6.1(4.0,7.5)	5.3(3.2,5.9)	5.9(4.9,7.4)	3.47(2.5,4.7)	6.1(2.0,8.2)	5.0(3.2,6.4)
Upper Arm Rotation	Right	23.0(11.1,28.4)	22.2(15.2,29.6)	24.1(14.2,38.6)	10.80(8.2,17.7)	6.8(2.9,9.7)	7.6(3.7,22.6)
	Left	28.6(21.2,40.2)	25.2(17.3,29.8)	27.5(17.0,31.4)	9.47(6.6,13.7)	7.9(5.2,11.1)	5.0(3.6,12.9)
Knee Flex/Ext	Right	5.9(2.8,8.4)	3.0(2.3,5.8)	6.4(1.9,7.7)	2.25(1.6,3.0)	2.0(1.4,3.0)	0.3(0.2,0.5)
	Left	4.2(2.8,8.2)	3.6(1.0,7.7)	3.6(2.0,8.4)	2.01(1.2,2.8)	2.2(1.7,2.7)	0.3(0.2,0.4)
Knee Add/Abd	Right	1.4(0.8,2.9)	1.8(1.4,3.5)	2.0(0.9,3.2)	0.99(0.7,1.7)	2.4(1.5,3.3)	0.4(0.2,0.5)
	Left	1.7(0.7,2.8)	1.8(0.5,2.3)	1.5(0.7,2.7)	0.74(0.5,1.5)	1.1(0.7,2.5)	0.2(0.1,0.3)
Knee Rotation	Right	0.3(0.1,0.6)	0.4(0.3,1.3)	0.3(0.2,0.5)	0.39(0.2,1.1)	1.0(0.4,2.3)	0.1(0.0,0.2)
	Left	0.2(0.1,0.4)	0.2(0.1,0.4)	0.2(0.1,0.4)	0.45(0.2,0.6)	0.8(0.5,1.5)	0.1(0.0,0.1)

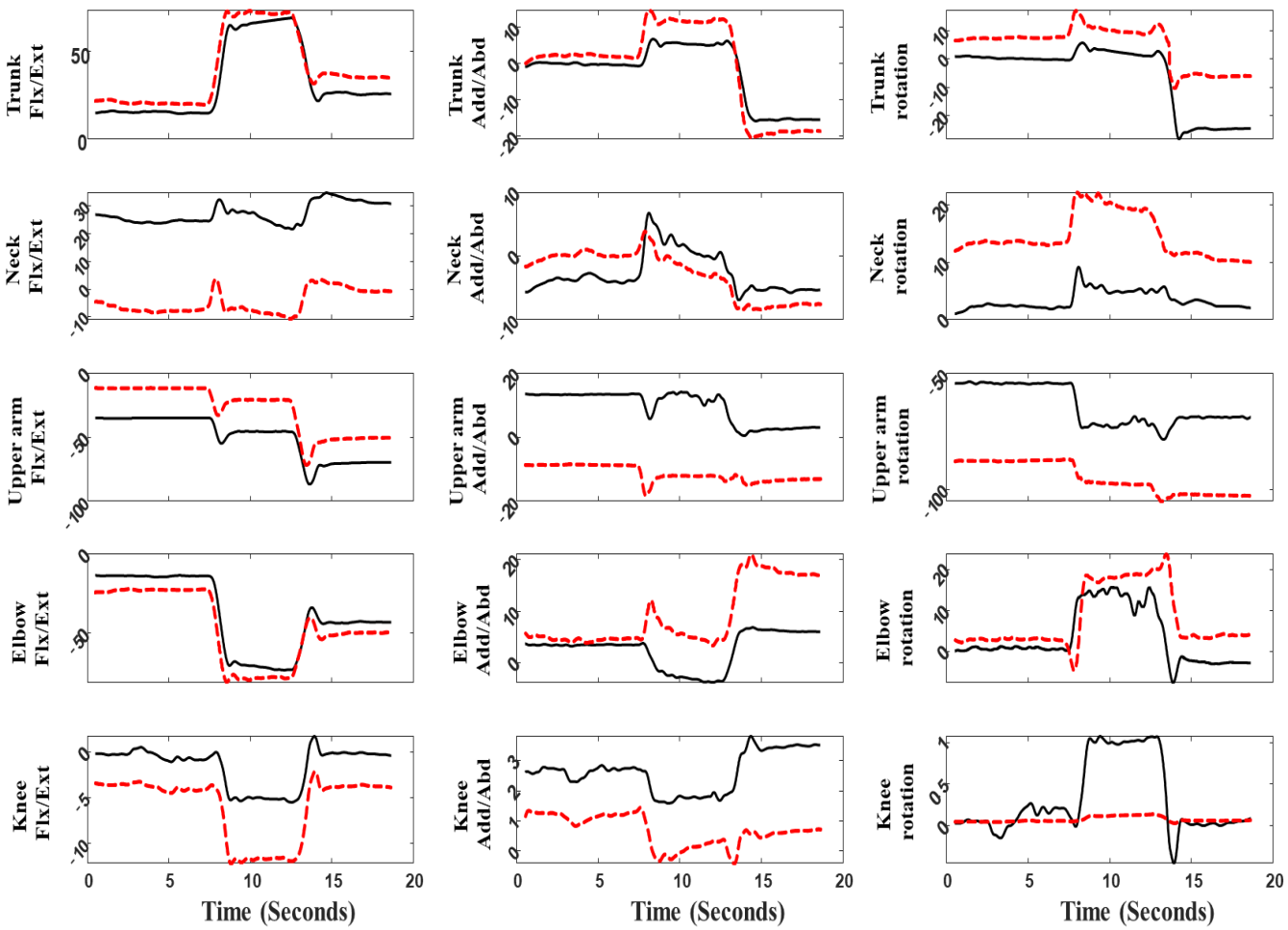

Figure A1: Joint angles (degrees) obtained from the marker-based system (3D joint angles) in sold black, IMU-based system (3D joint angles) in dashed red during the first trial of the manual material handling scenario 1 for participant 1. The joint angles for the trunk, neck, and right upper arm, right elbow, and right knee are presented.

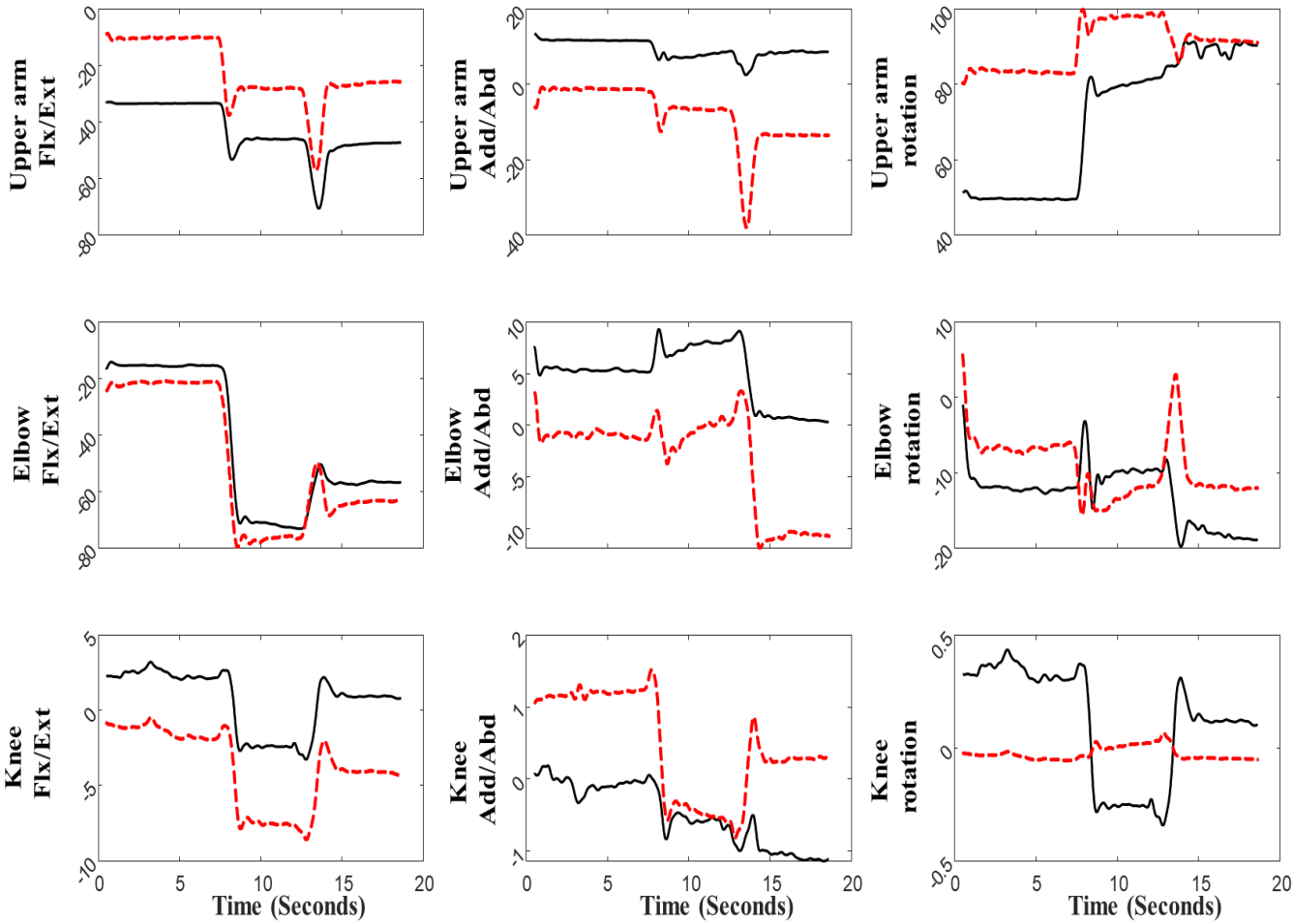

Figure A2: Joint angles (degrees) obtained from the marker-based system (3D joint angles) in sold black, IMU-based system (3D joint angles) in dashed red during the first trial of the manual material handling scenario 1 for 1 participant. The joint angles for left upper arm, left elbow, and left knee are presented.

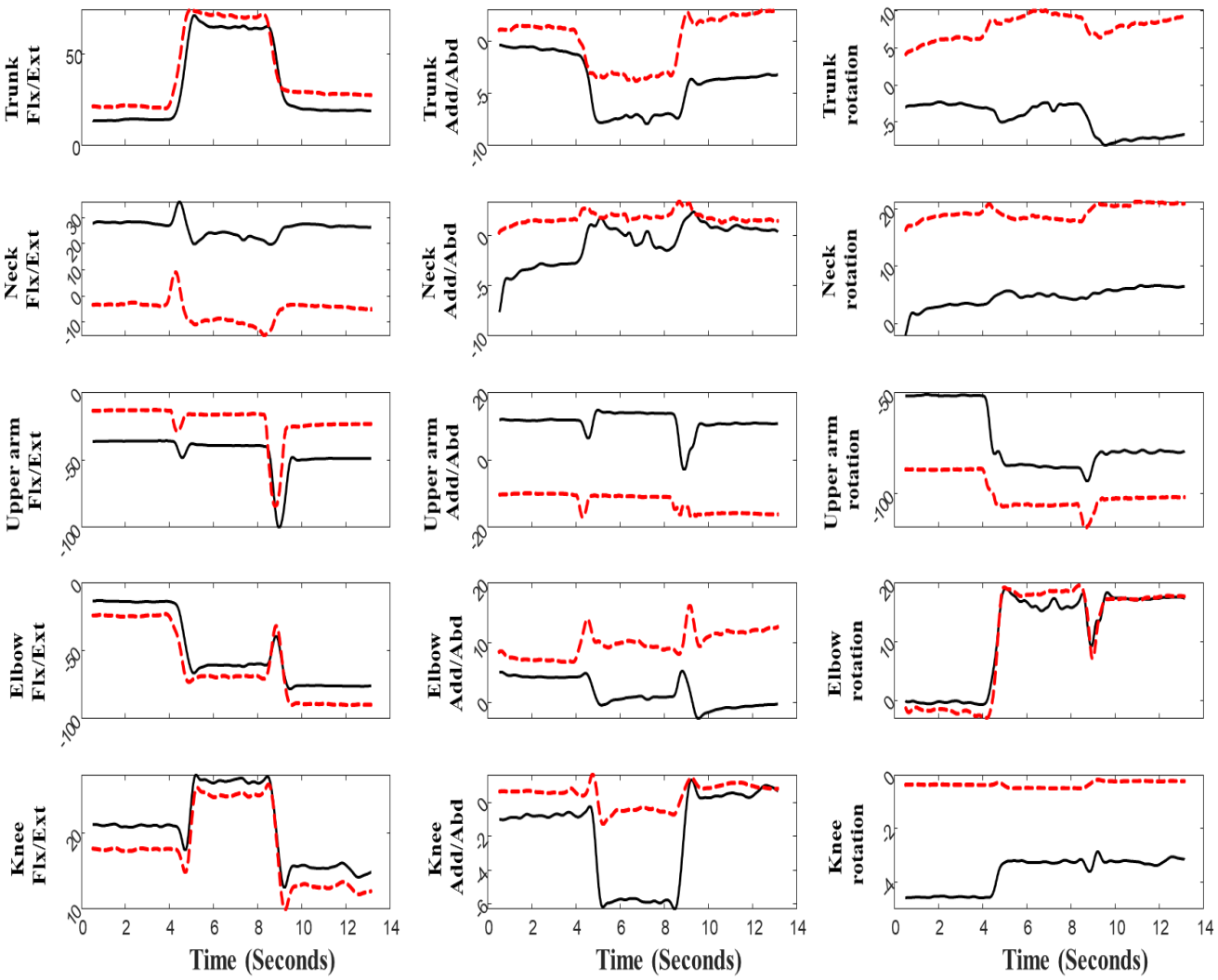

Figure A3: Joint angles (degrees) obtained from the marker-based system (3D joint angles) in sold black, IMU-based system (3D joint angles) in dashed red during the first trial of the manual material handling scenario 4 for participant 1. The joint angles for the trunk, neck, and right upper arm, right elbow, and right knee are presented.

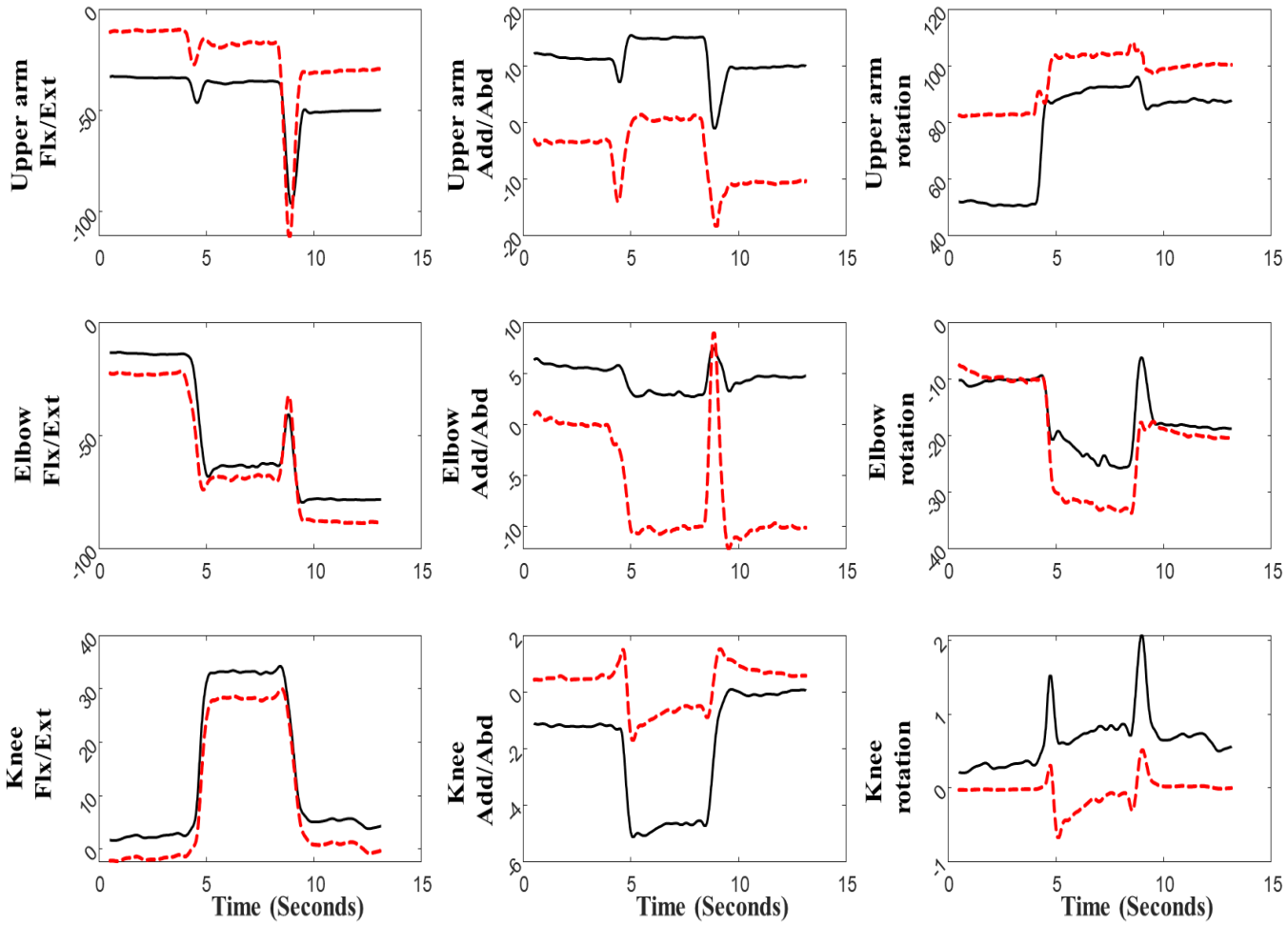

Figure A4: Joint angles (degrees) obtained from the marker-based system (3D joint angles) in sold black, IMU-based system (3D joint angles) in dashed red during the first trial of the manual material handling scenario 4 for 1 participant. The joint angles for the left upper arm left elbow, and the left knee are presented.

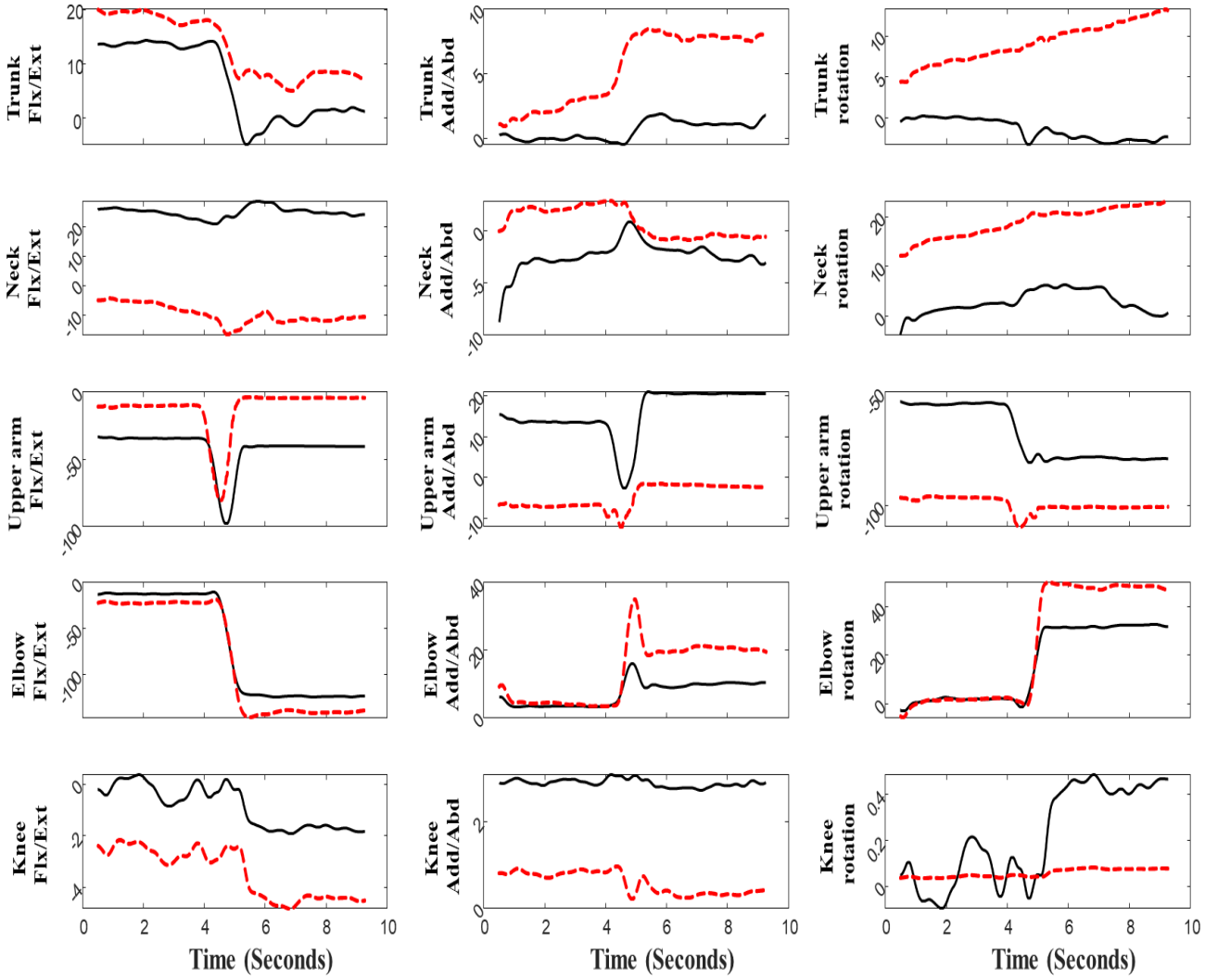

Figure A5: Joint angles (degrees) obtained from the marker-based system (3D joint angles) in sold black, IMU-based system (3D joint angles) in dashed red during the first trial of the manual material handling scenario 5 for participant 1. The joint angles for the trunk, neck, and right upper arm, right elbow, and right knee are presented.

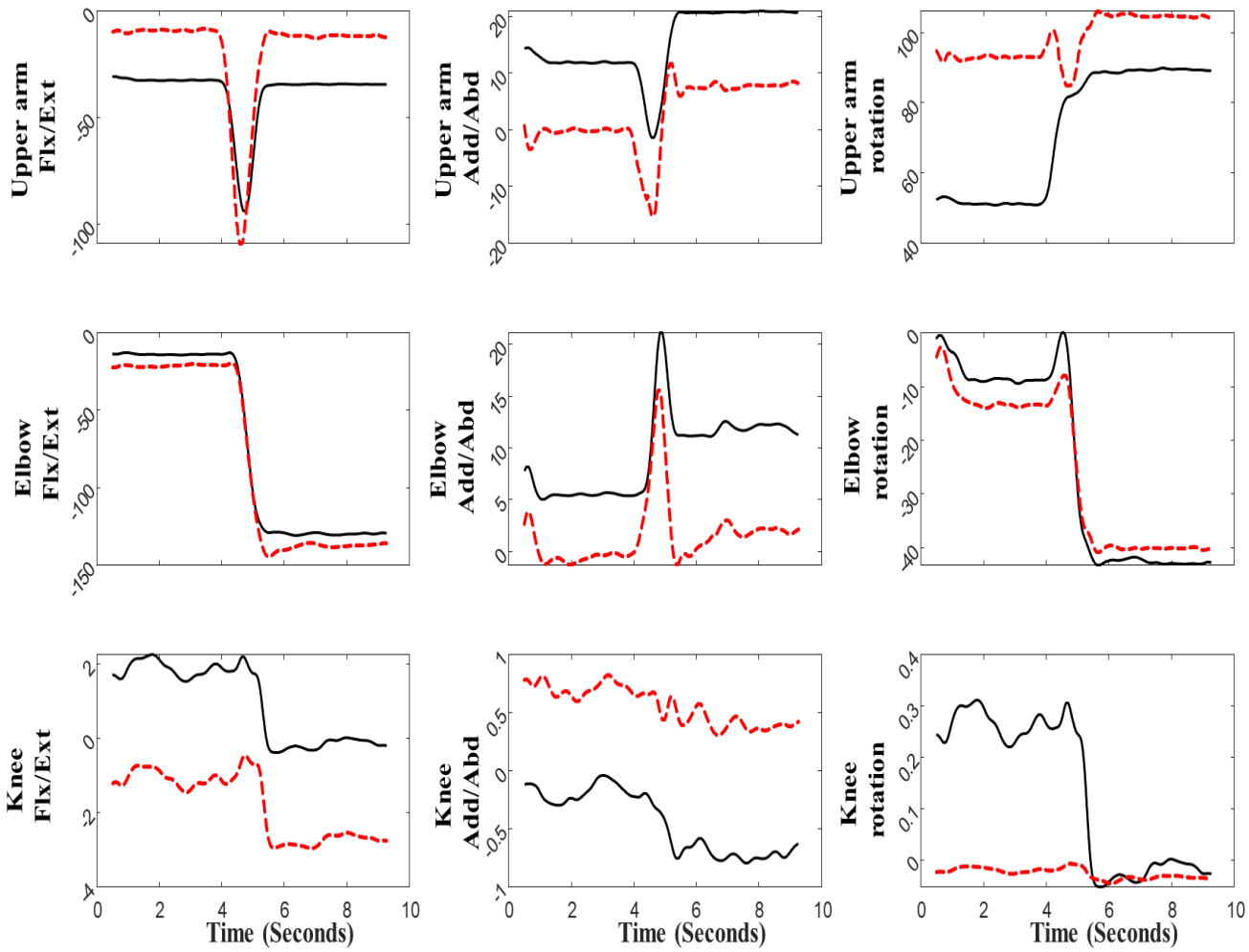

Figure A6: Joint angles (degrees) obtained from the marker-based system (3D joint angles) in sold black, IMU-based system (3D joint angles) in dashed red during the first trial of the manual material handling scenario 5 for 1 participant. The joint angles for the left upper arm left elbow, and left knee are presented.

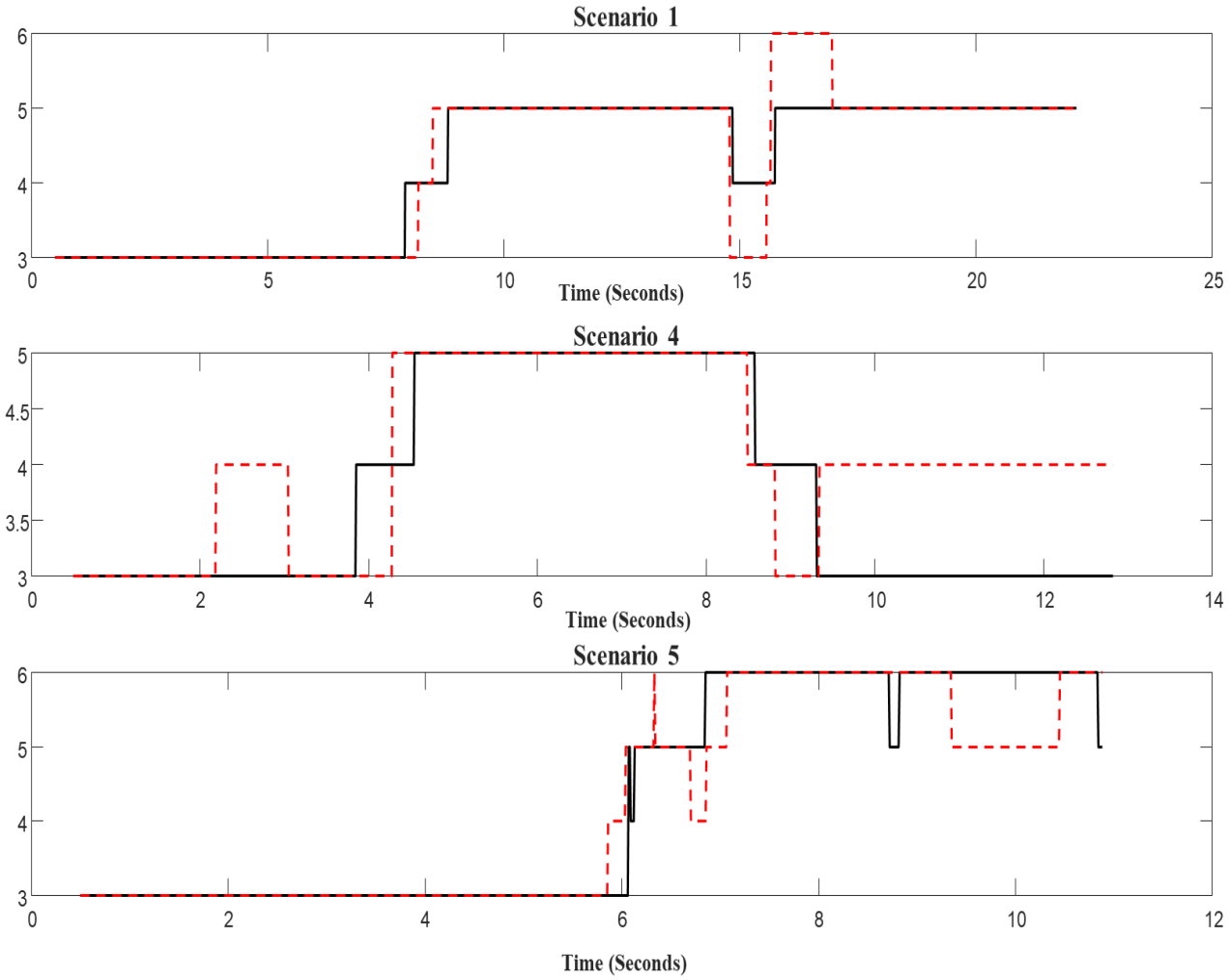

Figure A7: RULA scores obtained from the marker-based system (3D joint angles) in sold black, IMU-based system (3D joint angles) in dashed red during the first trial of the manual material handling scenarios (1, 4, and 5) for participant 1 right body side.

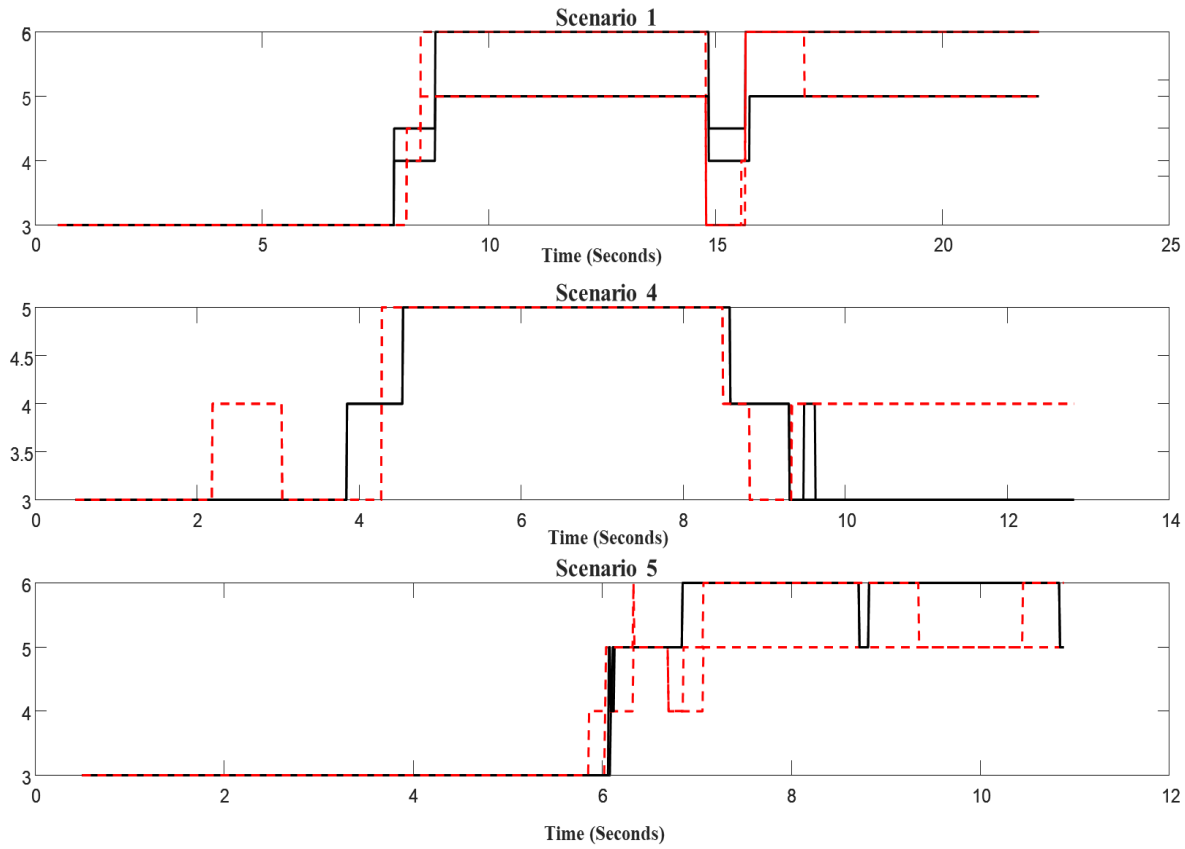

Figure A8: RULA scores obtained from the marker-based system (3D joint angles) in sold black, IMU-based system (3D joint angles) in dashed red during the first trial of the manual material handling scenarios (1, 4, and 5) for participant 1 left body side.

Appendix B: 2D joint angles for the IMU-based system and marker-less system.

Table B1 and Table B2 contain offset and the RMSE after removing the offset (the offset was calculated at the first 200 frames) for all joint angles and for all scenarios. Figure B1 to Figure B10 contains joint angles obtained from the marker-based system, IMU-based system, and marker-less system of the manual material handling. Figure B11 and Figure B12 contain RULA scores obtained from the marker-based system and IMU-based system and marker-less system during the manual material handling scenarios. Figure B13 illustrates RULA scores obtained from the marker-based system (2D joint angles) of the manual material handling scenarios (1 to 5) for 11 participants for left and right body side. This figures visually depicts the inter-participant variability of the recorded RULA scores. Figure B14 to figureB14 illustrate the comparison between the accuracy of the IMU-based system and marker-less system for joint angle measurement for all scenarios. The accuracy of each system was defined as its obtained RMSE against marker-based motion-capture system. The p-value for these comparisons are reported based on Friedman test.

Table B1. Offset and RMSE of the 2D joint angles in the comparison between Marker-based system and IMUs-based system presented in 50th (25th, 75th) percentile of the participants.

	Body side	Offset					RMSE				
		Scenario 1	Scenario 2	Scenario 3	Scenario 4	Scenario 5	Scenario 1	Scenario 2	Scenario 3	Scenario 4	Scenario 5
Neck Flex/Ext		10.7(6.2,17.0)	10.3(5.5,19.2)	11.4(5.2,16.5)	11.5(5.5,16.1)	10.1(5.6,15.0)	2.1(1.6,2.9)	3.1(2.2,4.4)	3.5(2.4,4.2)	2.7(2.2,3.7)	2.2(1.7,4.1)
Neck Lat Bend		3.3(1.6,5.2)	3.8(1.7,6.1)	2.5(1.3,5.0)	2.2(0.9,4.5)	2.9(1.4,4.9)	4.5(3.3,5.4)	7.4(4.4,8.5)	6.4(3.9,11.6)	3.5(2.2,7.4)	8.3(5.9,10.6)
Trunk Flex/Ext		1.7(0.9,2.9)	1.9(1.0,3.7)	1.5(0.6,3.7)	2.5(0.7,5.1)	2.1(1.1,3.5)	3.1(1.9,4.0)	3.2(2.6,6.1)	4.4(2.6,7.1)	3.3(2.4,4.1)	3.1(1.5,3.9)
Trunk Lat Bend		1.5(0.8,2.7)	1.6(0.4,2.8)	1.2(0.7,1.9)	2.6(0.7,3.7)	1.4(1.0,2.9)	3.4(2.8,4.4)	7.0(5.3,10.1)	1.8(1.3,2.9)	2.3(1.5,3.2)	1.4(0.8,2.4)
Trunk Rotation		1.9(0.8,3.0)	2.5(0.95,5.5)	1.6(0.6,2.2)	0.9(0.5,2.0)	0.9(0.5,1.9)	4.8(3.6,5.4)	10.9(7.8,12.9)	2.0(1.6,2.9)	2.6(2.0,4.4)	1.5(1.0,2.1)
Upper Arm Flex/Ext	Right	3.1(1.4,4.3)	3.9(0.7,5.4)	3.2(1.5,4.7)	3.3(1.8,4.4)	3.0(0.9,4.8)	3.9(2.7,5.3)	6.3(4.7,8.7)	5.8(4.0,8.8)	5.2(3.7,7.3)	5.8(3.5,7.5)
	Left	1.9(0.5,2.9)	1.7(1.0,3.2)	2.3(1.2,3.4)	2.4(1.0,3.8)	2.4(0.7,3.3)	3.0(2.4,4.4)	6.0(4.9,7.0)	5.2(3.7,7.0)	4.0(3.4,5.0)	3.7(2.5,6.3)
Upper Arm Add/Abd	Right	5.9(2.3,9.8)	6.3(2.0,8.7)	4.5(1.4,10.5)	4.1(1.5,10.3)	6.5(1.5,10.6)	4.6(3.2,6.4)	15.5(8.2,29.7)	9.7(6.5,19.8)	11.0(8.7,20.6)	15.0(9.1,26.8)
	Left	7.5(5.7,10.8)	8.1(6.9,10.8)	7.9(6.9,10.4)	8.0(7.6,12.7)	9.0(6.7,11.9)	4.3(2.7,7.2)	19.3(12.2,28.0)	10.0(7.6,24.3)	13.1(11.0,16.1)	13.8(7.8,24.7)
Upper Arm [a]	Right	4.1(2.3,7.9)	4.0(2.7,6.7)	4.5(2.3,7.9)	4.3(3.1,5.4)	3.9(2.2,6.4)	3.5(2.0,5.8)	5.0(4.3,7.0)	4.2(3.0,7.0)	3.6(3.1,7.1)	3.7(2.7,5.9)
	Left	6.1(3.2,7.2)	6.2(4.7, 8.6)	6.1(4.3,8.6)	6.9(3.0,8.8)	5.5(3.2,8.2)	2.8(1.8,6.4)	4.3(3.1,6.8)	4.2(3.0,6.3)	4.1(2.7,6.8)	2.9(1.9,5.0)
Lower Arm Add/Abd	Right	11.4(8.5,18.9)	12.0(7.3,17.6)	11.6(6.0,17.0)	9.2(7.4,16.1)	9.4(5.7,14.3)	4.3(2.7,7.6)	7.4(4.7,12.9)	10.0(6.9,23.5)	7.4(6.0,10.7)	12.5(10.8,15.9)
	Left	19.9(12.4,24.1)	17.2(11.6,21.1)	12.6(7.0,16.9)	18.4(11.4,26.6)	12.5(9.1,16.3)	5.7(3.4,9.6)	9.4(5.9,13.4)	12.7(7.6,21.0)	9.7(6.4,14.5)	16.6(12.6,19.3)
Elbow Flex/Ext	Right	28.8(22.1,30.7)	29.8(22.9,33.9)	26.3(22.3,30.8)	29.5(23.6,32.3)	29.9(25.1,33.5)	3.1(2.3,5.8)	4.3(3.0,7.7)	4.3(2.7,7.2)	3.7(3.0,6.7)	5.8(3.5,12.7)
	Left	24.9(21.2,26.9)	24.6(21.8,29.2)	23.3(21.6,28.0)	26.4(22.7,29.1)	27.0(24.4,29.5)	2.6(1.9,5.2)	4.3(2.8,6.9)	3.0(2.1,6.3)	3.1(2.2,7.7)	6.2(2.6,9.0)
Shoulder Add/Abd	Right	6.3(3.3,10.7)	8.9(4.2,12.5)	6.2(3.8,12.2)	6.6(4.3,13.1)	6.1(3.1,12.3)	4.8(3.3,6.9)	6.8(5.3,7.9)	6.3(3.6,8.5)	7.2(5.9,8.4)	3.8(2.3,10.2)
	Left	1.9(1.0,7.6)	1.6(0.6,6.7)	2.1(1.3,6.8)	2.8(1.2,7.5)	1.9(0.7,3.9)	2.6(2.0,3.4)	5.1(3.5,9.6)	5.7(4.1,8.2)	6.3(4.4,7.7)	8.3(4.2,10.9)
Knee Flex/Ext	Right	1.7(0.8,4.6)	3.0(1.5,6.4)	2.8(1.6,5.8)	3.6(2.3,6.9)	2.2(1.3,6.8)	3.6(2.4,4.89)	3.6(2.3,4.6)	5.1(3.4,7.2)	3.0(1.5,3.9)	1.2(0.6,2.1)
	Left	1.8(0.7,5.0)	2.3(1.0,5.6)	3.0(1.1,5.8)	4.0(1.7,5.9)	2.6(1.2,6.1)	4.0(2.3,6.1)	3.8(2.3,7.1)	3.8(2.8,6.5)	2.1(1.8,3.1)	1.5(0.7,2.0)

[a] Angle between the Upper-arm vector and the Trunk vector without projection.

Table B2. Offset and RMSE of the 2D joint angles in the comparison between Marker-based system and Microsoft Kinect presented in 50th (25th, 75th) percentile of the participants.

	Body Side	Offset					RMSE				
		Scenario 1	Scenario 2	Scenario 3	Scenario 4	Scenario 5	Scenario 1	Scenario 2	Scenario 3	Scenario 4	Scenario 5
Neck Flex/Ext		25.8(27.9,33.7)	28.5(32.6,37.1)	28.4(32.8,36.7)	29.9(33.1,39.6)	27.3(31.5,37.6)	3.7(2.7,5.7)	11.5(7.2,15.2)	16.2(11.0,27.9)	13.0(7.8,15.5)	17.0(13.8,21.1)
Neck Lat Bend		1.4(3.7,5.5)	9.4(11.5,15.7)	2.2(5.3,9.4)	1.8(3.6,5.5)	1.9(4.7,8.7)	8.9(6.4,14.6)	12.9(9.4,15.7)	12.7(8.0,15.5)	8.3(5.9,9.7)	11.3(6.6,16.5)
Trunk Flex/Ext		2.7(4.8,5.7)	0.6(2.0,3.0)	2.7(3.8,5.4)	2.2(3.5,4.0)	2.4(3.6,4.1)	13.0(10.2,16.8)	12.6(11.1,13.9)	18.5(13.3,32.2)	11.5(10.0,15.5)	2.7(1.2,3.9)
Trunk Lat Bend		1.1(2.2,3.9)	0.7(1.8,3.0)	0.5(1.2,2.1)	0.6(1.3,2.3)	0.6(1.4,2.2)	6.9(5.3,9.3)	16.8(13.7,20.5)	5.7(2.9,9.7)	2.9(1.6,3.8)	2.1(1.5,2.8)
Trunk Rotation		1.2(2.0,3.4)	0.7(2.0,3.6)	0.3(0.8,1.5)	0.9(1.8,2.2)	0.7(1.1,1.9)	11.1(7.3,15.6)	20.4(25.1,17.7)	7.1(3.9,12.8)	3.1(2.0,5.9)	2.2(1.6,3.3)
Upper Arm Flex/Ext	Right	0.5(2.3,5.6)	1.8(3.4,5.0)	2.6(4.8,7.1)	3.9(4.9,6.4)	4.3(6.1,7.5)	13.2(10.7,15.1)	17.1(13.7,22.3)	29.1(15.6,41)	17.3(12.5,22.0)	28.7(23.0,32.1)
	Left	0.9(2.2,3.8)	0.9(2.6,5.1)	1.7(3.6,6.2)	1.9(3.6,6.4)	2.7(6.6,10.5)	12.3(10.4,15.2)	21.4(16.2,25.5)	25.5(13.9,39.4)	17.9(14.2,21.7)	24.9(29.1,32.6)
Upper Arm Add/Abd	Right	1.8(4.8,8.8)	11.0(15.2,17.3)	2.7(4.4,7.6)	2.9(4.5,6.5)	2.1(4.2,6.1)	11.5(8.9,15.5)	23.0(18.6,33.0)	39.9(18.3,49.0)	34.2(25.7,41.5)	31.4(28.0,36.0)
	Left	10.8(13.7,16.6)	3.0(6.6,8.1)	2.0(5.0,7.5)	1.6(3.7,6.2)	1.9(3.8,9.4)	8.5(6.3,13.3)	38.9(26.7,48.4)	36.2(18.6,52.8)	33.7(24.7,40.7)	27.3(29.7,33.3)
Upper Arm[a]	Right	2.4(5.4,9.2)	10.4(12.9,15.4)	2.1(4.8,7.8)	2.4(5.1,7.1)	1.8(5.2,7.0)	10.8(8.4,12.7)	12.6(10.9,14.8)	23.0(13.9,35.4)	15.7(12.6,18.1)	25.9(21.1,28.6)
	Left	10.3(12.4,15.8)	2.0(5.3,8.2)	1.4(5.0,8.0)	1.5(3.9,8.1)	2.9(6.3,11.3)	7.6(6.1,9.7)	22.8(16.0,27.4)	20.3(11.7,33.2)	14.9(12.9,16.8)	20.8(25.0,28.3)
Lower Arm Add/Abd	Right	5.4(9.2,15.0)	3.0(6.1,9.2)	5.2(10.1,13.1)	7.3(10.1,13.3)	6.7(9.6,13.5)	21.2(15.8,26.3)	21.7(16.0,28.3)	15.1(10.7,23.8)	11.9(10.4,14.5)	16.1(11.8,19.5)
	Left	5.8(11.2,19.0)	3.0(8.6,12.8)	5.4(10.7,15.2)	7.6(9.9,16.4)	3.9(8.6,13.9)	17.2(14.4,19.0)	22.5(16.5,28.8)	15.6(10.2,29.7)	10.2(7.7,13.4)	9.1(11.8,14.8)
Elbow Flex/Ext	Right	11.1(16.6,26.9)	6.5(10.5,16.5)	13.7(17.5,23.4)	15.8(19.1,28.1)	10.9(14.8,20.3)	19.2(14.7,22.5)	17.9(14.3,21.7)	15.1(10.7,23.8)	9.7(8.6,12.8)	16.8(14.0,20.0)
	Left	4.8(8.9,14.4)	12.4(16.4,21.2)	10.3(15.7,25.0)	10.0(13.6,23.1)	11.2(13.5,22.5)	16.0(13.6,21.6)	22.2(15.4,26.8)	15.1(9.9,35.2)	10.5(8.6,13.1)	12.4(15.4,19.1)
Shoulder Add/Abd	Right	2.4(5.2,8.6)	4.6(6.1,8.0)	3.1(5.5,8.3)	4.1(6.6,8.9)	4.0(5.4,9.2)	7.8(6.1,11.1)	10.4(7.5,12.4)	11.3(8.0,15.3)	9.1(7.6,10.9)	5.5(3.8,9.9)
	Left	1.0(4.0,6.7)	1.7(4.8,7.5)	2.3(4.5,9.1)	2.3(3.4,6.2)	1.6(2.5,5.1)	8.2(6.6,11.1)	8.9(5.9,12.2)	11.9(8.7,16.9)	8.2(4.9,10.2)	4.6(7.3,12.9)
Knee Flex/Ext	Right	1.4(4.5,9.5)	1.5(3.0,4.6)	1.5(3.3,6.4)	1.8(4.0,6.7)	2.0(4.8,6.9)	8.0(4.9,16.3)	13.4(12.0,17.2)	28.1(23.5,47.6)	17.5(15.6,22.3)	1.7(1.1,2.5)
	Left	2.2(4.5,7.4)	2.0(3.7,7.0)	1.3(3.7,5.5)	2.1(3.7,7.2)	1.8(4.4,8.4)	6.7(5.0,11.6)	16.7(12.8,22.0)	26.0(22.6,39.3)	14.8(11.6,18.9)	1.2(2.1,4.5)

[a] Angle between the Upper-arm vector and the Trunk vector without projection.

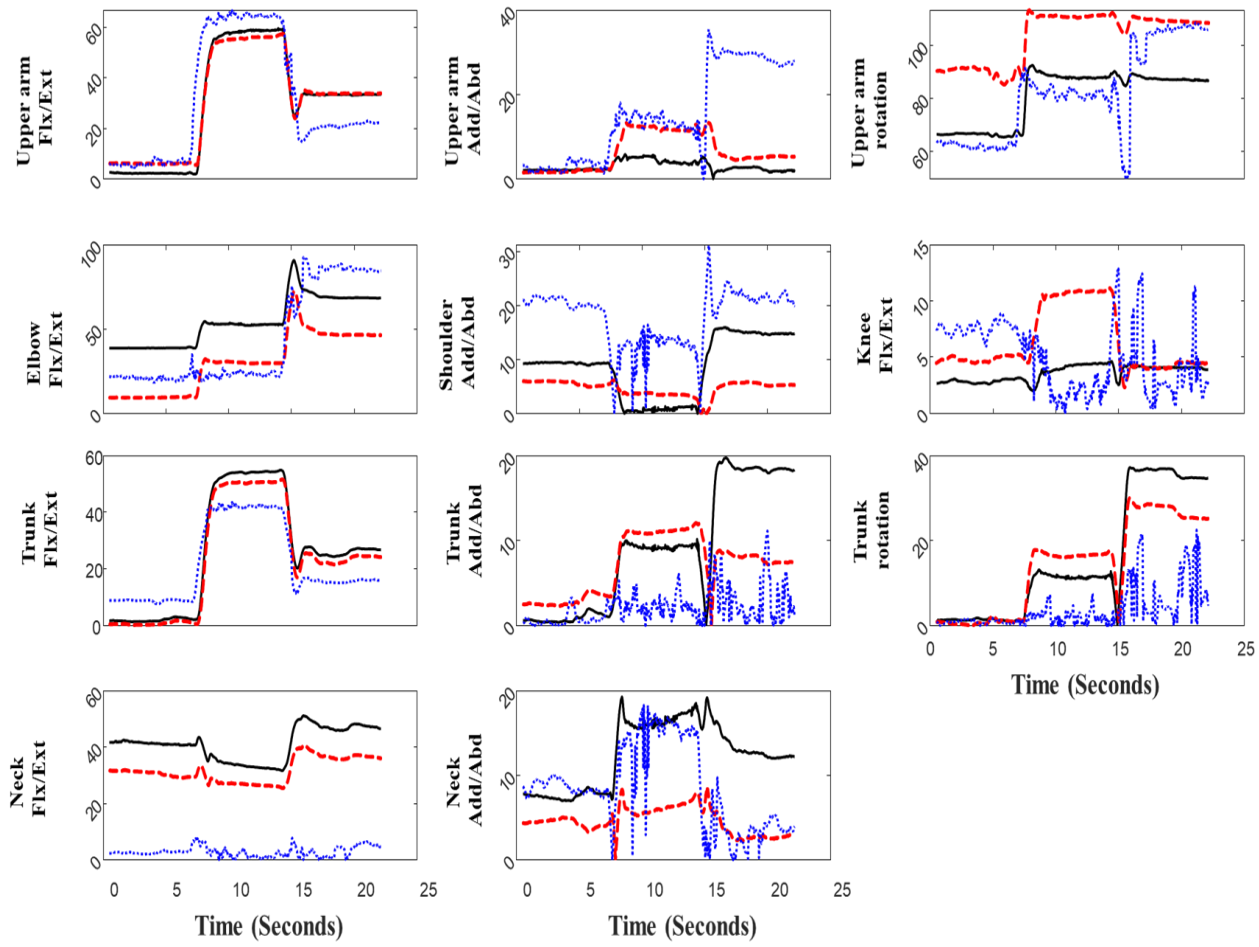

Figure B1: Joint angles (degrees) obtained from the marker-based system (2D joint angles) in sold black, IMUs-based system (2D joint angles) in dashed red, and marker-less system in dashed blue during the first trial of the manual material handling scenario 1 for participant 1. The joint angles for the trunk, neck, and right upper arm, right elbow, and right shoulder, and right knee are presented.

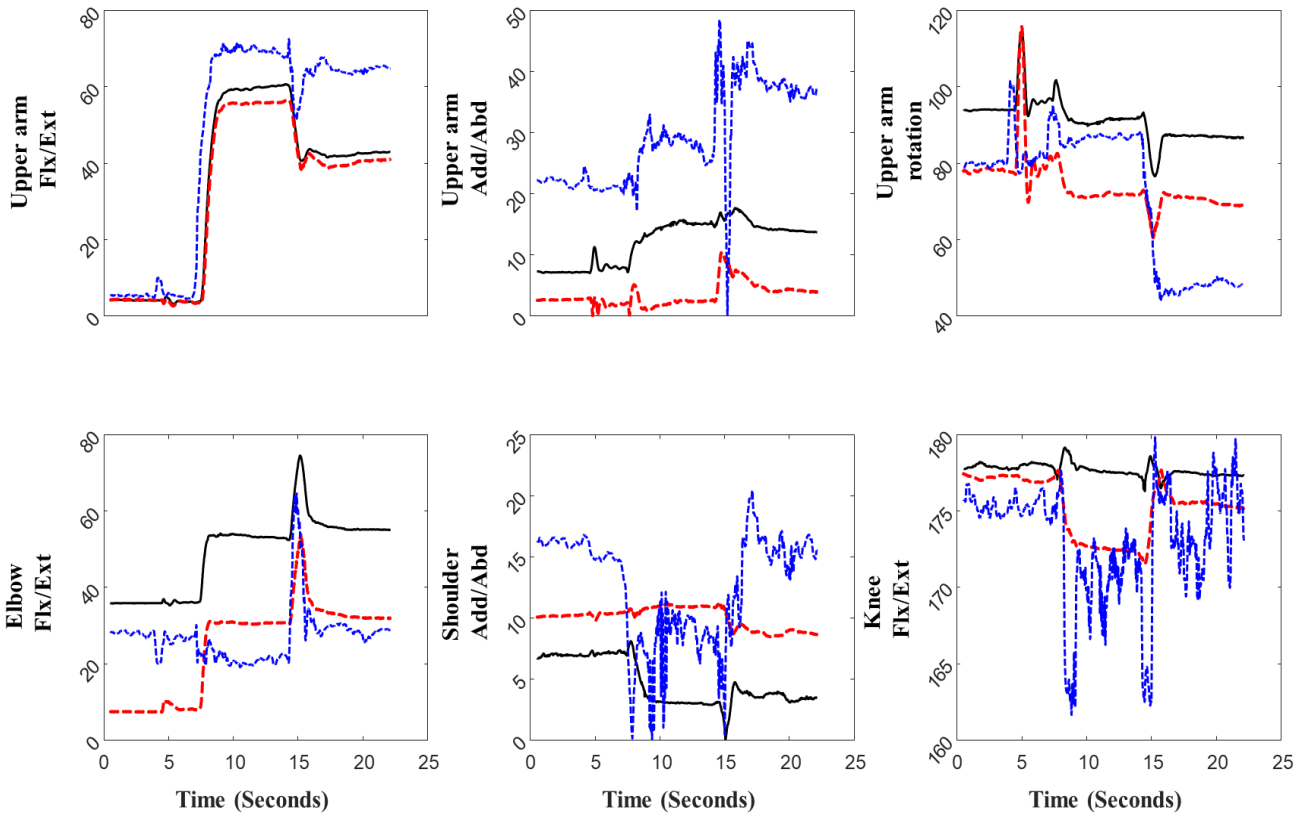

Figure B2: Joint angles (degrees) obtained from the marker-based system (2D joint angles) in sold black, IMUs-based system (2D joint angles) in dashed red, and marker-less system in dashed blue during the first trial of the manual material handling scenario 1 for 1 participant. The joint angles for left upper arm, left elbow, left shoulder, and left knee are presented. .

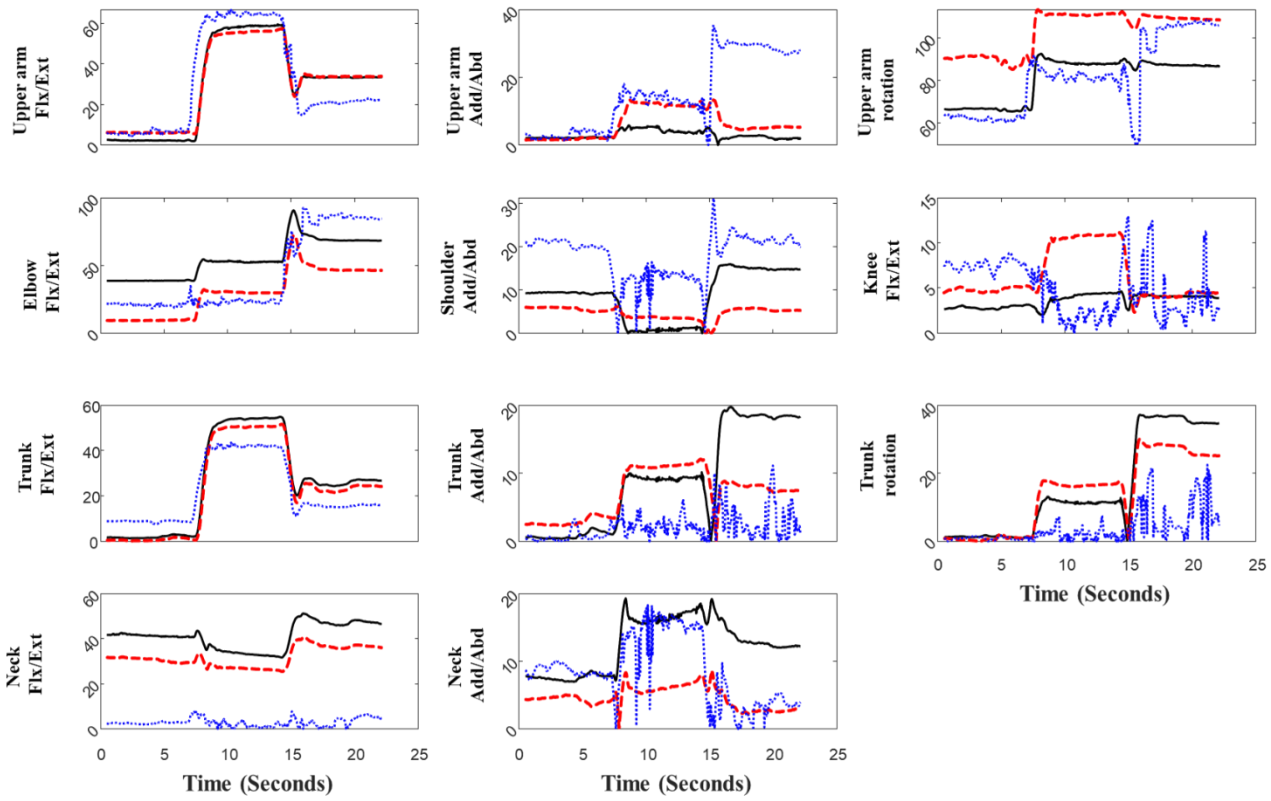

Figure B3: Joint angles (degrees) obtained from the marker-based system (2D joint angles) in sold black, IMUs-based system (2D joint angles) in dashed red, and marker-less system in dashed blue during the first trial of the manual material handling scenario 2 for participant 1. The joint angles for trunk, neck, and right upper arm, shoulder, elbow, and knee.

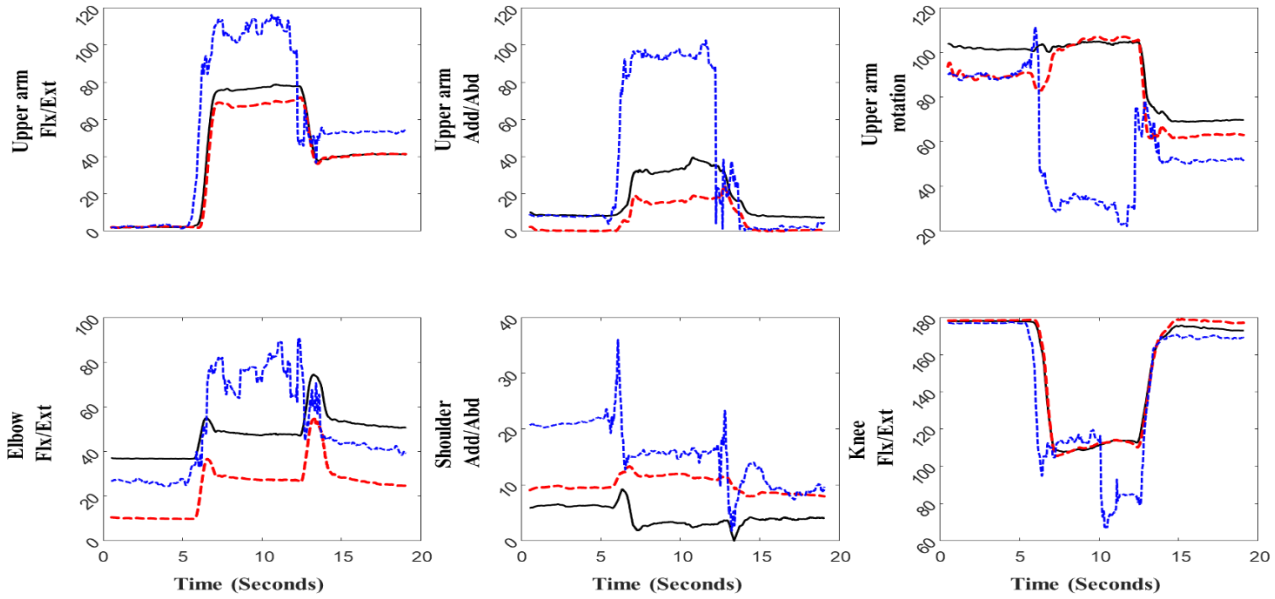

Figure B4: Joint angles (degrees) obtained from the marker-based system (2D joint angles) in sold black, IMU-based system (2D joint angles) in dashed red, and marker-less system in dashed blue during the first trial of the manual material handling scenario 2 for 1 participant. The joint angles for left upper arm, left elbow, left shoulder, and left knee are presented

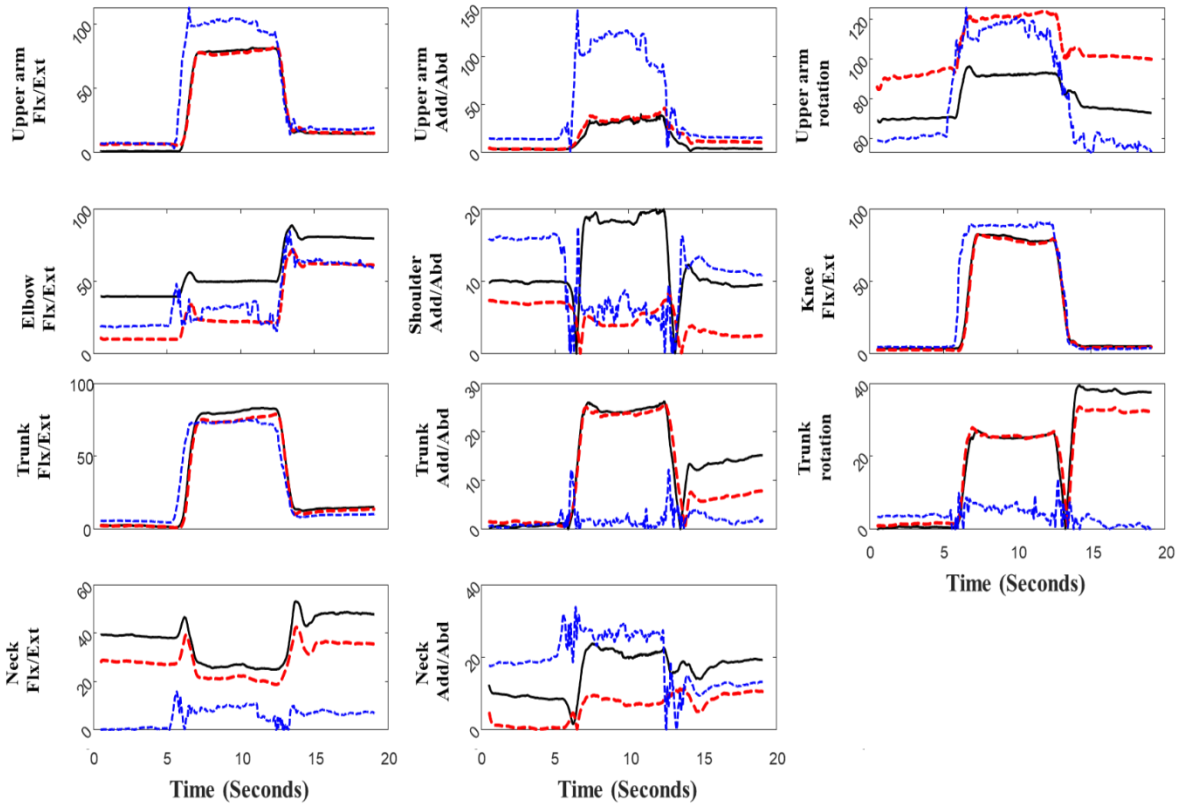

Figure B5: Joint angles (degrees) obtained from the marker-based system (2D joint angles) in sold black, IMU-based system (2D joint angles) in dashed red, and marker-less system in dashed blue during the first trial of the manual material handling scenario 3 for participant 1. The joint angles for trunk, neck, and right upper arm, right elbow, and right shoulder, and right knee are presented.

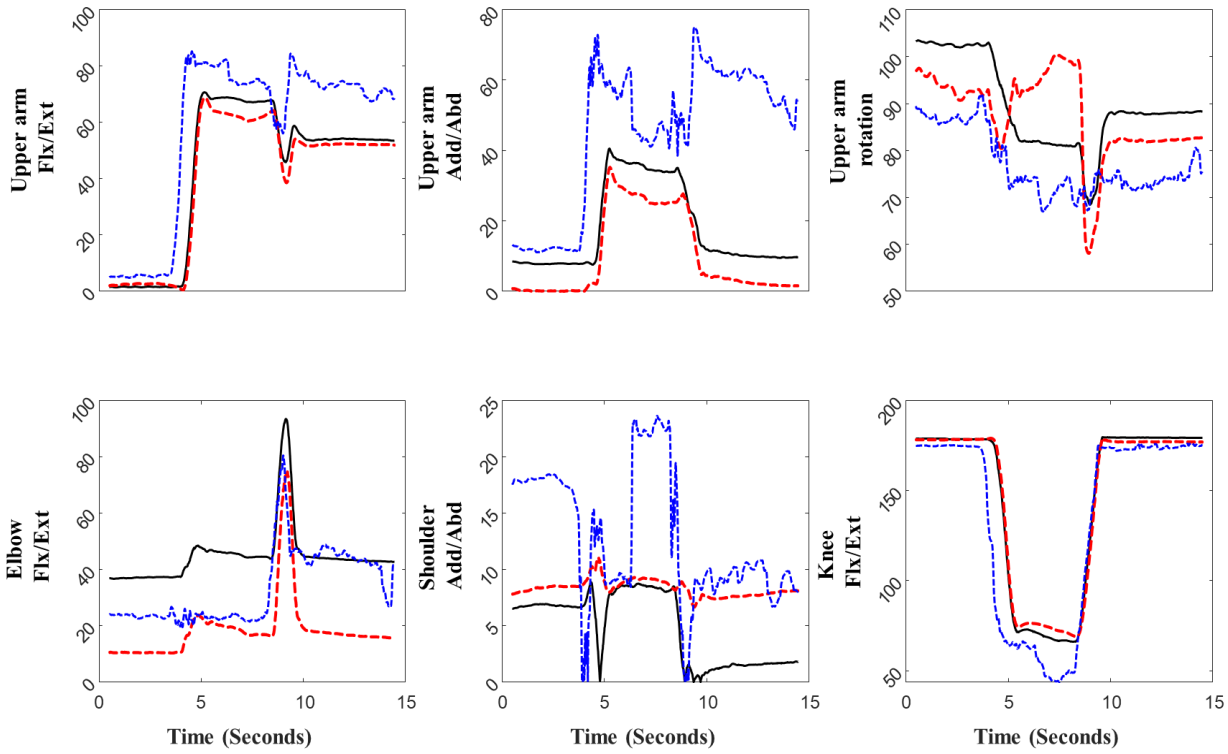

Figure B6: Joint angles (degrees) obtained from the marker-based system (2D joint angles) in sold black, IMU-based system (2D joint angles) in dashed red, and marker-less system in dashed blue during the first trial of the manual material handling scenario 3 for 1 participant. The joint angles for left upper arm, left elbow, left shoulder, and left knee are presented

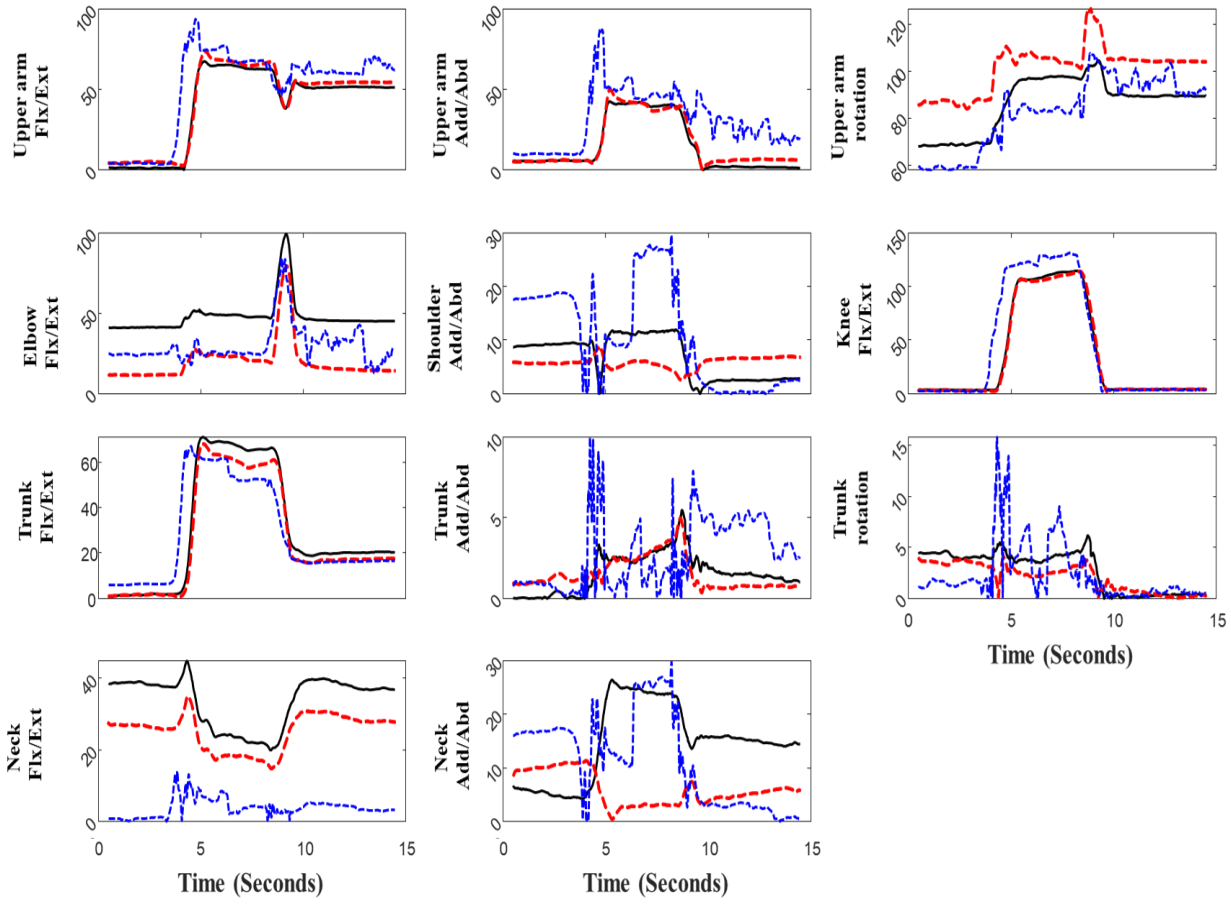

Figure B7: Joint angles (degrees) obtained from the marker-based system (2D joint angles) in sold black, IMU-based system (2D joint angles) in dashed red, and marker-less system in dashed blue during the first trial of the manual material handling scenario 4 for participant 1. The joint angles for trunk, neck, and right upper arm, right elbow, and right shoulder, and right knee are presented.

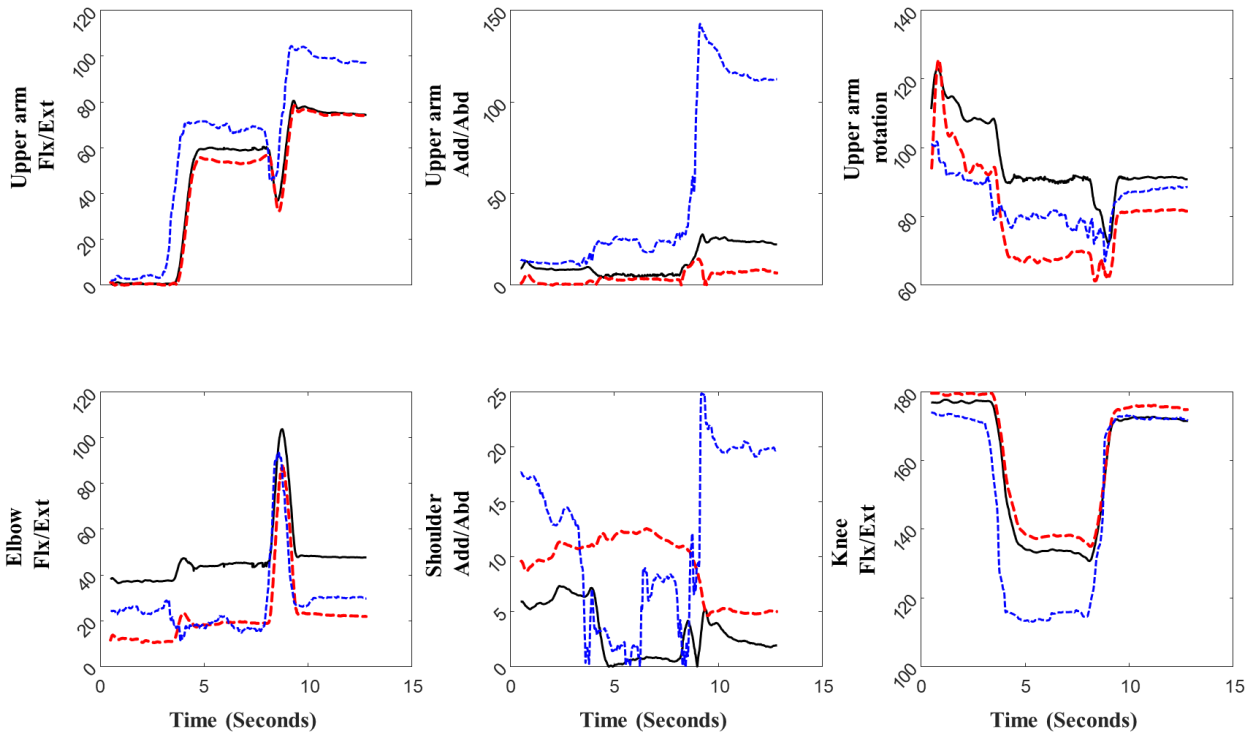

Figure B8: Joint angles (degrees) obtained from the marker-based system (2D joint angles) in sold black, IMU-based system (2D joint angles) in dashed red, and marker-less system in dashed blue during the first trial of the manual material handling scenario 4 for 1 participant. The joint angles for left upper arm, left elbow, left shoulder, and left knee are presented

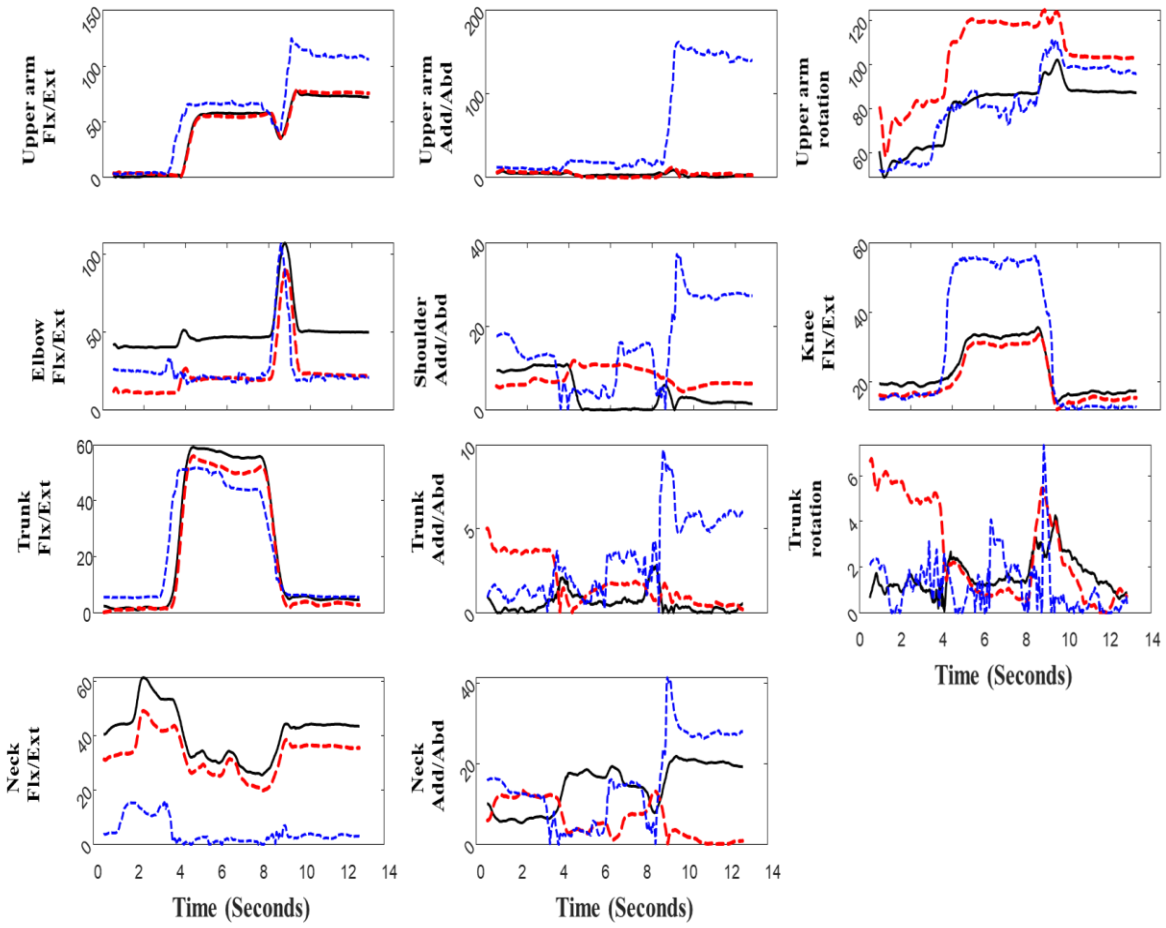

Figure B9: Joint angles (degrees) obtained from the marker-based system (2D joint angles) in sold black, IMU-based system (2D joint angles) in dashed red, and marker-less system in dashed blue during the first trial of the manual material handling scenario 5 for participant 1. The joint angles for trunk, neck, and right upper arm, right elbow, and right shoulder, and right knee are presented.

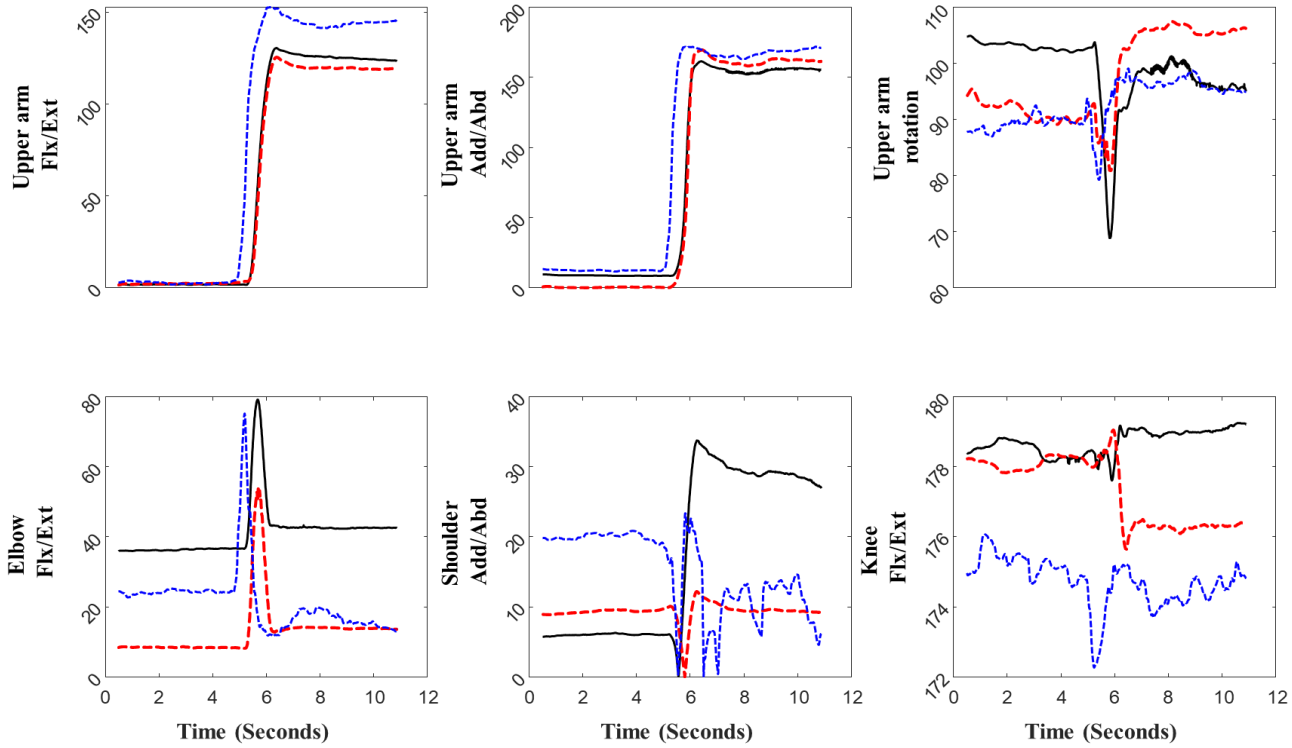

Figure B10: Joint angles (degrees) obtained from the marker-based system (2D joint angles) in sold black, IMU-based system (2D joint angles) in dashed red, and marker-less system in dashed blue during the first trial of the manual material handling scenario 5 for 1 participant. The joint angles for left upper arm, left elbow, left shoulder, and left knee are presented

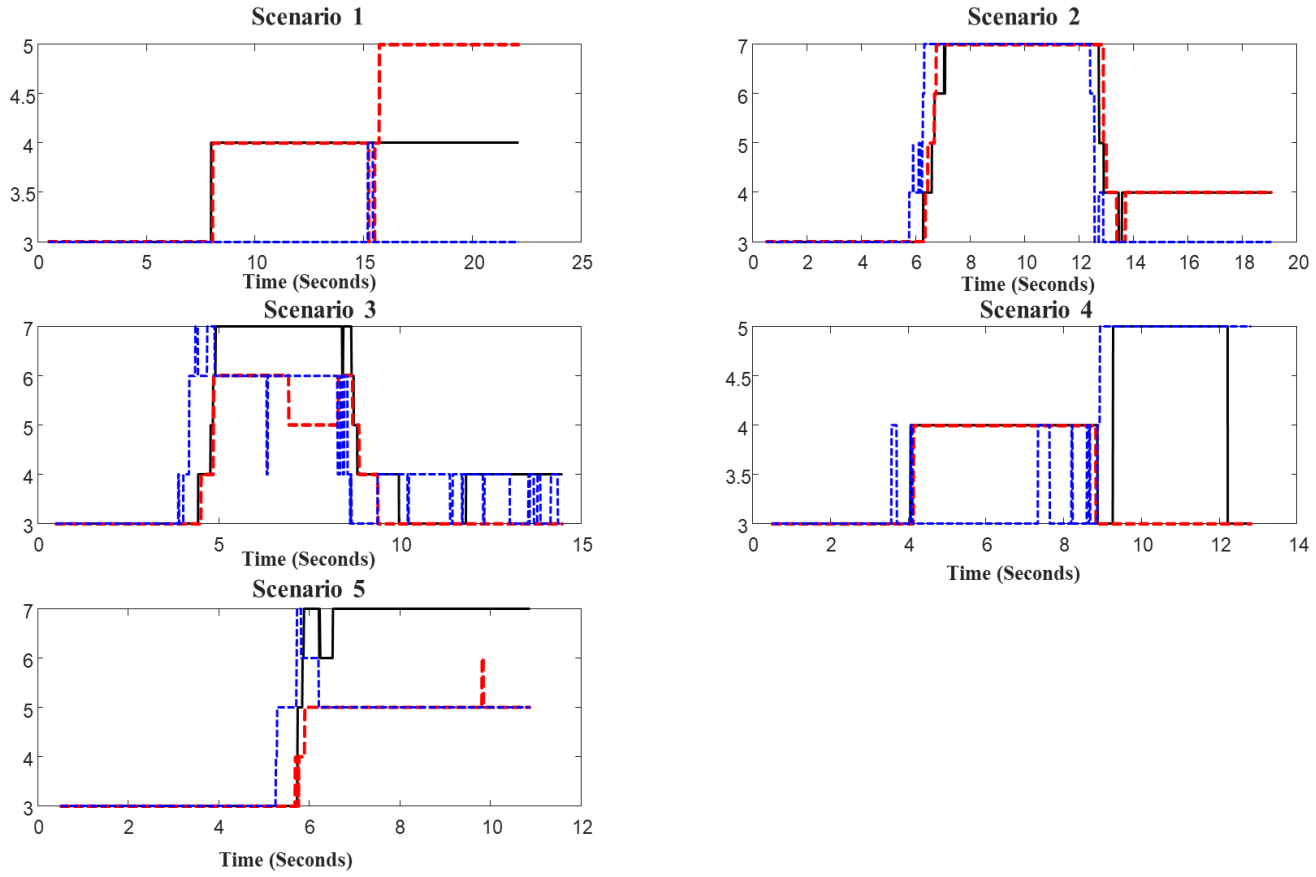

Figure B11: RULA scores obtained from the marker-based system (2D joint angles) in sold black, IMU-based system (2D joint angles) in dashed red, and marker-less system (2D joint angles) in dashed blue during the first trial of the manual material handling scenarios (1 to 5) for participant 1 right body side.

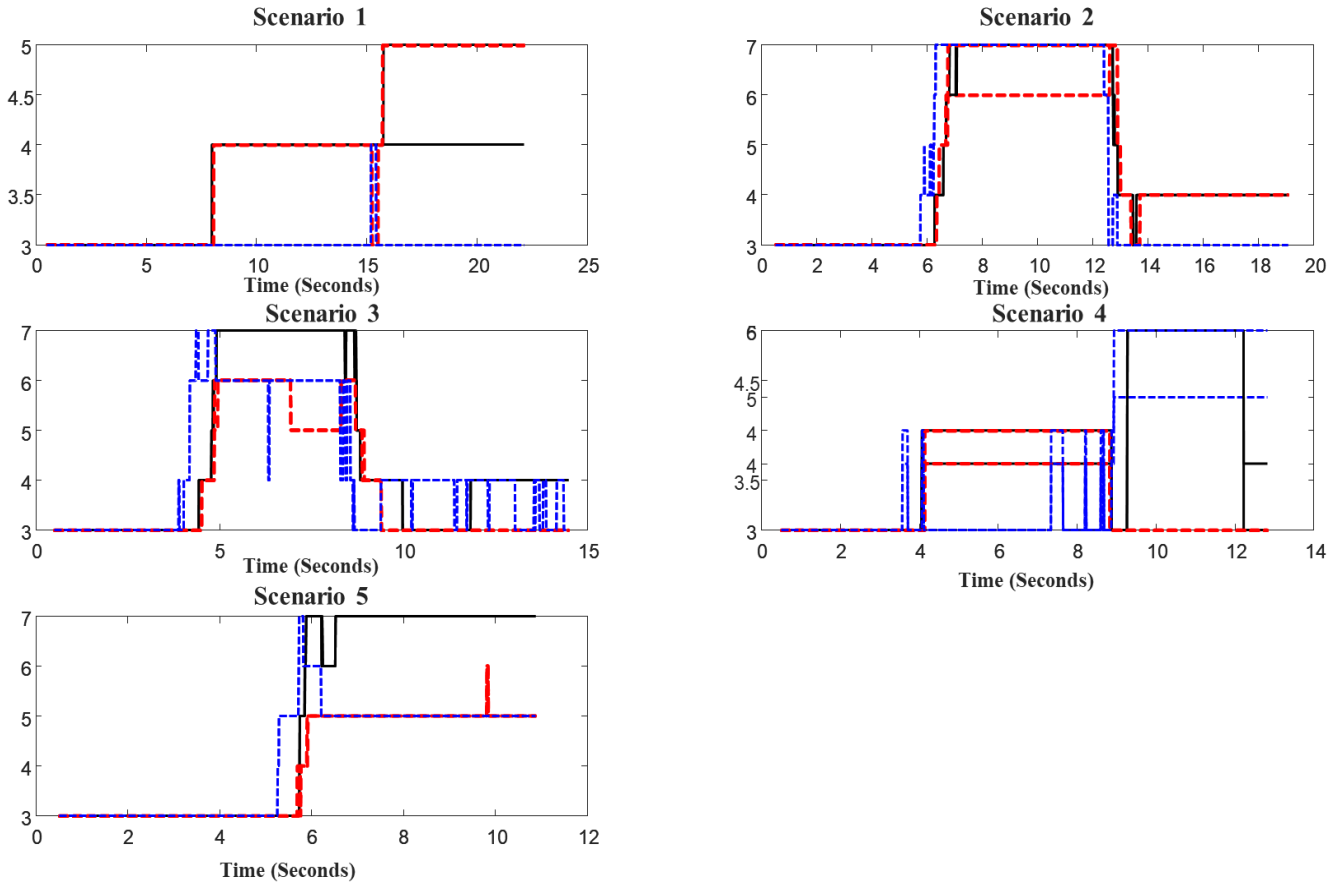

Figure B12: RULA scores obtained from the marker-based system (2D joint angles) in sold black, IMU-based system (2D joint angles) in dashed red, and marker-less system (2D joint angles) in dashed blue during the first trial of the manual material handling scenarios (1 to 5) for participant 1 left body side.

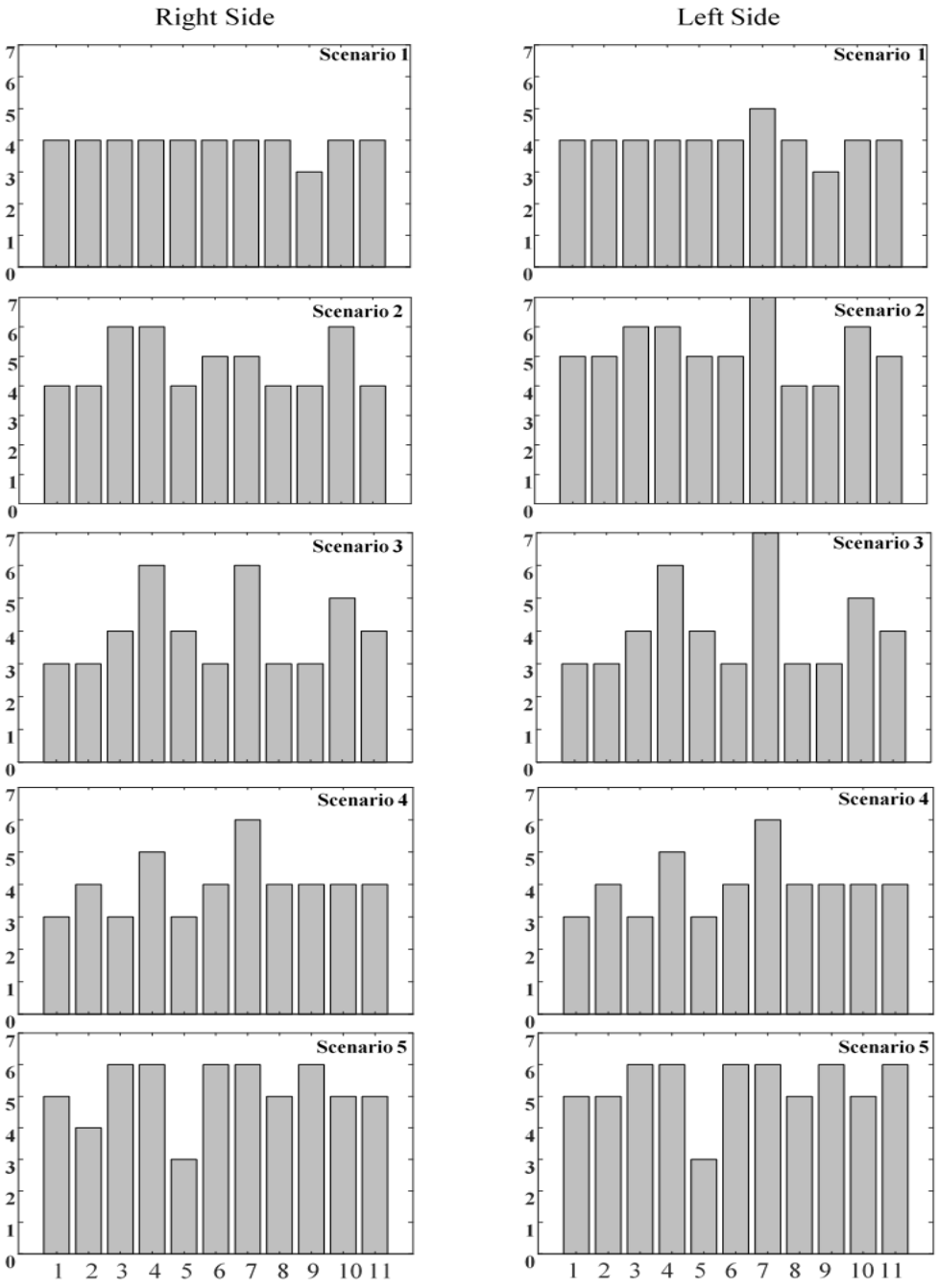

Figure B13: RULA scores (median among trial for each participant) obtained from the marker-based system (2D joint angles) of the manual material handling scenarios (1 to 5) for 11 participants for left and right body side.

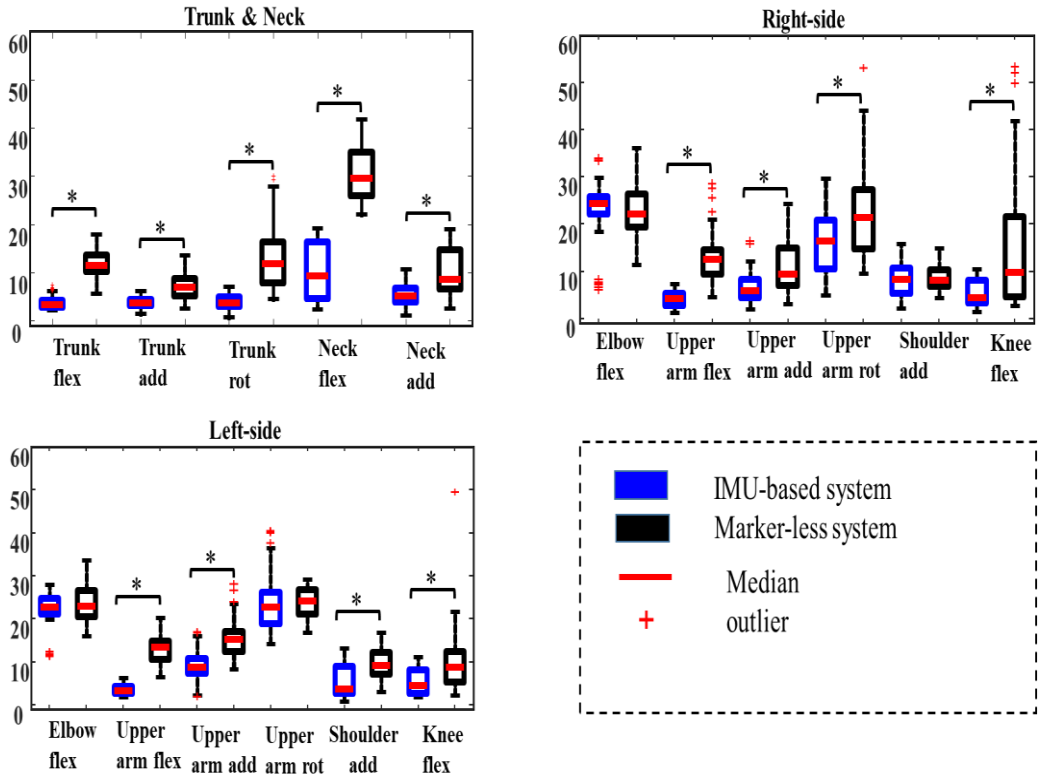

Figure B14: Comparison between the accuracy of the IMU-based system and marker-less system for joint angle measurement in scenario 1. The accuracy of each system was defined as its obtained RMSE against marker-based motion-capture system. The p-value for these comparisons are reported based on Friedman test (* if significant, with a significance level of 5%).

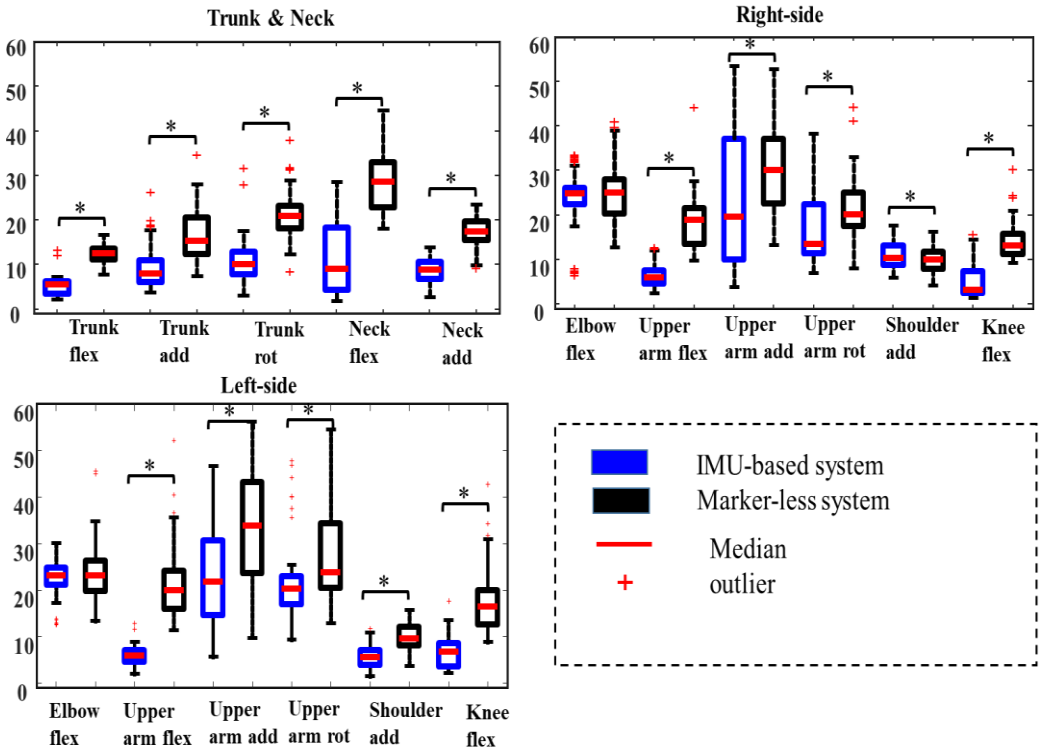

Figure B15: Comparison between the accuracy of the IMU-based system and marker-less system for joint angle measurement in scenario 2. The accuracy of each system was defined as its obtained RMSE against marker-based motion-capture system. The p-value for these comparisons are reported based on Friedman test (* if significant, with a significance level of 5%).

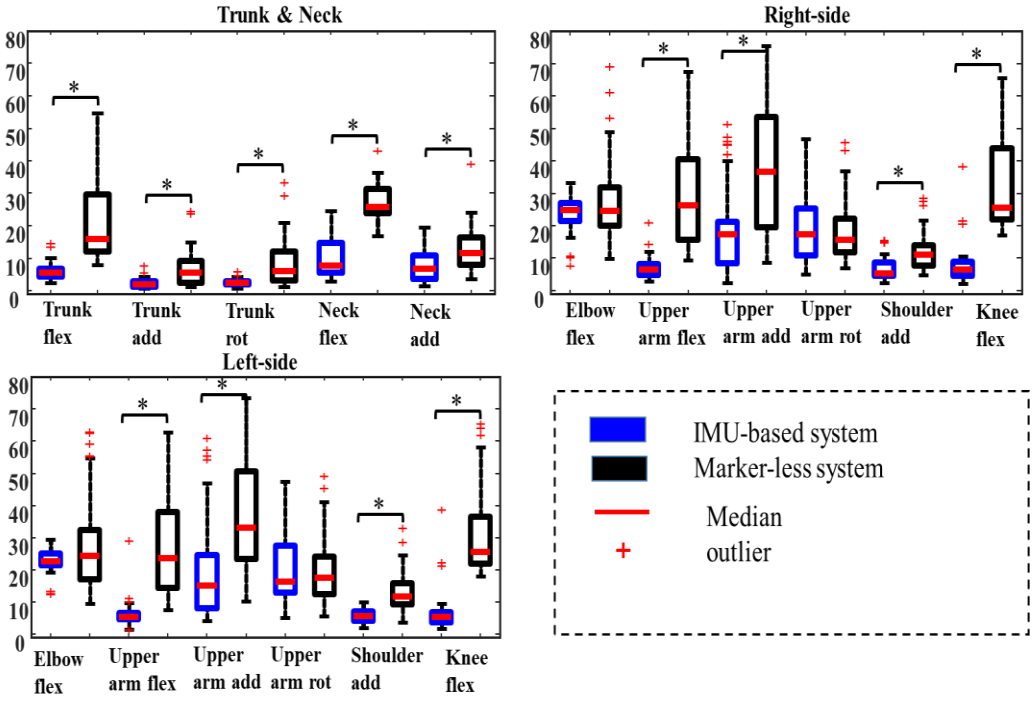

Figure B16: Comparison between the accuracy of the IMU-based system and marker-less system for joint angle measurement in scenario 3. The accuracy of each system was defined as its obtained RMSE against marker-based motion-capture system. The p-value for these comparisons are reported based on Friedman test (* if significant, with a significance level of 5%).

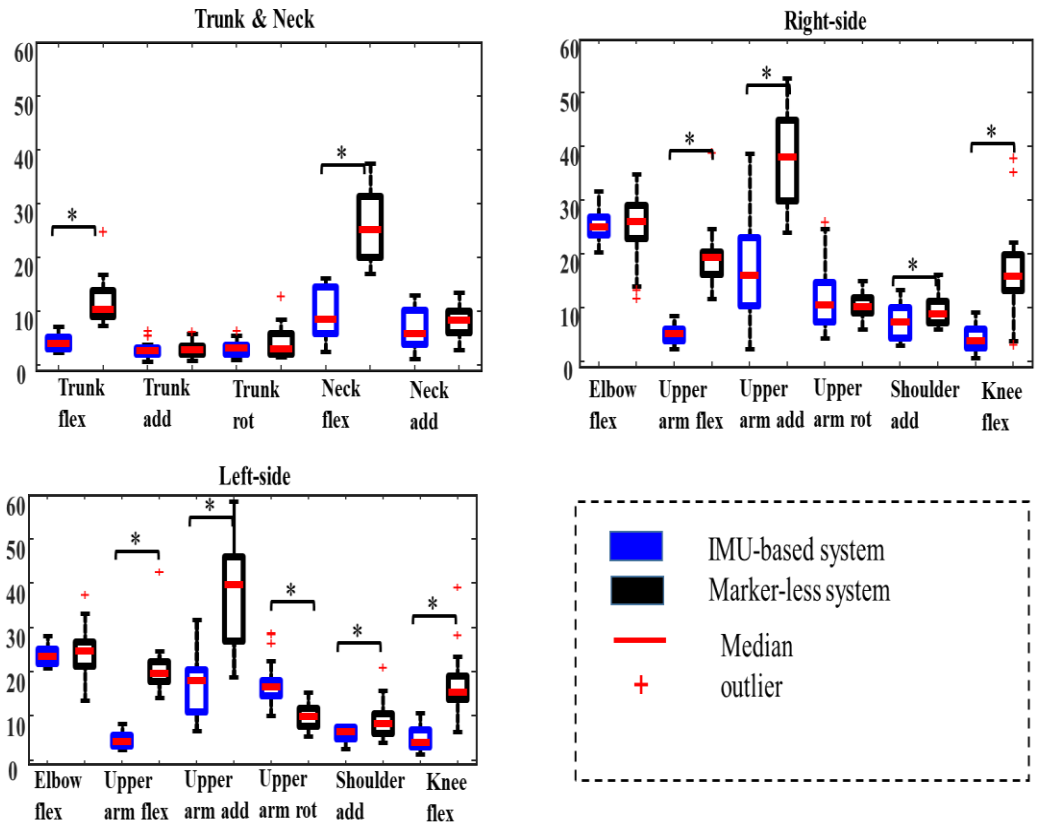

Figure B17: Comparison between the accuracy of the IMU-based system and marker-less system for joint angle measurement in scenario 4. The accuracy of each system was defined as its obtained RMSE against marker-based motion-capture system. The p-value for these comparisons are reported based on Friedman test (* if significant, with a significance level of 5%).

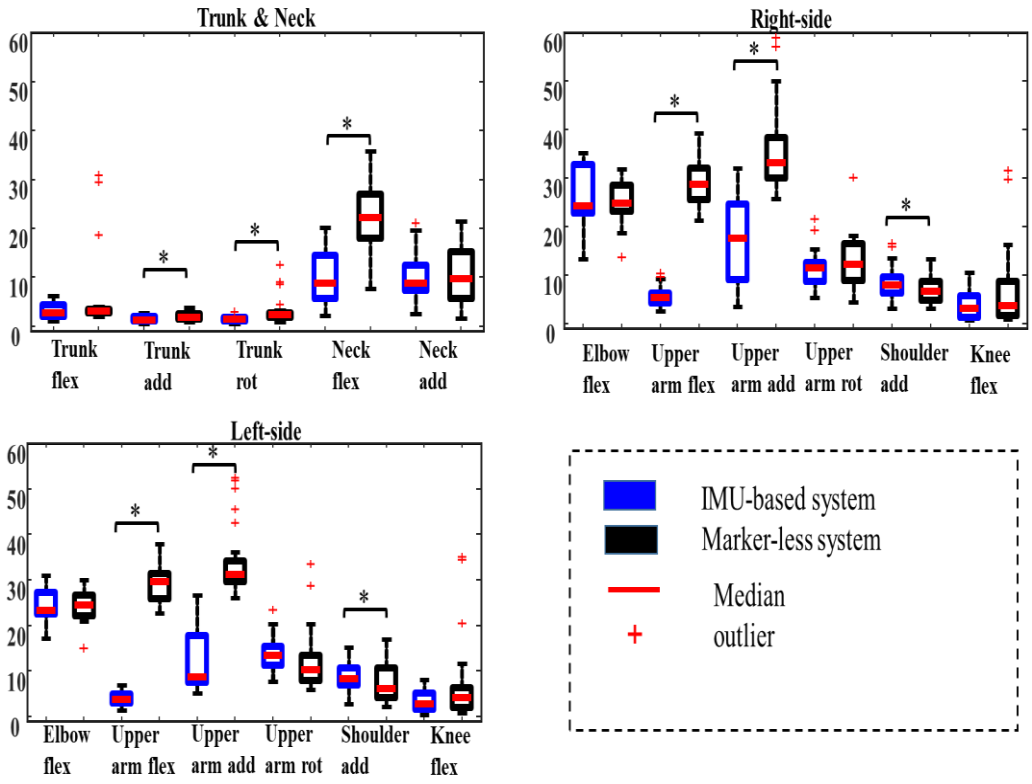

Figure B18: Comparison between the accuracy of the IMU-based system and marker-less system for joint angle measurement in scenario 4. The accuracy of each system was defined as its obtained RMSE against marker-based motion-capture system. The p-value for these comparisons are reported based on Friedman test (* if significant, with a significance level of 5%).